Robust Heteroclinic Cycles and Frequency Locking

Tsung-Lung Tsai

Downing College, Cambridge

Dissertation submitted

for the degree of

Doctor of Philosophy

at the

University of Cambridge

April 2009

To my family

Declaration

This dissertation is my own work and contains nothing which is the outcome of work done in collaboration with others, except as specified in the text and Acknowledgements. A short preliminary account of some of the results in Chapters 3 and 4 has been published in collaboration with my supervisor in *Physical Review E*, 2006, and has been approved by the Board of Graduate Studies for inclusion in this dissertation. No parts of this dissertation have been submitted for a degree, diploma or other qualification at this or any other University.

Acknowledgements

This dissertation would not have been possible without the support of numerous people. I would like to acknowledge that support now. First to my wife, Hui-Chuan Li, and my daughters, Yun-Shan Tsai (Sandra) and Yun-Ciao Tsai. thank you for understanding the importance of my work even though it often took me away from my role as a husband and father.

A heartfelt thank you goes to Dr. Jonathan H.P. Dawes, my supervisor, for his wisdom and intellectual vision, who has been constantly supportive and encouraging. I will always appreciate his invaluable suggestions and insightful questions during my PhD study.

I would also like to thank my parents, mother in law and all my relatives in Taiwan, for encouraging me always to do my best.

I am grateful to the Government of Taiwan, Cambridge Trust and my parents for funding my PhD study, and to Downing College, the Department of Applied Mathematics and Theoretical Physics and Cambridge Philosophical Society for financial support towards attending conferences.

Summary

In this dissertation, I study the synchronization between two oscillators. Specifically, in Chapters 3 and 4, one of the oscillators involved is a robust heteroclinic cycle.

Chapter 1 of this dissertation is introductory material. In Chapter 2, I include some basic background and examples of robust heteroclinic cycles followed by a review of circle maps and the '0-1 test', both of which will be used in my later discussion. I then study a robust heteroclinic ODE system perturbed by a periodic function in Chapter 3 and 4.

Chapter 3 gives the detailed derivation of the Poincaré map of the ODE system. The Poincaré map method is normally used for studying the dynamics near a cycle in a dynamical system. The idea of this method is to put a plane, called a cross section, transversely crossing the cycle which we are going to study and then observe the dynamics of points where an arbitrary orbit near the cycle intersects this plane. This result reduces the ODE system to a two-dimensional map.

In Chapter 4, the dynamics and bifurcations of the system when varying the forcing frequency is carried out. In short, my results show that the ODE system is equivalent to a damped pendulum with constant torque if the attracting strength of the heteroclinic cycle is weak. In contrast, it is equivalent to a circle map when the attracting strength of the heteroclinic cycle is strong. Depending on the value of the forcing frequency, the circle map can be invertible or noninvertible.

Chapter 5 deals with coupled systems with two cells. The ODE systems in both cells possess cyclic symmetry. I prove that if there exists a non-trivial symmetric periodic solution in one cell, then the non-trivial periodic solution in the other cell must have the same symmetry. I also consider the ratio of the frequencies of the periodic solutions in the two cells. A necessary condition for non-trivial periodic solutions with this ratio to be cyclically symmetric is identified.

Contents

Chapter 1

Introduction

Modeling biological systems is a very hard task due to their intrinsic complexity. However, regular patterns, which can be described roughly by symmetry in mathematics, are ubiquitous in our natural world, such as: spots on a leopard, stripes on a tiger and cylindrical stripes on a shell. Therefore, one may make an assumption when modeling biological systems that, without any noise and any coupling with other system, the underlying system is perfectly symmetric. In this sense, symmetry can be considered as one of the building blocks with which our real world is established. Consequently, studying symmetric systems is an essential step in understanding natural phenomena.

Mathematically, we model real world scenarios by dynamical systems. Spatial patterns correspond to stable equilibria of dynamical systems while spatial-temporal patterns may be driven by the instability of systems. Symmetry also constrains our study of some objects in dynamical systems. For example, a heteroclinic cycle in a dynamical system is a topological cycle which consists of saddle-type equilibrium points, periodic orbits or chaotic attractors, and connecting trajectories between them. One question that arises is whether heteroclinic cycles are structurally stable within some fixed symmetric setting, i.e. if hetero-

clinic cycles exist generically for some dynamical system.

Normally, a heteroclinic cycle is structurally unstable in a dynamical system without any symmetric setting. A well-known example is the undamped pendulum system [59]. With an arbitrary small perturbation, the ideal heteroclinic cycle breaks.

In systems with some fixed symmetric structure, the situation is different. For systems that are equivariant under a symmetry group acting on the phase space, heteroclinic cycles within them become robust in the sense that heteroclinic cycles always exist even if a small perturbation preserving symmetry is added. In this case, symmetry forces the connections to lie in invariant subspaces; this makes the cycle robust. More precisely, suppose Γ is a compact Lie group and $f(x, \lambda)$ is a family of one-parameter vector fields in $\chi_G = \{g : g(\gamma x) = \gamma g(x), \forall \gamma \in \Gamma\}$, i.e. the set of all equivariant vector fields with respect to Γ. Assume that $f(x, 0) \in \chi_G$ contains a heteroclinic cycle and each heteroclinic connection lies on a fixed point subspace Fix(Σ) for some subgroup $\Sigma \subset \Gamma$. Then there is an open set V in the parameter space such that each $f(x, \lambda)$ also possesses a heteroclinic cycle for every $\lambda \in V$.

Therefore, systems with robust heteroclinic cycles, but not general heteroclinic cycles, can be good candidates for modeling our real world. Indeed, examples of robust heteroclinic cycles connecting equilibrium points have been found in many contexts [52, 33, 38, 47, 45, 46, 72, 26, 17, 10]. They appear in various fields: ecological models of competing species [37, 52], thermal convection [12, 14, 8, 62], game theory [25, 69] and neuroscience [63, 79, 76, 66, 77, 4, 5, 65]. In principle, systems with heteroclinic cycles represent mathematically the concept of "Winnerless Competition" which has been identified as a better description than "Winner-takes-all" of many scenarios in game theory and evolutionary biology [57].

M. Krupa [42] classified all the possible contexts in which the existence of robust heteroclinic cycles have been shown into three categories: mathematical biology and game theory (MBGT), spontaneous symmetry breaking (SSB) and forced symmetry breaking (FSB). In this dissertation, we discuss only cycles connecting equilibrium points. Examples of cycles connecting periodic orbits or chaotic attractors can be found in [23] and [19], for instance. They demonstrate more complicated dynamics, such as cycling chaos.

The first example of a heteroclinic cycle modeling a biological system was given by R. M. May and W. J. Leonard in 1975 [52]. In their paper, a three dimensional Lotka-Volterra system

$$\begin{cases} \dot{x} &= x(1-(x+y+z)-cy+ez) \\ \dot{y} &= y(1-(x+y+z)-cz+ex) \\ \dot{z} &= z(1-(x+y+z)-cx+ey) \end{cases}, \tag{1.1}$$

which is a model with three competing species, is proved to possesses an attracting non-periodic cycle which connects three saddle equilibrium points. Moreover, the time spent near each saddle point increases. In fact, although the authors didn't point out the robustness of this cycle, it is robust due to the biological constraint: once a species is extinct, it will be extinct forever. In other words, the coordinate planes $\{x = 0\}$, $\{y = 0\}$ and $\{z = 0\}$ form the invariant planes supporting the connections.

J. Guckenheimer and P. Holmes in [33] confirmed that robust heteroclinic cycles do exist generically in the subspace of C^r vector fields on $\mathbb{R}^3$ which are equivariant with respect to a symmetry group generated by two elements, namely, cyclic permutation of the coordinate axes and the reflection of the coordinate planes. In addition to this, they also proved that a codimension 1 bifurcation is sufficient to produce heteroclinic cycles, which is called 'spontaneous symmetry breaking bifurcation' by M. Krupa in [42].

In addition to spontaneous symmetry breaking bifurcation, 'forced symmetry breaking bifurcation' also gives rise to the occurrence of robust heteroclinic cycles. Examples of this kind are shown, for example in [38, 47, 45, 46, 58], by forcing small perturbations on symmetric systems to break a part of the symmetry but keep the rest of the symmetry to support the cycles.

The main feature of the dynamics near an attracting heteroclinic cycle is intermittency: each trajectory spends relatively a much longer time passing through the vicinity of an equilibrium point than when transiting to the next equilibrium point. This is due to the strong linear influence near the equilibrium points. Moreover, a trajectory will move closer to each equilibrium point and spend increasing amounts of time passing each of them; these are critical differences in the dynamics from trajectories near periodic orbits. In ecological terminology, these characteristics mean that each species will be getting increasingly more dominant both sizewise and timewise, after experiencing an almost extinct period. From this point of view, a model with heteroclinic cycles is not appropriate to describe the long term behavior of the biological world. However, this defect can be modified by forcing a small symmetry-breaking perturbation (noise) or by coupling two or more systems (interaction with other systems).

With suitable choice of parameters, a small perturbation added on to a 6-dimensional Lotka-Volterra system, for example

$$\dot{x}_i = x_i(1 - \sum_{j=1}^{6} \alpha_{ij} x_j) + \epsilon x_i x_{i+3},$$

would produce an attracting periodic solution in the vicinity of the original heteroclinic cycle [4].

In recent years, a modified Lotka-Volterra system has been utilized to model the dynamics of neuron ensembles. The N-neuron system studied in [79, 76, 66,

77, 4] is

$$\dot{x}_i = x_i \left(\sigma(\mathbf{H}, \mathbf{S}) - \sum_{j=1}^{N} a_{ij} x_j + H_i(t) \right) + S_i(t), \tag{1.2}$$

where $x_i > 0$ is the spiking rate of the ith neuron, H_i is the forcing from other neuron ensembles, S_i is the stimuli from the sensors acting on the i-th neuron and a_{ij} is the strength of inhibition on the i-th neuron by the j-th neuron. Since non of the neurons dominates the whole dynamics, Rabinovich et al. [66] called this phenomenon 'Winnerless competition' (WLC).

A neural ensemble normally consists of several neurons interacting with each other through an inhibitory way. Its dynamics can be studied experimentally by recording the spiking rate of each neuron. According to experimental results, a good mathematical model to describe the dynamics of a neural system, especially a sensory system, must have the ability to capture the features of robustness and sensitivity. More precisely, it must be robust under small perturbation (noise) and must be very sensitive to incoming input (stimulus) [63]. Robust heteroclinic cycles possess these two features: a fixed symmetry breaking stimulus destroys the heteroclinic cycle and gives rise to a periodic solution near the original cycle; this periodic solution is robust under small perturbation.

Robust heteroclinic cycles can also be applied to describe the transient behavior of neural systems [5, 63, 64]. To recognize the stimulus as soon as possible, a sensory system makes decisions by identifying the pattern of the transient sequence of the firing neurons before it settles down to a stable stationary state. As transient behavior in a dynamical system normally depends sensitively on initial conditions, it is very hard to find a mathematical model which can reproduce the same sequence of firing neurons when the stimulus is slightly different. Afraimovich et al. [5] constructed a model consisting of a stable heteroclinic sequence (SHS) which generates reproducible transient dynamics. In their model, a sequence of equilibrium points are connected by one-dimensional separatrices and

any trajectory near the SHS will visit equilibrium points in turn along the SHS. Moreover, due to the stability of the heteroclinic sequence, a small deviation of the initial point will produce the same transient sequence.

Constant perturbations to a robust heteroclinic cycle result in periodic orbits typically. For a heteroclinc system forced by a random perturbation, the returning time corresponding to a cross section for a trajectory near the original heteroclinic cycle becomes random, although the mean of it is well-defined [71]. But to date there has been no systematic investigation of the effects of time periodic perturbations. This is surprising, given the natural effects of external cyclical variations on population dynamics, for example. A natural mathematical comparison to make would be to compare the effects of time-periodic forcing on a heteroclinic cycle with the well-known effects of time-periodic forcing on periodic oscillations, for example frequency-locking. This comparison is the central motivation for the work described in this dissertation.

J. H. P. Dawes and I in [18] investigate the complex dynamics of the Lotka-Volterra system with periodic forcing,

$$\begin{cases} \dot{x} &= x(1-(x+y+z)-cy+ez)+\gamma(1-x)f(2\omega t) \\ \dot{y} &= y(1-(x+y+z)-cz+ex) \\ \dot{z} &= z(1-(x+y+z)-cx+ey) \end{cases}, \tag{1.3}$$

where f is a non-negative function in $PC^1(2\pi)$, the set of all 2π-periodic functions with continuous first-order derivative, $0 < \gamma \ll 1$ and $1 > c > e > 0$. It is a generalized version of the system studied by Rabinovich et al. [63]. In this dissertation, Chapter 3 and 4 sets out a mathematically rigorous and detailed approach to the analysis of the dynamics of (1.3). This provides a much greater level of insight into the dynamics than [63] was able to provide. Our preliminary results have recently been published [18].

By calculating the global and local maps of the system in Chapter 3, we con-

struct a two-dimensional Poincaré map defined on a cross section of the cycle. The numerical results show that the dynamics of map system fit the ODE system very well for a range of values of parameters when $\gamma << 1$ and $\omega > 0$. Moreover, the map we derived is valid for all c/e while the map derived by Afraimovich et al. in [3], in which they considered a similar system, is only correct when c/e near 1.

The general feature of the dynamics for the case c/e large when varying ω is the existence of a sequence of frequency-locking intervals with regions of complicated dynamics in between. In particular, the frequency-locking intervals indicate the existence of a stable periodic orbit of period $k\pi/\omega$ within it, where $k \in \mathbb{N}$. We prove in Chapter 4 that the system is equivalent to a circle map, which could be invertible or non-invertible depending on the size of ω. As for the case when c/e is near 1, except for the frequency-locking scenario, bistability could occur over some intervals in ω. In this case, the system is equivalent to a forced damped pendulum with torque. This part of discussion is also included in Chapter 4.

In addition to adding external perturbations to a single robust heteroclinic system, coupling two or more robust heteroclinic systems could also produce an applicable biological model.

For example, P. Varona et al. [77, 76] attempted to use (1.2) as a model to capture the irregular hunting behavior of *Clione*, a marine mollusk. *Clione* uses gravitational sensory organs, the statocysts, to determine its orientation. $S_i(t)$, in (1.2), represents the stimulus of the statocyst on the receptor neuron a_i. In their model, the statocyst consists of six neurons, which are divided into two subgroups of three neurons. Inside each subgroup, the inhibitory coupling terms are relatively stronger and produce heteroclinic connections between the three neurons. Later, Venaille et al. [79] weakly coupled two neuron ensembles. Each of the two ensembles is a six neuron statocyst which is modeled by the same way as P.

Varona did in [77, 76]. They found that synchronization of two ensembles occurs although the signals produced by individual ensembles are chaotic. These features are similar to the coordination of two distinct motor activities of *Clione* during hunting motion: acceleration of the wing and the bending of the tail, both of which change randomly but coordinate very well.

Mathematically, we call a system consisting of two or more dynamical systems coupling to each other a coupled cell system. Here, 'cell' means the individual dynamical system without coupling. Although a coupled cell system is merely a higher-dimensional dynamical system as a whole, we are interested in the properties of cell trajectories, which are the projections of a trajectory in the whole dynamical system to the individual cells, when we called the system 'coupled cell system'. Theory for coupled cell systems with symmetry has been developed by Stewart, Golubitsky, Pivato and Török [28]. Although we can freely couple dynamical systems in any way, coupling systems in a square or a hexagonal lattice is more common, for implicitly they resemble partial differential equations. In this case, regular or irregular spatio-patterns can be found [7, 80].

Periodic solutions with spatial-symmetry in a symmetric system automatically have temporal-symmetry [28]. M. Tachikawa [74] considered an ecological system consisting of two four-dimensional replicator equations coupled diffusively. In these two cells, there exist a stable and an unstable robust heteroclinic cycle respectively. His results showed numerically that frequency-locking intervals with specific ratios can be observed when varying the strength of the coupling. The author remarked that these specific ratios arise due to the existence of symmetric periodic solutions, but did not prove any result.

In Chapter 5, I consider a more general theory which shows that, in a system consisting of two cells with cyclic symmetry, symmetry is always snchronized between non-trivial periodic solutions in two cells. More precisely, if there exists a

symmetric periodic solution in one cell, then the periodic solution in the other cell must have the same symmetry. The intrinsic spatio-temporal-symmetry of a periodic solution allows us to classify all the ratios of frequencies between non-trivial periodic solutions in these two cells according to the symmetry they possess.

We now briefly describe the contents of this dissertation as follows.

In Chapter 2, I give some basic background on robust heteroclinic cycles followed by three examples of the existence of robust heteroclinic cycles. The review of the theory of circle maps, either invertible or noninvertible, is presented as this is necessary for our later discussion. This chapter closes with the description of '0-1 test' which is a new method to distinguish regular and chaotic dynamics from any timeseries of data.

Chapter 3, 4 and 5 contain the body of my research. In Chapter 3 and 4, I study heteroclinic systems with periodic perturbations. A detailed derivation of the Poincaré map of the system is carried out in Chapter 3 while a thorough analytic and numerical study is displayed in Chapter 4.

Chapter 5 deals with a different, but closely related, topic. I consider coupled systems of two cells with cyclic symmetry. Specifically, I am interested in the interactions between non-trivial periodic solutions in the two cells. As mentioned in the previous paragraph, I prove that the periodic solutions in the two cells must have the same symmetry. I also identify those ratios of frequencies where the non-trivial periodic solutions possess cyclic symmetry.

Conclusions and possible future research directions will be presented and discussed in Chapter 6.

Chapter 2

Preliminaries and Background

In this chapter, we give the definition of heteroclinic cycles in section 2.1, followed by three examples of the existence of heteroclinic cycles in section 2.2, which fall into the three categories classified by Krupa in [42]. We then review the theories of circle maps in section 2.3 and the 0-1 test in section 2.4. These theoretical results form the basis for our later analysis in Chapter 4.

2.1 Definition of a heteroclinic cycle

Suppose that $\Gamma \in \mathbf{O}(n)$ is a compact Lie group acting linearly on $\mathbb{R}^n$. Let $f : \mathbb{R}^n \to \mathbb{R}^n$ be a Γ-equivariant vector field. That is

$$f(\gamma x) = \gamma f(x), \forall \gamma \in \Gamma \text{ and } \forall x \in \mathbb{R}^n.$$

Definition 2.1.1 *Suppose that ξ_j, $j = 1, \cdots, m$ are hyperbolic equilibria of the vector field $f(x)$ and that the group orbits $\Gamma\xi_j = \{\gamma \in \Gamma : \gamma\xi_j\}$, $j = 1, 2, ..., m$ are distinct. Let $W^s(\xi_j)$ and $W^u(\xi_j)$ denote the stable and unstable manifolds of ξ_j, respectively. The set of group orbits of the unstable manifolds*

$$X = \{W^u(\gamma\xi_j), j = 1, \cdots, m, \gamma \in \Gamma\}$$

forms a heteroclinic cycle provided $dim W^u(\xi_j) \geq 1$ *for all* j *and*

$$W^u(\xi_j) - \{\xi_j\} \subset \bigcup_{\gamma \in \Gamma} W^s(\gamma \xi_{j+1}).$$

Here, we use indices modulo m, i.e. we set $m + 1 \equiv 1$. *If* $m = 1$, *we call it a homoclinic cycle.*

Suppose that $\Sigma \subset \Gamma$ is a subgroup, we define its fixed-point subspace by

$$Fix(\Sigma) = \{x \in \mathbb{R}^n : \sigma x = x, \forall \sigma \in \Sigma\}.$$

In particular, since $f(Fix(\Sigma)) \subset Fix(\Sigma)$ for every $\Gamma-$equivariant f and isotropy subgroup Σ, the following definition is natural:

Definition 2.1.2 *The cycle X is a robust heteroclinic cycle if for each* $j = 1, \cdots, m$, *there is a fixed-point subspace* $P_j = Fix(\Sigma_j)$ *where* $\Sigma_j \subset \Gamma$, *such that (i)* ξ_{j+1} *is a sink in* P_j *and (ii)* $W^u(\xi_j) \subset P_j$.

Remark 2.1.1 *(i) A robust heteroclinic cycle will persist under any small* $\Gamma-$*equivariant perturbations of the vector field.*
(ii) For a general vector field without symmetry, a heteroclinic cycle is necessarily structurally unstable.
(iii) Without loss of generality, we may assume that the subgroups Σ_j *are isotropy subgroups* $\Sigma_x = \{\gamma \in \Gamma : \gamma x = x\}$ *for some x, and that the* P_j *are the smallest possible subspace such that the conditions in the definition are satisfied.*

The stability of invariant sets is one of the most important issues in the theory of dynamical systems. There are various definitions of stability. Here, we only consider the strongest one: asymptotic stability.

Definition 2.1.3 *A heteroclinic cycle X is stable if for any open neighborhood U of X, there exists an open neighborhood V of X such that any forward trajectory*

$\{x(t) : t \geq 0, x(0) \in V\} \subset U$. *($x(t)$ is the solution of differential equation $\dot{x} = f(x)$). We said it is asymptotically stable if it is stable and any forward trajectory starting in V is asymptotic to X. The cycle is unstable if it is not stable.*

There have been many papers studying on this topic, for example [43], [44], [24], [36] and [60]. Krupa and Melbourne in [43] analyze the relative size of the eigenvalues of the linearizations at the equilibria and get a sufficient condition for asymptotic stability of a heteroclinic cycle. The following theorem is a part of their results:

Theorem 2.1.1 *Suppose X is a robust heteroclinic cycle. Then X is asymptotically stable provided the condition*

$$\prod_{j=1}^{m} min(c_j, e_j - t_j) > \prod_{j=1}^{m} e_j,$$

where $-c_j$ is the maximum real part of eigenvalues of (df) in $P_{j-1} - P_j$ at the j-th equilibrium point, e_j is the maximum real part of eigenvalues of (df) and t_j is the maximum real part of eigenvalues whose eigenvectors are normal to $P_{j-1} + P_j$.

Remark 2.1.2 *In $\mathbb{R}^3$, the condition above could be reduced to the very intuitive one*

$$\prod_{j=1}^{m} c_j > \prod_{j=1}^{m} e_j$$

2.2 Existence of heteroclinic cycles

In this section, we will consider three examples of heteroclinic cycles. The first one is from Guckenheimer and Holmes ([33]) which shows that the symmetry-breaking bifurcations of equilibria can naturally lead to the existence of robust heteroclinic cycles. The second example is from Hou and Golubitsky ([38]) which

displays that symmetry breaking may result in the occurrence of heteroclinic cycles. The final example is a Lotka-Volterra system; an application will be also discussed.

2.2.1 Spontaneous symmetry breaking

Let $G \subset \mathbf{O}(3)$ be the symmetry group generated by

$$r_x = \begin{pmatrix} -1 & 0 & 0 \\ 0 & 1 & 0 \\ 0 & 0 & 1 \end{pmatrix}$$

and

$$\sigma = \begin{pmatrix} 0 & 0 & 1 \\ 1 & 0 & 0 \\ 0 & 1 & 0 \end{pmatrix},$$

in other words, G consists of cyclic permutations of the coordinate axes in $\mathbb{R}^3$ and reflections about the coordinate planes.

Guckenheimer and Holmes prove the following theorem [33]:

Theorem 2.2.1 *Consider the space $\chi_G(\mathbb{R}^3)$ of $C^r(r \geq 3)$ vector fields on $\mathbb{R}^3$ that are equivariant with respect to the group G. There is an open set $U \subset \chi_G$ of vector fields in χ_G such that*
(i) all vector fields in U are topologically equivalent, and
(ii) vector fields in U have heteroclinic cycles consisting of three saddle points and trajectories joining these. All trajectories that do not lie on the coordinate planes, or the lines $x = \pm y = \pm z$ are asymptotic to the heteroclinic cycle.

Remark 2.2.1 *In the original paper [33] by Guckenheimer and Holmes, the continuous differentiability of $\chi_G(\mathbb{R}^3)$ was set to be $r \geq 1$. However, since the Taylor*

expansion up to order three of these vector fields will be considered in the following, we consider vector fields in $\chi_G(\mathbb{R}^3) \cap C^r$ *for* $r \geq 3$ *here.*

In the following, we will show only the existence and the stability of robust heteroclinic cycles within $\chi_G(\mathbb{R}^3)$.

Firstly, note that the vector field

$$X = (f(x,y,z), g(x,y,z), h(x,y,z)) \in \chi_G(R^3)$$

if and only if $f(x,y,z) = g(y,z,x) = h(z,x,y)$ and $f(x,y,z) = -f(-x,y,z) = -f(x,-y,z) = -f(x,y,-z)$, which ensures that the only system of equations defining a vector field in $\chi_G(\mathbb{R}^3)$ has a truncated Taylor expansion at the origin of the form,

$$\begin{cases} \dot{x} = x(\lambda + a_1x^2 + a_2y^2 + a_3z^2) \\ \dot{y} = y(\lambda + a_1y^2 + a_2z^2 + a_3x^2) \\ \dot{z} = z(\lambda + a_1z^2 + a_2x^2 + a_3y^2) \end{cases} \tag{2.1}$$

Secondly, the symmetry of group G forces the lines defined by $x = \pm y = \pm z$, the coordinate axes and the coordinate planes to be invariant under the action of any vector field $X \in \chi_G(\mathbb{R}^3)$.

Assume $a_1 < 0$, so that the bifurcation is supercritical. Let $P_1 = (\sqrt{-\frac{\lambda}{a_1}}, 0, 0)$ and $P_2 = \sigma P_1 = (0, \sqrt{-\frac{\lambda}{a_1}}, 0)$. Then

$$\begin{matrix} Df(P_1) = \lambda \cdot diag\left(-2, \frac{a_1-a_3}{a_1}, \frac{a_1-a_2}{a_1}\right) \\ Df(P_2) = \lambda \cdot diag\left(\frac{a_1-a_2}{a_1}, -2, \frac{a_1-a_3}{a_1}\right) \end{matrix} . \tag{2.2}$$

Hence if we assume that

$$a_2 < a_1 < a_3, \tag{2.3}$$

then P_1 is a saddle and P_2 is a sink for the flow of (1) restricted to $\{(x,y,z) : z = 0\}$. (Obviously, if $a_3 < a_1 < a_2$ then we can do the same thing and get a cycle moving in the opposite direction.)

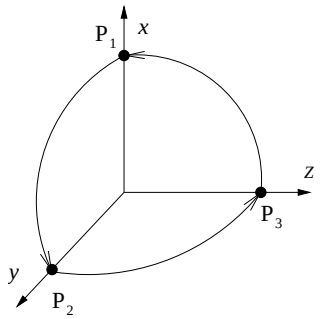

Figure 2.1: The heteroclinic cycle in the Guckenheimer-Holmes system (2.1) in the first octant.

Now consider the restriction of (2.1) to P:

$$\begin{cases} \dot{x} = x(\lambda + a_1 x^2 + a_2 y^2) \\ \dot{y} = y(\lambda + a_1 y^2 + a_3 x^2) \end{cases} \tag{2.4}$$

We can easily show that (2.4) admits no equilibria other than the origin, $\pm P_1$ and $\pm P_2$ if we have (2.3). Besides, we can prove that the unstable manifold $W^u(P_1)$ is located in a bounded region. More precisely, choose $K > \sqrt{-\frac{\lambda}{a_1}}$ and consider $D = \{(x, y) : 0 < x < K, 0 < y < K\}$. Then the flow within D will not leave it since

$$\dot{x} = K(\lambda + a_1 K^2 + a_2 y^2) < 0$$

on $\{x = K\} \cap \bar{D}$, and

$$\dot{y} = K(\lambda + a_1 k^2 + a_3 x^2) < 0$$

on $\{y = K\} \cap \bar{D}$. Hence, by the Poincaré-Bendixson theorem, there exists a connection between P_1 and P_2. By applying σ to this connection, we have proved the following lemma:

Lemma 2.2.1 *The heteroclinic cycle exists for $\lambda > 0$ in the system (2.1) if $a_1 < 0$ and the condition (2.3) holds.*

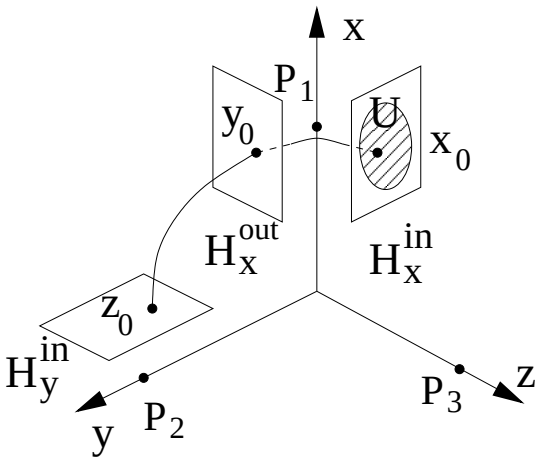

Figure 2.2: The cross sections H_x^{in}, H_x^{out} and H_y^{in}.

Moreover, this lemma proves that the existing cycle is robust for small symmetry-preserving perturbations. (See Figure 2.1).

To identify the stability of the heteroclinic cycle, we use the Poincaré map method to analyze the dynamics near the cycle we have found.

Let $\delta > 0$ be a small real number and $H_x^{in} = \{z = \delta\}$, $H_x^{out} = \{y = \delta\}$ and $H_y^{in} = \{x = \delta\}$ be cross sections near P_1 and P_2. Let $x_0 \in H_x^{in}, y_0 \in H_x^{out}, z_0 \in H_y^{in}$ be points on the connecting orbits $P_3 \longrightarrow P_1, P_1 \longrightarrow P_2, P_1 \longrightarrow P_2$, respectively (see Figure 2.2). Let $U = \{(u, w, \delta)\}$ be a small neighborhood of x_0, $U^+ = \{(u, w, \delta) : w > 0\} \cap U$ and $U^- = \{(u, w, \delta) : w < 0\} \cap U$. Then the trajectories starting from U^+ and U^- will hit H_y^{in} if we choose U small enough. On the other hand, the trajectories starting from $U \backslash (U^+ \cup U^-)$ will converge to P_1 since P_1 is a stable equilibrium in the x-plane. Define $g : U^+ \to H_x^{in}$ by $g = \sigma^{-1}h$, where h is the first hit map from U to H_y^{in}. If we identify points in U with points in $\mathbb{R}^2$ then we can write $g(u, w) = g(x_0 + (u, w, \delta)) = (g_1(u, w), g_2(u, w))$. Now extending g to be defined on U by setting $g(u, w) = (g_1(u, -w), -g_2(u, -w))$, if $w < 0$, we get a Poincaré map g^3 which reduce the 3-dimensional flow system to a 2-dimensional

map system. In the following discussion, we will assume $w > 0$ without loss of generality.

Note that the cycle that we have found is asymptotically stable if 0 is asymptotically stable fixed point of g. On the other hand, the cycle is unstable if 0 is a repelling fixed point of g.

Before we derive the leading-order approximation of g, we define some notation from [43]. Let

$$r = -2\lambda, e = \lambda \cdot \frac{a_1 - a_3}{a_1}, c = \lambda \cdot \frac{a_2 - a_1}{a_1},$$

where $r, e, -c$ denote the radial, expanding and contracting eigenvalues of the linearized system of (2.1), respectively. We expect that if $c > e$, then the cycle will be asymptotically stable. Moreover, the radial eigenvalue r plays no role in determining stability.

Now we begin to derive the lowest order expression of g. Let ψ and ϕ denote the first hit maps from U^+ to H_x^{out} and from a neighborhood of y_0 in H_x^{out} to H_y^{in}. Since the flow near the hyperbolic equilibrium P_1 is equivalent to the flow of the linearized system, ψ is of the form

$$\psi(u, w, \delta) = (\delta^{-\frac{r}{e}} u w^{\frac{r}{e}}, \delta, \delta^{1-\frac{c}{e}} w^{\frac{c}{e}}).$$

The map ϕ is a diffeomorphism. Using a Taylor expansion near y_0, we can approximate

$$\phi(u, \delta, v) = (\delta, a_0(u, v), b_0(u, v)v),$$

where a_0 and b_0 are smooth functions. Thus, from the fact that $g(u, w) = \sigma^{-1}\phi \circ \psi$ we get the following lemma.

Lemma 2.2.2 *At leading order, the map g has the form*

$$g(u, w) = (a(u, w), b(u, w)w^{c/e}),$$

for some continuous functions a and b, $b(u,w) > 0$ for $w > 0$. Moreover there exist constants $K, \alpha > 0$ such that

$$|a(u,w)| \leq Kw^{\alpha}; |b(u,w)| \leq K, (u,w) \in U$$

Suppose $c/e > 1$ and let $g = (g_1, g_2)$. If $w < max\{(2K)^{c/e-1}, 1, 1/2K\}$, then $g_2 \leq Kw^{c/e} \leq w/2$ which implies that $|(g_2)^n(u,w)| \leq (w/2)^n \to 0$ as $n \to \infty$. On the other hand, $|g_1^n(u,w)| = |a^n(u,w)| \leq (Kw^{\alpha})^n < (1/2)^n \to 0$ as $n \to \infty$. Hence, we have proved the following corollary which describing the stability of the heteroclinic cycle.

Corollary 2.2.1 *The heteroclinic cycle in system (2.1) is stable if $2a_1 > a_2 + a_3$.*

2.2.2 Forced symmetry breaking

In this section, we will follow the result of Hou and Golubitsky ([38]) which gives an example of a robust cycle arising through forced symmetry breaking.

Let $\Gamma \subset \mathbf{O}(n)$ be a Lie group acting on $\mathbb{R}^n$ and let $f : \mathbb{R}^n \longrightarrow \mathbb{R}^n$ be a $\Gamma-$equivariant vector field. Consider systems of differential equations:

$$\dot{z} = f(z) \tag{2.5}$$

$$\dot{z} = f(z) + \epsilon g(z), \tag{2.6}$$

where ϵ is small and g is only $\Delta-$equivariant with $\Delta \subset \Gamma$ a Lie subgroup.

Suppose equation (2.5) has an equilibrium at z_0. Then equivariance implies that the manifold

$$X_0 = \Gamma z_0 = \{\gamma z_0 : \gamma \in \Gamma\}$$

is a group orbit of equilibria. We assume that X_0 is not a set of disconnected equilibria. Moreover, we also assume that X_0 is normally hyperbolic and asymptotically stable. The definition of normal hyperbolicity can be found in [81]. Roughly

speaking, we call X_0 normally hyperbolic if it expands or contracts more quickly in its normal directions than in its tangent directions. When ϵ is small, normal hyperbolicity guarantees that there is a perturbed flow invariant manifold X_ϵ for the perturbed system (2.6) which is diffeomorphic to X_0

Lauterbach and Roberts ([47]) show that, when dim $\Delta <$ dim Γ and ϵ is small enough, the dynamics on the perturbed group orbit X_ϵ is generally more complicated than just consisting of equilibria. More precisely, the residual symmetry Δ forces the occurrence of one-dimensional flow invariant sets connecting these equilibria. Hence the symmetry-breaking perturbation will result in the occurrence of heteroclinic cycles. In their example, $\Gamma = \mathbf{O}(3)$ and $\Delta = \mathbf{T}$ (the group of symmetries of the tetrahedron). Later on, Lauterbach *et al.* ([45], [46]) classified all pairs for which $\Gamma = \mathbf{O}(3)$ or $\mathbf{SO}(3)$ and Δ is any proper Lie subgroup which may force heteroclinic cycles.

Hou and Golubitsky considered the system in $\mathbb{R}^4 \cong \mathbb{C}^2$with $\Gamma = \mathbf{D}_4 \ltimes \mathbf{T}^2, \Delta = \mathbf{D}_2$. The action of $\mathbf{D}_2$ on $\mathbb{C}^2$ is generated by the reflections

$$\begin{aligned} \kappa_1 \cdot (z_1, z_2) &= (\overline{z}_1, z_2) \\ \kappa_2 \cdot (z_1, z_2) &= (z_1, \overline{z}_2) \end{aligned}$$

The action of $\Gamma = \mathbf{D}_4 \ltimes \mathbf{T}^2$ on $\mathbf{C}^2$ is generated by κ_1 and

$$\begin{aligned} \kappa \cdot (z_1, z_2) &= (z_2, z_1) \\ (\theta, \phi) \cdot (z_1, z_2) &= (e^{i\theta} z_1, e^{i\phi} z_2) \end{aligned}$$

where $(\theta, \phi) \in \mathbf{T}^2$.

We will prove that there exists an equilibrium in the unperturbed system (2.5) of the form $z_0 = (\mu, \mu)$ where $\mu > 0$. We call such an equilibrium a mixed mode solution. Since the isotropy subgroup of z_0 is $\mathbf{D}_4$ generated by κ and κ_1, the group orbit X_0 of z_0 is diffeomorphic to the 2-torus $\mathbf{T}^2$.

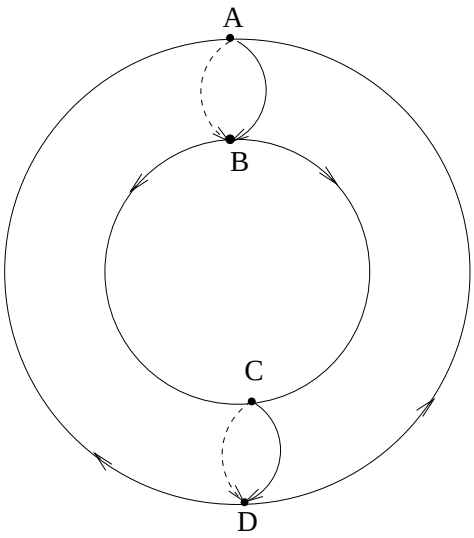

Figure 2.3: Fixed-point subsets on the 2-torus X_ϵ and the connections.

As we mentioned before, there is a perturbed flow invariant manifold X_ϵ for the perturbed system which is diffeomorphic to X_0 so that only the dynamics of X_0 is needed to be considered. Moreover, there are some points in X_0 which are also in X_ϵ. In fact, the fixed-point subsets of subgroup of $\mathbf{D}_2$ acting on X_0 are

$$\begin{aligned} Fix^0(\kappa_1) &= \{(0,\phi) : \phi \in [0,2\pi)\} \cup \{(\pi,\phi) : \phi \in [0,2\pi)\} \\ Fix^0(\kappa_2) &= \{(\theta,0) : \theta \in [0,2\pi)\} \cup \{(\theta,\pi) : \theta \in [0,2\pi)\} \\ Fix^0(\mathbf{D}_2) &= \{(0,0),(\pi,0),(0,\pi),(\pi,\pi)\}. \end{aligned}$$

(In other words, the fixed-point subset for each κ_i is the disjoint union of two circles, while that of $\mathbf{D}_2$ consists of four points. See Fig.2.3) Therefore, the four fixed points in $Fix^0(\mathbf{D}_2)$ are four equilibria on X_ϵ for the perturbed system (2.6). We call them $\mathbf{D}_2-$equilibria.

Note that the two invariant circles $Fix^0(\kappa_1)$ and $Fix^0(\kappa_2)$ are connections of these $\mathbf{D}_2-$ equilibria as depicted in Figure 2.3 Thus, if we can show that (i) all these four $\mathbf{D}_2-$equilibria are saddles and (ii) there is no other equilibria on $Fix^0(\kappa_1)$ and $Fix^0(\kappa_2)$, then we prove the existence of a heteroclinic cycle.

Orbit representative	Isotropy subgroup	Fixed-point subspace	Dimension
$(0,0)$	$\mathbf{D}_4 \ltimes \mathbf{T}^2$	$(0,0)$	0
$(x,0), x \in \mathbb{R}$	$\mathbf{D}_2 \ltimes \mathbf{S}^1$	$(x,0)$	1
$(x,x), x \in \mathbb{R}$	$\mathbf{D}_4$	(x,x)	1
$(x,y), x,y \in \mathbb{R}$	$\mathbf{D}_2$	(x,y)	2

Table 2.1: Isotropy subgroups of $\mathbf{D}_4 \cdot \mathbf{T}^2$ acting on $\mathbb{C}^2$.

The existence of stable mixed mode solutions of (2.5) will be shown first. Then we will prove the existence of perturbation term $g(z)$ such that all the $\mathbf{D}_2-$equilibria are saddles with inflow and outflow consistent with a cycle. After that, we will prove that there are no other equilibria on the cycle which ensures the existence of heteroclinic cycles. The asymptotic stability of the cycle will be established in the following. After all this, we give the main result of [38].

The existence of stable mixed mode solutions

There are four isotropy subgroups arising from the group action of $\mathbf{D}_4 \ltimes \mathbf{T}^2$ acting on $\mathbb{C}^2$, as listed in Table 2.1. We call the points with isotropy subgroup $\mathbf{D}_2 \ltimes \mathbf{S}^1$ pure modes and the points with isotropy subgroup $\mathbf{D}_4$ mixed modes.

Consider the $\mathbf{D}_4 \ltimes \mathbf{T}^2$-equivariant vector field $f(z,\lambda)$ which depends on a bifurcation parameter λ

$$\dot{z} = f(z,\lambda). \tag{2.7}$$

The general form of this vector field is

$$f(z_1,z_2,\lambda) = (A(|z_1|^2,|z_2|^2,\lambda)z_1, A(|z_2|^2,|z_1|^2,\lambda)z_2), \tag{2.8}$$

where $A : \mathbb{R}^2 \times \mathbb{R} \to \mathbb{R}$. Assume $A(0,0,0) \neq 0$. After properly rescaling λ and

Solution Type	Subgroup	Subspace	Equation	Eigenvalues
Trivial	$\mathbf{D}_4 \ltimes \mathbf{T}^2$	$(0,0)$	$z_1 = z_2 = 0$	λ(twice)
Pure mode	$\mathbf{D}_2 \ltimes \mathbf{S}^1$	$(x,0)$	$\lambda = -ax^2$	$2ax^2, (b-a)x^2$
Mixed mode	$\mathbf{D}_4$	(x,x)	$\lambda = -(a+b)x^2$	$2(a \pm b)x^2$

Table 2.2: Linear stability of different modes.

then Taylor expanding A, we have

$$A(|z_1|^2, |z_2|^2, \lambda) = \lambda + a|z_1|^2 + b|z_2|^2 + \text{higher order terms},$$

where $a, b \in \mathbb{R}$.

Let

$$K(z,\lambda) = ((\lambda + a|z_1|^2 + b|z_2|^2)z_1, (\lambda + a|z_1|^2 + b|z_2|^2)z_2) \tag{2.9}$$

be the third-order truncation of $f(z,\lambda)$. We say that a $\mathbf{D}_4 \ltimes \mathbf{T}^2$-equivariant vector field $f(z,\lambda)$ is nondegenerate if $a \neq 0$ and $a \neq \pm b$. The following theorem proved in [72] asserts that the stability of the equilibria of the vector field $f(z,\lambda)$ are determined by K.

Theorem 2.2.2 *A nondegenerate $\mathbf{D}_4 \ltimes \mathbf{T}^2$-equivariant vector field $f(z,\lambda)$ is $\mathbf{D}_4 \ltimes \mathbf{T}^2$-equivalent to $K(z,\lambda)$.*

Therefore, we may assume that $f(z,\lambda)$ is in normal form (2.9) and only compute the result from K.

The invariant subspaces of vector field K can be classified into three different types depending on which subgroup acting on it. See Table 2.2 for the branching equation.

Since fixed point subspaces are always flow-invariant, we can restrict our dis-

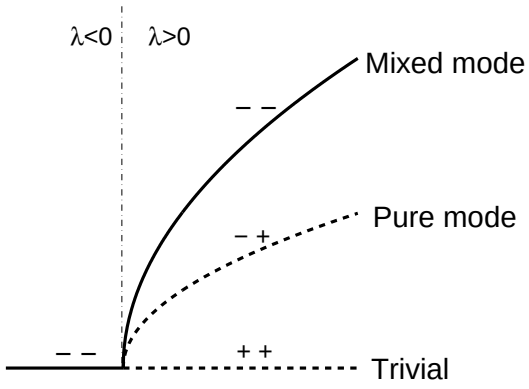

Figure 2.4: Bifurcation diagram in $a > |b|$ region.

cussion to $Fix(\mathbf{D}_2)$. Compute

$$(dK)|_{Fix(\mathbf{D}_2)} = \begin{pmatrix} \lambda + 3ax_1^2 + bx_2^2 & 2bx_1x_2 \\ 2bx_1x_2 & \lambda + bx_1^2 + 3ax_2^2 \end{pmatrix},$$

we get the eigenvalues of points on these three different types of invariant subspaces. See Table 2.2 for the details. Note that the stable mixed modes occur only in the region $\{(a,b) : a > |b|\}$. See Figure 2.4 for the bifurcation diagram in this region.

Stability of $\mathbf{D}_2-$equilibria

From this section on, we assume that the coefficients (a,b) of the truncated vector field (2.9) satisfy the condition $a > |b|$. This assumption will guarantee the existence of an orbitally stable mixed mode solution which is a normally hyperbolic 2-torus X_0.

By the previous section, we know that there are four mixed mode equilibria which are also in $Fix^0(\mathbf{D}_2)$ for the unperturbed system: $(\pm\mu, \pm\mu)$ where $\mu =$

$\sqrt{\lambda/(a+b)}$.

Now consider the perturbed system:

$$\dot{z} = F(z, \lambda, \epsilon), \tag{2.10}$$

where

$$F(z, \lambda, \epsilon) = f(z, \lambda) + \epsilon g(z). \tag{2.11}$$

According to the previous discussion, we know that for fixed $\lambda > 0$ small and ϵ small there is a flow invariant 2-torus X_ϵ.

Since $g = (g_1, g_2)$ is a $\mathbf{D}_2$ equivariant vector field, it has the form:

$$\begin{aligned} g_1 &= a_1(z_1 + \bar{z}_1, z_2 + \bar{z}_2, z_1\bar{z}_1, z_2\bar{z}_2)z_1 + b_1(z_1 + \bar{z}_1, z_2 + \bar{z}_2, z_1\bar{z}_1, z_2\bar{z}_2)\bar{z}_1 \\ g_2 &= a_2(z_1 + \bar{z}_1, z_2 + \bar{z}_2, z_1\bar{z}_1, z_2\bar{z}_2)z_2 + b_2(z_1 + \bar{z}_1, z_2 + \bar{z}_2, z_1\bar{z}_1, z_2\bar{z}_2)\bar{z}_2 \end{aligned}, \tag{2.12}$$

where a_1, b_1, a_2 and b_2 are real functions defined on $\mathbb{R}^4$. We define

$$\begin{aligned} K_1 &= g_{1,\bar{z}_1}(0,0) + g_{1,\bar{z}_2}(0,0) \\ K_2 &= g_{1,\bar{z}_1}(0,0) - g_{1,\bar{z}_2}(0,0) \\ L_1 &= g_{2,\bar{z}_2}(0,0) + g_{2,\bar{z}_1}(0,0) \\ L_2 &= g_{2,\bar{z}_2}(0,0) - g_{2,\bar{z}_1}(0,0) \end{aligned}$$

where $g_{1,\bar{z}_1}$ is the partial derivative of g_1 with respect to $\bar{z}_1$.

Note that the orbital stability of the mixed mode solutions to the unperturbed problem guarantees that the $\mathbf{D}_2-$equilibria are stable in directions transverse to the 2-torus X_ϵ so that we just need to consider the eigenvalues corresponding to the eigenvectors of dF which are tangent to X_ϵ. We denote the eigenvalues of dF in the $(i, 0)$ and $(0, i)$ directions by $\sigma_1(\epsilon)$ and $\sigma_2(\epsilon)$, respectively. The authors of [38] prove:

Theorem 2.2.3 *For fixed small λ and for small ϵ,*

$$sgn(K_2) = -sgn(K_1);\ sgn(L_1) = -sgn(K_1);\ sgn(L_2) = sgn(K_1). \tag{2.13}$$

Equilibria	$sgn(\sigma_1(\epsilon))$	$sgn(\sigma_2(\epsilon))$
$A(\mu,\mu)$	$-sgn(K_1\epsilon)$	$-sgn(L_1\epsilon)$
$B(\mu,-\mu)$	$-sgn(K_2\epsilon)$	$-sgn(L_2\epsilon)$
$C(-\mu,-\mu)$	$-sgn(K_1\epsilon)$	$-sgn(L_1\epsilon)$
$D(-\mu,\mu)$	$-sgn(K_2\epsilon)$	$-sgn(L_2\epsilon)$

Table 2.3: The signs of the eigenvalues of equilibria in the tangent direction.

are necessary and sufficient conditions for proving that $\mathbf{D}_2-$*equilibria on* X_ϵ *have inflow and outflow directions that are consistent with having a heteroclinic cycle.*

To prove this theorem, the authors of [38] show that the sign of $\sigma_1(\epsilon)$ and $\sigma_2(\epsilon)$ are as Table 2.3.

Having the result of Table 3, we can easily verify the necessary and sufficient condition for the saddleness of each $\mathbf{D}_2-$equilibria by checking $\sigma_1(\epsilon)\cdot\sigma_2(\epsilon)$ directly. Moreover, the direction of inflow and outflow can be verified as Figure 2.3. We shall not go through the proof of Table 3 since it needs only some tedious calculations.

The existence of heteroclinic cycles

To prove the existence of heteroclinic cycles, we just need to prove there are no equilibria other than the $\mathbf{D}_2-$equilibria on the one-dimensional invariant manifolds on X_ϵ connecting the $\mathbf{D}_2-$equilibria. In fact, we only need to prove that the assertion is true on the unperturbed invariant subspace X_0, and then use the continuity to establish the result for small enough ϵ.

Suppose (y,λ,ϵ) is an equilibrium of F that is in Fix(κ_2) but not in Fix($\mathbf{D}_2$). Let Y be the group orbit of y under the action of $\mathbf{T}^2$ and let

$$\pi : \mathbb{C}^2 \to T_yY$$

be the orthogonal projection defined by

$$\pi(w_1, w_2) = (w_1 - \tfrac{y_1}{|y_1|^2} Re(w_1\bar{y}_1), w_2 - \tfrac{y_2}{|y_2|^2} Re(w_2\bar{y}_2)).$$

Here, T_yY denotes the tangent space of Y at y.

It is easy to compute that

$$\begin{aligned} \pi(F(y,\lambda,\epsilon)) &= \epsilon\left(i\tfrac{y_1}{|y_1|^2} Im(\bar{y}_1)b_1, i\tfrac{y_2}{|y_2|^2} Im(\bar{y}_2)b_2\right) \\ &= 0. \end{aligned}$$

Note that if $y \notin Fix(\kappa_2)$, then $b_1|_y = 0$ since the coefficient of b_2 will not vanish in this case. Similarly, if $y \notin Fix(\kappa_1)$, then $b_2|_y = 0$. Thus, all we have to do is to find out the conditions that make $b_1|_{Fix^0(\kappa_2)}$ and $b_2|_{Fix^0(\kappa_1)}$ away from zero on X_0.

Clearly, (2.13) implies

$$|g_{1,\bar{z}_2}(0,0)| < |g_{1,\bar{z}_1}(0,0)| \text{ and } |g_{2,\bar{z}_1}(0,0)| < |g_{2,\bar{z}_2}(0,0)|. \tag{2.14}$$

If we compute $b_1|_{Fix^0(\kappa_2)}$ and $b_2|_{Fix^0(\kappa_1)}$ by substituting $z_1 = \mu e^{i\phi_1}$ and $z_2 = \mu e^{i\phi_2}$, then we have

$$\begin{aligned} b_2|_{Fix^0(\kappa_1)} &= 2(b_{2,1}(0) + b_{2,2}(0)\cos(\phi_2))\mu + O(\mu^2) \\ b_1|_{Fix^0(\kappa_2)} &= 2(b_{1,2}(0) + b_{1,1}(0)\cos(\phi_1))\mu + O(\mu^2). \end{aligned}$$

Moreover,

$$\begin{aligned} b_{1,1}(0) &= g_{1,\bar{z}_1}(0,0) \qquad b_{1,2}(0) = g_{1,\bar{z}_2}(0,0) \\ b_{2,1}(0) &= g_{2,\bar{z}_1}(0,0) \qquad b_{2,2}(0) = g_{2,\bar{z}_2}(0,0). \end{aligned}$$

Therefore, (2.13) implies that the b_j are uniformly bounded away from zero and hence the only equilibria of F are $\mathbf{D}_2-$equilibria. This proves the existence of the heteroclinic cycles.

Asymptotic stability of cycles

In the previous section, for fixed $\lambda > 0$ and for all sufficient small ϵ, we have found heteroclinic cycles connecting the four $\mathbf{D}_2-$equilibria on the flow invariant

2-torus X_ϵ if the conditions $a > |b|$ and (2.13) are valid. In this section, we will prove that in addition to these, if

$$sgn(\epsilon) = sgn(L_1K_2 - K_1L_2)\ sgn(K_1) \tag{2.15}$$

also holds, then the heteroclinic cycles are asymptotically stable.

By using the Theorem2.7 in [42], all we need is to check if the product of the four attracting eigenvalues is greater than the product of the four repelling eigenvalues, which is equivalent to $L_1^2K_2^2 - K_1^2L_2^2 > 0$. Since (2.13) implies $L_1K_2 + K_1L_2 > 0$ and (2.15) implies $L_1K_2 - K_1L_2 > 0$, the asymptotically stable cycles exist when both of them valid.

We summarize this section by the main result in [38]:

Theorem 2.2.4 *Consider the system of ODEs (2.5) and (2.6) and assume $a > |b|$ and (2.13). Then for each fixed small $\lambda > 0$ and for every sufficiently small nonzero ϵ, there exist structurally stable heteroclinic cycles in (2.10) connecting the $\mathbf{D}_2-$equilibria. When (2.15) is also valid, the heteroclinic cycles are asymptotically stable.*

2.2.3 Biological models with heteroclinic cycles

Suppose that there are n species living in an ecosystem. Let x_i denote the density of species i and assume that the growth rate for each capita, $\dot{x}_i/x_i$, depends on the density of all the species involved. Then, the dynamical system which describes the dynamics of these n species is:

$$\dot{x}_i = x_i f_i(x),$$

for $i = 1, ..., n$. If f_i is affine for all i, then we obtain the Lotka-Volterra equation:

$$\dot{x}_i = x_i(r_i + (Ax)_i), \tag{2.16}$$

for $i = 1, ..., n$ where $A = (a_{ij})$ is a $n \times n$ matrix. Here r_i is the intrinsic growth rate of the ith species and a_{ij} are competition coefficients expressing the strength with which the jth species affects the growth rate of the ith.

Different choices of parameters, r_i and a_{ij}, describes different biological systems. For example, in two dimensional cases, if $r_1 > 0 > r_2$ and $a_{21} > 0 = a_{11} = a_{22} > a_{12}$, we obtain the prey-predator system. In contrast, a competing model between two species sharing the same resource can be modeled by setting $r_1, r_2 > 0$ and $a_{ij} \neq 0$ for $i \neq j$.

The dynamics of two dimensional Lotka-Volterra systems with f_i affine can be easily analyzed as there exist no limit cycles in them. For instance, there are only three possibilities for the competing case: (i) the two species coexist, (ii) only one of the species is able to dominate the other one, regardless of initial condition, and (iii) either of the species is able to dominate the other one, depending on the initial condition.

In higher dimensional cases the situation becomes more complicated, even in only three dimensions. If we make some symmetry assumptions: $r_1 = r_2 = r_3 = r$, $a_{12} = a_{23} = a_{31} = 1 + c$ and $a_{21} = a_{32} = a_{13} = 1 - e$(i.e. cyclic interaction between the species), rescale x_i and time t to make $a_{ii} = 1$ and $r = 1$, then we obtain the 3-dimensional Lotka-Volterra system as considered by R. M. May and W. J. Leonard in [52]:

$$\begin{cases} \dot{x} &= x(1 - (x + y + z) - cy + ez) \\ \dot{y} &= y(1 - (x + y + z) - cz + ex) \\ \dot{z} &= z(1 - (x + y + z) - cx + ey) \end{cases} . \tag{2.17}$$

May and Leonard prove the following theorem:

Theorem 2.2.5 *If $c > e > 0$ and $e < 1$, then there exists a stable heteroclinic cycle in system (2.17).*

The construction of system (2.17) shows us that it is equivariant with respect to $\mathbf{Z}_3$, the cyclic permutation group. Moreover, it can be easily converted into the Guckenheimer-Holmes system (2.1) by setting $x = X^2, y = Y^2$ and $z = Z^2$; it then gains $\mathbf{Z}_2^3$ symmetry. In other words, these two systems are equivalent and share the same dynamics. (The biological constraint: once a species is extinct, it will be extinct forever, forces the coordinate hyperplanes to be invariant. These invariant hyperplanes also exist in a mathematical system with $\mathbf{Z}_2^n$ symmetry.)

Remark 2.2.2 *Note that an identical result can be found by comparing Theorem 2.2.5 with Corollary 2.2.1.*

Remark 2.2.3 *The non-$\mathbf{Z}_3$ symmetry system was considered by Chi, et al. ([13]) in which they prove that if the parameters satisfy $a_{13} > 1 > a_{12} > 0, a_{21} > 1 > a_{23} > 0, a_{32} > 1 > a_{31} > 0$ and the conditions in Theorem2.1.1, then there exists a stable heteroclinic cycle in this system.*

The Lotka-Volterra system has long been utilized as a powerful ecological as well as game-theoretical model ([70], [25]), and has been proved as an effective archetype in describing the dynamics of sensory neurons [76]. It has also been used in describing the mode interactions in rotating Rayleigh-Beńard convection ([12, 14]). In a two-species competitive Lotka-Volterra system, the ”winner -take-all” scenario occurs due to the lack of cycles. Nevertheless, dramatically different dynamics appear when it comes to higher dimensions. The coordinate planes, corresponding to the extinction of some species, support heteroclinic connections between saddle points, which results in the existence of a robust heteroclinic cycle. In this case, the system becomes winnerless.

Recently, this system has also been used in modeling the networks of competing neuron ensembles([63, 79, 76, 66, 77, 4]). According to experimental results, the desired model to simulate the activity of a neural ensemble should have the

following features: (i) It is strongly sensitive so that the neurons can be turned on immediately as soon as a stimulus occurs. We use a function σ to control it. (ii) It is robust against small perturbation (noise). (iii) It admits no attracting equilibrium points so that the neurons can be fired in turns. In other words, a stable cycle is preferable.

V. S. Afraimovich, et al. propose the following system:

$$\dot{x}_i = x_i \left(\sigma(\mathbf{H}, \mathbf{S}) - \sum_{j=1}^{N} a_{ij} x_j + H_i(t) \right) + S_i(t), \tag{2.18}$$

where $x_i > 0$ is the firing rate of the ith neuron, H_i is the forcing from other neuron ensembles, S_i is the stimuli from the sensors acting on the i-th neuron and a_{ij} is the strength of inhibition on the i-th neuron by the j-th neuron. If $\sigma = 1$ and $\mathbf{H} = \mathbf{S} = 0$, we retrieve the Lotka-Volterra system.

Here, they set $\sigma(\mathbf{H}, \mathbf{S}) = -1$, if $\mathbf{H} = \mathbf{S} = \mathbf{0}$, and $\sigma(\mathbf{H}, \mathbf{S}) = 1$, otherwise. More precisely, all neurons are silent when there are no any stimuli, from sensors or other neuron ensembles, on it, while all neurons are activated when stimuli occur.

A remarkable application is proposed by P. Varona et al.([77, 76]), who attempt to use this model to capture the hunting behavior of *Clione*, a marine mollusk. *Clione* uses a gravitational sensory organs, the statocysts, to determine its orientation. The $S_i(t)$, here, represents the stimuli of the statocyst on the receptor neuron a_i. In their model, statocyst consists of six neurons(see Fig. 2.5), which are divided into two coupling subgroups of three neurons in each. Inside each subgroup, a relatively stronger inhibitory constants construct heteroclinic connections between three neurons. More precisely, the parameters they choose for computing are: $a_{13} = a_{35} = a_{51} = 5, a_{46} = a_{24} = a_{62} = 2, a_{16} = a_{21} = a_{32} = a_{43} = a_{54} = a_{65} = 1.5$, $a_{ii} = 1$, for all i and $a_{ij} = 0$, otherwise. As soon as its food appears, the hunting neurons are activated, i.e. $\mathbf{H} \neq 0$. In this case, chaotic dynamics are observed, similar to the irregular hunting behavior of *Clione*.

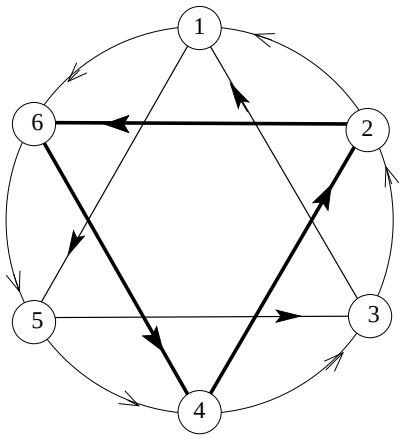

Figure 2.5: Two groups of heteroclinic cycles, $1 \to 5 \to 3 \to 1$ and $2 \to 6 \to 4 \to 2$, and their weak couplings between six neurons. The thickness of connection curves denote the strength of the inhibitions.

Based on this statocyst model, Venaille et al. [79] considered a coupled system with two such statocyst models. They studied the coordination and synchronization between two neuron ensembles by examining numerically the dynamics of the two cells for different coupling ways and coupling strengths. If there is only two neurons coupled together, then synchronization between these two neurons can be observed. However, the rest of the neurons can not be synchronized and there is no activation sequence locking within them. In contrast, coupling three corresponding neurons in each cell results in the existence of activation sequence locking. In the case of coupling all the corresponding neurons in each cell, the dynamics of the system can be fully synchronized or chaotic depending on the coupling strength. These results give an example that coupled cell systems provide a more complicated dynamics which increase the signals the system can produce in terms of neuron activities.

As we have mentioned in the Introduction, a small perturbation destroying the symmetry of a heteroclinic system may results in the birth of a periodic solution.

In other words, the above system looks like a periodic cycle interacting with a heteroclinic cycle, or two periodic cycles interacting with each other. Therefore, a thorough study in heteroclinic systems with periodic perturbations becomes very important for understanding the coordination of neuron ensembles.

2.3 Circle maps

In this section, we review some basic properties of the maps of circle. Theory on circle homeomorphisms, i.e. invertible circle maps, has been well-established and can be found in almost any textbooks on dynamical systems such as [20], [35], [34] and [9]. We discuss briefly this case in section 2.3.1.

On the other hand, although non-invertible circle maps have been well-studied in the literature, see for example [49, 40, 51, 48, 50, 78, 11, 21], they are not presented normally in any textbooks. Therefore, we will give a more detailed review on circle maps in section 2.3.2.

2.3.1 Invertible circle maps

Suppose $f : \mathbf{S}^1 \to \mathbf{S}^1$ is an orientation preserving homeomorphism of circle $\mathbf{S}^1 = \mathbb{R}/\mathbb{Z} = [0, 1)$. A function $F : \mathbb{R} \to \mathbb{R}$ is called a lift of f if it satisfies $\pi \circ F = f \circ \pi$, where $\pi : \mathbb{R} \to \mathbf{S}^1$ is the projection defined by $\pi(x) = (cos(2\pi x), sin(2\pi x)) \in \mathbf{S}^1$. Note that the lift of a circle map is not unique; nevertheless, two different lifts are equal up to translation by some integer.

It is well known that for the rigid rotation $f(x) = x + \omega \ (mod\ 1)$, all the points on $[0, 1)$ are periodic if ω is a rational number. In contrast, all the points will travel densely around $[0, 1)$ if ω is irrational. As for a general circle map, which could be nonlinear, we expect that there are only finitely many periodic points if they exist. In this case, a typical non-periodic point could travel a different distance

in each iteration. This suggests that it is useful to measure the average amount a point rotates by over many iterations.

Definition 2.3.1 *Let f be an orientation-preserving circle homeomorphism and let F be a lift of it. The rotation number of f is defined by*

$$\rho(f) = \lim_{n\to\infty} \frac{F^n(x) - x}{n},$$

$x \in [0, 1)$.

This definition is, in fact, well-defined; that is, it is easy to prove that the rotation number exists and that it is independent of the initial point x. Moreover, suppose $m,\ n \in \mathbb{N}$ and $(m, n) = 1$, i.e. m and n are coprime, then $\rho(f) = \frac{m}{n}$ if and only if f has a periodic point x with $f^n(x) = x + m$.

Consider a one-dimensional differential equation $\dot{x} = a + b\sin(2\pi x)$ defined on $[0, 1)$ which describes the dynamics of a periodic system perturbed by a periodic function. By using Euler's method to discretise it, we have a difference equation $x_{n+1} = x_n + \alpha + \frac{\beta}{2\pi}\sin(2\pi x_n)$, where $\alpha = ah$, $\beta = 2\pi bh$ and h is the step size for Euler's method. In other words, the dynamics of the map

$$F(x, \alpha, \beta) = x + \alpha + \frac{\beta}{2\pi}\sin(2\pi x) \ \ (mod\ 1) \tag{2.19}$$

can be used to describe the dynamics of the differential equation. (2.19) is called the standard or canonical family of circle maps and it is a homeomorphism if $\beta \in [0, 1]$. Normally, we restrict α only in $[0, 1]$ as we get the same dynamics for the other cases.

The dynamics of (2.19) are quite regular when $\beta \in [0, 1]$. For $\beta = 0$, the map becomes the simple rotation of $\mathbf{S}^1$ and we have $\rho(F) = \frac{m}{n}$ if and only if $\alpha = \frac{m}{n}$, where $m, n \in \mathbb{N}$ and $(m, n) = 1$. For a fixed $\beta \in (0, 1)$ and a fixed rational number m/n in $[0, 1]$, there exists a closed interval in α in which the rotation number

of F is m/n. These intervals grow as β increases to 1 when the measure of the union of these intervals in α is exactly equal to 1. In other words, the standard family has a periodic orbit for almost all values of α in $[0,1]$ when $\beta = 1$. In addition, for each $\beta \in (0,1)$ and for each irrational number $\bar{\rho}$, there exist a unique α such that $\rho(F(\alpha,\beta)) = \bar{\rho}$. It follows that the bifurcation diagram of (2.19) in the parameter space (α,β) consists of the so-called 'Arnold tongues' in each of which the rotation number of F is a rational constant and periodic orbits exist within it.

2.3.2 Non-invertible circle maps

In this section, we consider the case when f is a continuous circle map, i.e. $f \in C_0(\mathbf{S}^1)$. Specifically, we concentrate through out this section on non-invertible circle maps as the invertible case has been discussed in section 2.3.1.

The rotation number as defined in Definition 2.3.1 was first introduced by Poincaré. Its definition has been extended to any continuous circle map by Newhouse et al. in [55]:

Definition 2.3.2 *Let f be a continuous circle map and let F be a lift of f. The rotation number of a point $x \in [0,1]$ is defined by*

$$\rho(F,x) = \lim_{n\to\infty} \frac{F^n(x) - x}{n},$$

if the limit exists. The rotation set of F is defined by

$$\rho(F) = \{\rho(F,x) : x \in [0,1]\}$$

Different x may have different rotation numbers and, in some cases, this limit may not exist [51]. Nevertheless, R. Ito in [40] proved that the rotation set of F is either a point or a bounded closed interval $[\rho_1,\rho_2]$, which is called the rotation interval of F.

By definition, ρ is clearly a monotonically increasing function of F, meaning that if $F \leq G$ then $\rho(F, x) \leq \rho(G, x)$ for all x where the limit exists. Therefore, one way to find the rotation interval of a function F is to find two monotone functions F_+ and F_- such that $F_- \leq F \leq F_+$, and $\rho(F, x_+) = \rho(F_+)$ and $\rho(F, x_-) = \rho(F_-)$ for some x_+ and $x_- \in [0, 1)$. Note that since F_+ and F_- are monotone, they have rotation numbers that are well-defined and independent of the initial point x.

P. Boyland [11] constructed the least monotone upper bound F_+ and the greatest monotone lower bound F_- of F as follows:

$$F_+(x) = \sup_{y \leq x} F(y),$$

$$F_-(x) = \inf_{y \geq x} F(y),$$

and proved that $\rho(F) = [\rho(F_-), \rho(F_+)]$. We will use this method to calculate the rotation interval of a circle map numerically in section 4.4.2.

For a circle map having a rotation interval instead of a rotation number, there exist infinitely many periodic orbits which have rational rotation numbers, and quasiperiodic orbits which have irrational rotation numbers. On the other hand, having a single rotation number does not imply having a single periodic orbit. For example, through a sequence of period-doubling bifurcations by varying the parameters in the family of circle maps, we may arrive at a map which has single rotation number but infinitely many coexisting periodic orbits with period of the form $q \cdot 2^n$, for all integers n and some q. As the existence of infinitely many periodic orbits is a typical feature of chaos, the question then arises as to the relationship between chaos and rotation numbers.

R.S. MacKay and C. Tresser in [49] considered the following class of circle maps:

Definition 2.3.3 *([49]) Class A^r, $r \geq 1$, is the subset of $C^r(\mathbf{S}^1)$ such that for $f \in A^r$, and F a lift of f:*

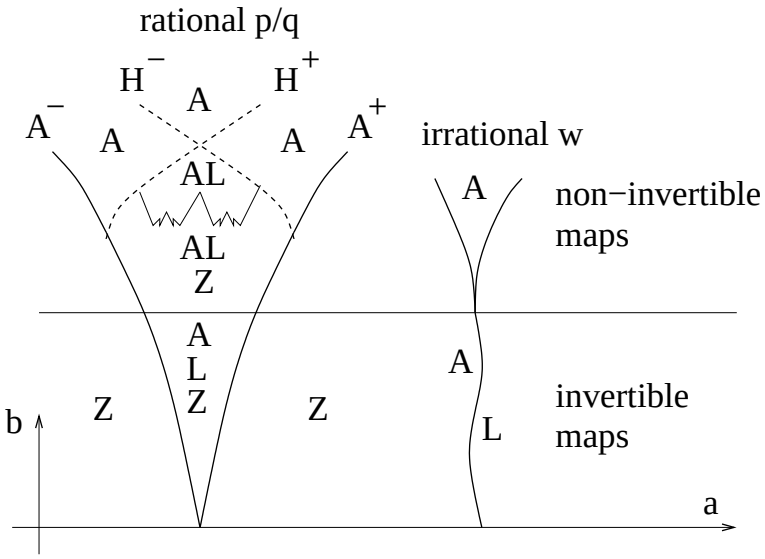

Figure 2.6: The schematic bifurcation diagram of a two-parameter family $F_{a,b}$ of circle maps. We denote A as the Arnold tongue region in which the rotation number p/q or w, respectively, exists for some point $x \in [0,1]$. L is the region where the circle map has single rotation number, i.e. frequency locked region, and Z is the region where the circle map has zero topological entropy. The boundaries of the Arnold tongue and the region where heteroclinic connections exist are denoted by A^+, A^-, H^+ and H^-.

(i) $\log DF$ *has bounded variation on every compact interval where* DF *is strictly positive.*

(ii) If F *is non-monotone, then every common critical point of the monotone bounds* $F_\pm$ *is non-flat.*

Here, a critical point of a map F *is a point* x *where* $DF(x) = 0$. *We say that a critical point of* F *is non-flat if there exist positive constants* ϵ, A, B, c *such that* $|DF|^{-1/2}$ *is convex on* $(x-\epsilon, x)$ *and* $(x, x+\epsilon)$, *and for all* $|t| < \epsilon$, $B|t|^c \le |DF(x+t)| \le A|t|^c$.

MacKay and Tresser identified the Arnold tongue regions (A), frequency-locking regions (L) and zero topological entropy regions (Z) of circle maps in A^r.

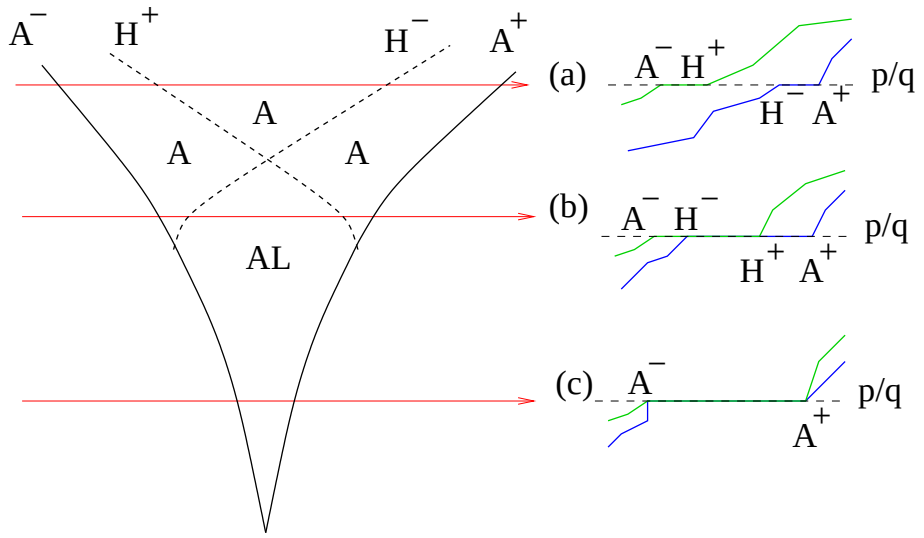

Figure 2.7: Three possible routes when varying parameters of a family of circle maps and their corresponding upper (green) and lower (blue) bounds of rotation intervals. The vertical axes of the right figures are the possible rotation numbers of the maps. Note that on the right of H^- and on the left of H^+, we have p/q as the minimum and maximum, respectively, of the rotation intervals. In addition, frequency-locking intervals can be observed in the cases (*b*) and (*c*).

See Figure 2.6 for a schematic diagram of these regions. A map F is located in the Arnold tongue region $A_{p/q}$ or A_w if there exists a point x such that $\rho(F, x) = p/q$ or $\rho(F, x) = w$, respectively. Frequency-locking regions consist of maps which have single rotation number, i.e. $\rho(F, x) = p/q$ or w, for all $x \in \mathbf{S}^1$. For a map which is not in region (L), we expect a rotation interval instead of a single rotation number. Figure 2.7 shows three possible routes when varying parameters of a family of circle maps and their corresponding upper (green) and lower (blue) bounds of rotation intervals.

As for the zero topological entropy regions, we first give the following definition:

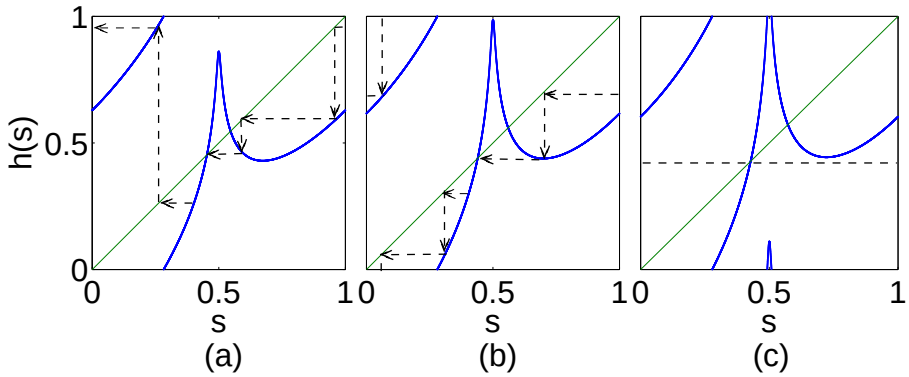

Figure 2.8: The graphs of one-parameter family of circle maps (2.20) for (a) $\omega = 0.016$, (b) $\omega = 0.019$ and (c) $\omega = 0.022$. When $\omega = 0.016$, there exists a homoclinic connection between the unstable fixed point and itself. This connection disappears, for instance in the case $\omega = 0.022$, after the family undergoes a homoclinic bifurcation at $\omega = 0.019$.

Definition 2.3.4 *([49]) The topological entropy of a function f is defined by*

$$h(f) = \lim_{\epsilon \to 0} \overline{\lim_{n \to \infty}} \frac{1}{n} \log H(f, n, \epsilon),$$

where $H(f, n, \epsilon)$ is the maximal cardinality of (n, ϵ)-separated sets. Given a continuous map $f : X \to X$ where X is a compact metric space with metric d, and given $\epsilon > 0$, $n \in \mathbb{Z}^+$, we say that a set S is (n, ϵ)-separated if

$$[x, y \in S, x \neq y] \Rightarrow [\exists m : 0 \leq m < n \text{ such that } d(f^m(x), f^m(y)) > \epsilon].$$

We say there is topological chaos if the topological entropy is positive.

Maps in the region $A \setminus Z$ are topologically chaotic. Moreover, there exists a region $L \setminus Z$ in which maps have single rotation number but are topologically chaotic.

In figure 2.6, there are two curves H^+ and H^- which separate the Arnold tongue region into two subregions: frequency-locking region and non-frequency-

locking region. Boyland [11] proved that these curves are the maps where heteroclinic (homoclinic) bifurcations occur. A heteroclinic (homoclinic) bifurcation occurs when the preimage of the unstable fixed point of a map is its minimum or maximum. For example, consider a one-parameter family of circle maps, which will be studied in section 4.4.2:

$$\bar{s} = h(s) = s + \frac{\omega}{\pi}\mu - \frac{\omega}{\pi}\xi \log(1 + \sqrt{a_1}\cos(2\pi s)), \tag{2.20}$$

where $\mu = 232, \xi = 19.06$ and $a_1 = 0.998$ are constants. As depicted in Figure 2.8, when $\omega = 0.016$, there exists a homoclinic connection between the unstable fixed point and itself. This connection disappears in the case $\omega = 0.022$ after the family undergoes a homoclinic bifurcation at $\omega = 0.019$.

Note that H^+ and H^- also form a part of the boundary of the region where the topological entropy of the map is positive. R.S. MacKay and C. Tresser [49] proved that maps with non-trivial rotation interval have positive topological entropies. Consequently, non-trivial rotation interval implies topological chaos. We will use this fact in section 4.4.2.

2.4 0-1 Test

In this section, we give a brief review of the 0-1 test which is a binary test for chaotic dynamics developed by G.A. Gottwald and I. Melbourne [29, 30, 32]. This test will be performed later in section 4.4.3 to prove numerically the chaotic dynamics for the system we are going to study.

The usual method to detect chaotic dynamics for a deterministic dynamical system is to calculate numerically the maximal Lyapunov exponent λ [1]. For positive λ, the nearby trajectories separate exponentially and hence the underlying system demonstrates chaotic dynamics. In contrast, the system is regular (i.e. periodic or quasiperiodic dynamics) if $\lambda < 0$. However, this method is only valid

for dynamical systems whose equations are known. In the case when the equation is unknown or we have only a series of experimental data, then λ may be estimated by the phase space reconstruction method [75], approximating the linearisation of the evolution operator [68], or by the direct method [67].

0-1 test has been proved to be an easier way to detect chaotic dynamics for a time-series of data [29, 32, 31, 22, 39], even with noise [30]. J.H.P. Dawes and M.C. Freeland [16] utilized a modified 0-1 test to distinguish quasiperiod and strange non-chaotic attractor, both of which have no positive maximal Lyapunov exponent. The benefit of this test is that it does not require to know the equation of the underlying dynamical system. In other words, even experimental data can be analysed without knowing the mechanism behind the data. Moreover, it is easy to identify chaotic from regular dynamics due to the binary output. The test returns 0 or 1 if the underlying data is regular or chaotic, respectively.

We describe the 0-1 test in the following:

Consider the following Euclidean group extension of dynamical system $\phi(n)$:

$$\begin{cases} \varpi(n+1) &= \varpi(n) + c \\ p(n+1) &= p(n) + \phi(n)\cos\varpi(n) \\ q(n+1) &= q(n) + \phi(n)\sin\varpi(n) \end{cases},$$

where ϖ and (p, q) are the rotation and translation, respectively, in the plane. It has been shown in [56] that the dynamics on the group extension is bounded if the underlying dynamics is regular and unbounded if the underlying dynamics is chaotic. Moreover, if the chaotic attractor is uniformly hyperbolic, then p and q behave asymptotically like Brownian motion. Therefore, one way to detect if a set of data $\phi(n)$ is chaotic or not is to see if p and q are asymptotically bounded.

Thus, for a given set of data $\phi(j)$ with $j = 1, ..., N$, G.A. Gottwald and I.

Melbourne considered the translation variables

$$p_\varpi(n)=\sum_{j=1}^{n}\phi(j)\cos(j\varpi),$$
$$q_\varpi(n)=\sum_{j=1}^{n}\phi(j)\sin(j\varpi),$$

and their mean square displacement

$$M_\varpi(n)=\lim_{N\to\infty}\frac{1}{N}\sum_{j=1}^{N}[p_\varpi(j+n)-p_\varpi(j)]^2+[q_\varpi(j+n)-q_\varpi(j)]^2,$$

for $n \leq n_{cut}$ and $n_{cut} \ll N$. The 0-1 test is based on the asymptotic growth rate of $M_\varpi(n)$ as $n \to \infty$. In the practical use, all the data $\phi(j)$ must be taken to be on the attractor and N must be taken large enough so that the asymptotic behavior of p_ϖ and q_ϖ can be observed. The authors suggested that $n_{cut} = N/10$ is sufficient to get good results.

Since, for those $\phi(n)$ with absolute summability, this mean square displacement satisfies

$$M_\varpi(n) = V(\varpi)n + V_{osc}(\varpi, n) + e(\varpi, n),$$

where $e(\varpi, n)/n \to 0$ as $n \to \infty$ uniformly in $\varpi \in (0, \pi)$ and

$$V_{osc}(\varpi, n) = (E\phi)^2\frac{1-cosn\varpi}{1-cos\varpi},$$

in which

$$E\phi = \lim_{N\to\infty}\frac{1}{N}\sum_{j=1}^{N}\phi(j),$$

they then subtract the oscillation term $V_{osc}(\varpi, n)$ from $M_\varpi(n)$ and define

$$D_\varpi(n) = M_\varpi(n) - V_{osc}(\varpi, n).$$

Although theoretically M_ϖ and D_ϖ get the same result as both n and N tend to infinity in the 0-1 test, the latter performs better in practice than the former for finite n. Therefore, we will calculate the asymptotic growth rate of D_ϖ instead of M_ϖ for the system we are studying in section 4.4.3.

There are two ways to calculate the asymptotic growth rate of D_ϖ: the regression method and the correlation method. The regression method involves the calculation of a linear regression for the log-log plot of the mean square displacement. The asymptotic growth rate K_ϖ is defined by

$$K_\varpi = \lim_{n\to\infty} \frac{\log \tilde{D}_\varpi(n)}{\log n},$$

where $\tilde{D}_\varpi(n) = D_\varpi(n) - \min_{n=1,\cdots,n_{cut}} D_\varpi(n)$. Here, we take $\tilde{D}_\varpi(n)$ instead of $D_\varpi(n)$ due to the fact that the latter could be negative and hence may result in problem when taking the log in the definition.

In the case of the correlation method, the authors of [32] defined the linear correlation coefficient of D_ϖ as its asymptotic growth rate

$$K_\varpi = corr(\vec{n}, \Delta),$$

where $\vec{n} = (1, 2, \cdots, n_{cut})$, $\Delta = (D_\varpi(1), D_\varpi(2), \cdots, D_\varpi(n_{cut}))$ and the function *corr* is the linear correlation coefficient defined by

$$corr(x, y) = \frac{cov(x, y)}{\sqrt{var(x)var(y)}},$$

where

$$cov(x, y) = \frac{1}{n}\sum_{j=1}^{n}(x_j - \bar{x})(y_j - \bar{y})$$

is the covariance of x and y, $var(x) = cov(x, x)$ is the variance of x and $\bar{x} = \frac{1}{n}\sum_{j=1}^{n} x_j$.

In many cases, the correlation method performs better than the regression method although they should agree theoretically as both n and N tend to infinity.

By definition, the asymptotic growth rate K_ϖ depends on the choice of ϖ. In some resonant cases where ϖ is such that $p_\varpi(n) \sim n$, and hence $M_\varpi(n) \sim n^2$, $K_\varpi = 2$ irrespective of regular or chaotic dynamics. To avoid this situation, we

compute K_ϖ for N_ϖ values of $\varpi \in (0, \pi)$ and then take the median value of these K_ϖ as our final asymptotic growth rate K of the data. In [32], the authors examined the effect of increasing N_ϖ in the 0-1 test for the logistic map and found that $N_\varpi = 100$ is sufficient. Therefore, in section 4.4.3, we apply 0-1 test to our system by taking 100 values of ϖ.

Chapter 3

The Poincaré Map

3.1 Introduction

Poincaré method is normally used for studying the dynamics near a cycle in a dynamical system [41, 60]. The idea of this method is to put a plane, called a cross section, transversely crossing the cycle which we are going to study and then observe the dynamics of points where an arbitrary orbit near the cycle intersects this plane.

For a heteroclinic cycle, due to the time spent by an orbit on passing by an equilibrium point is much greater than that on travelling between two equilibrium points, and the strong linear effects happening only around equilibrium points, we split the Poincaré map into two kinds of maps: local maps near equilibrium points and global maps between their neighbourhoods.

Papers, such as [43, 44, 54, 61, 53], utilize the Poincaré map method to study the dynamics of autonomous systems with heteroclinic cycles. But to date it has not been done rigorously for the non-autonomous case. V.S. Afraimovich et al. in [3] have derived a Poincaré map for a system which is similar to the system we are going to investigate. However, their result has some limitations which are not

pointed out by the authors. We will discuss this in more detail at the end of this chapter and at the beginning of next chapter.

In this chapter, we derive the Poincaré map of the system (1.3)

$$\begin{cases} \dot{x} &= x(1-(x+y+z)-cy+ez)+\gamma(1-x)f(2\omega t) \\ \dot{y} &= y(1-(x+y+z)-cz+ex) \\ \dot{z} &= z(1-(x+y+z)-cx+ey) \end{cases},$$

where f is a non-negative function in $PC^1(2\pi)$, the set of all 2π-periodic functions with continuous first-order derivative, $0 < \gamma \ll 1$ and $1 > c > e > 0$. We may assume that $f(s) \sim O(1)$ to ensure that the perturbation term is $O(\gamma)$. In order to keep the intrinsic biological meaning of the unperturbed system, the assumption of non-negativeness of f is needed to ensure the first octant is invariant.

The derivation involves careful calculation of the local and global maps. Because of the time-periodic perturbation, the local linearisation now includes non-autonomous terms. Actually, these time-dependent terms play a very important role in obtaining an accurate corresponding local map. Therefore, we will not neglect them as was done by Afraimovich et al. in [3]. As for the global parts, our calculation takes the periodicity of the diffeomorphism between two cross sections into account and this has been shown numerically to produce a better map than the one we have published in [18].

This chapter is divided into four sections. In section 3.2, we study the local dynamics of (1.3). The complete derivation of the Poincaré map of the system (1.3) will be displayed in section 3.3. We will discuss some assumptions on the parameters of our Poincaré map in section 3.5. The chapter closes with a more general discussion in section 3.6.

3.2 Local dynamics

Before deriving the Poincaré map of system (1.3), we will analyze the local dynamics of the system.

In the absence of the periodic forcing term, the system is equivalent to the Guckenheimer-Holmes system, which has been proved in chapter 2 to possess a robust heteroclinic cycle connecting the three equilibrium points $P_1(1,0,0)$, $P_2(0,1,0)$ and $P_3(0,0,1)$. The condition $c > e > 0$ ensures the asymptotic stability of the heteroclinic cycle. Otherwise, all orbits would flow exponentially away from it.

For $\gamma > 0$, symmetry is broken and we expect that there are periodic solutions near the original heteroclinic cycle. In fact, P_2 and P_3 are no longer equilibrium points. Instead, two periodic orbits exist nearby. For instance, near P_3 on the xz-plane, the dynamics looks like

$$\begin{aligned} \dot{x} &= ex + \gamma f(2\omega t) + O(\gamma^2) \\ \dot{w} &= -w - (1+c)x + O(\gamma^2), \end{aligned} \tag{3.1}$$

where $x, w \equiv z-1 \sim O(\gamma)$. The following lemma proves the existence of a periodic orbit near P_3:

Lemma 3.2.1 *System (3.1) has a periodic solution if $f(s)$ is a periodic function of period 2π.*

Proof: All we have to prove is that there exists an initial point (x_0, w_0) at time $t = 0$ such that the solution $(x(t), w(t))$ of (3.1) satisfies $(x(t+\pi/\omega), w(t+\pi/\omega)) = (x(t), w(t)), \forall t \in \mathbb{R}$.

The solution of the first equation of (3.1) is

$$x(t) = \mathrm{e}^{et} x_0 + V(t), \tag{3.2}$$

where $V(t) = \gamma e^{et} \int_0^t e^{-e\tau} f(2\omega\tau)d\tau$. Then $x(t)$ is π/ω-periodic if and only if

$$\begin{aligned}
& x_0 = \tfrac{V(t+\pi/\omega)-V(t)}{e^{et}-e^{e(t+\pi/\omega)}},\ \forall t \in \mathbb{R} \\
\Leftrightarrow\ & (V(t+\pi/\omega) - V(t))' \left(e^{et} - e^{e(t+\pi/\omega)}\right) - (V(t+\pi/\omega) - V(t)) \left(e^{et} - e^{e(t+\pi/\omega)}\right)' \\
& = 0,\ \forall t \in \mathbb{R} \\
\Leftrightarrow\ & [e(V(t+\pi/\omega) - V(t)) + \gamma f(2\omega(t+\pi/\omega)) - \gamma f(2\omega t)] \left(e^{et} - e^{e(t+\pi/\omega)}\right) \\
& -e(V(t+\pi/\omega) - V(t)) \left(e^{et} - e^{e(t+\pi/\omega)}\right) = 0,\ \forall t \in \mathbb{R}.
\end{aligned}$$

The terms involving $V(t)$ are cancelled out, so $x(t)$ is periodic if and only if $f(2\omega(t+\pi/\omega)) - f(2\omega t) = 0,\ \forall\ t \in \mathbb{R}$. This equality is always true since f is periodic function of period 2π. Thus, we have found a desired

$$x_0 = \left(e^{e\pi/\omega} \int_0^{\pi/\omega} e^{-e\tau} f(2\omega\tau)\gamma d\tau\right) / \left(1 - e^{e\pi/\omega}\right).$$

The same derivation can be done for the second equation of system (3.1). Since the solution $x(t)$, with respect to this initial point x_0, of the first equation of (3.1) is a periodic function, we can apply the same argument again and then get a point w_0 and a corresponding periodic solution $w(t)$. Hence, we are done. ■

A result similar to Lemma 3.2.1 also holds for P_2 because the approximated ODEs have the same form. We denote the periodic orbits near P_2 and P_3 by P_2' and P_3', respectively. Note that P_3' oscillates below the plane $\{x = 0\}$, while P_2' oscillates above this plane.

Remark 3.2.1 *The explicit form of the x-coordinate of P_3' can be derived by simply changing variables. From (3.2),*

$$\begin{aligned}
x(t) &= e^{et} \tfrac{e^{e\pi/\omega}}{1-e^{e\pi/\omega}} \int_0^{\pi/\omega} \gamma e^{-e\tau} f(2\omega\tau)d\tau + \gamma e^{et} \int_0^t e^{-e\tau} f(2\omega\tau)d\tau \\
&= \gamma e^{et} \tfrac{e^{e\pi/\omega}}{1-e^{e\pi/\omega}} \left\{ \int_0^{\pi/\omega} e^{-e\tau} f(2\omega\tau)d\tau + e^{-e\pi/\omega} \int_0^t e^{-e\tau} f(2\omega\tau)d\tau \ . \right. \\
&\quad \left. - \int_0^t e^{-e\tau} f(2\omega\tau)d\tau \right\}
\end{aligned}$$

The second term in the curly brackets is equal to

$$\int_{\pi/\omega}^{t+\pi/\omega} e^{-e\tau} f(2\omega\tau)d\tau.$$

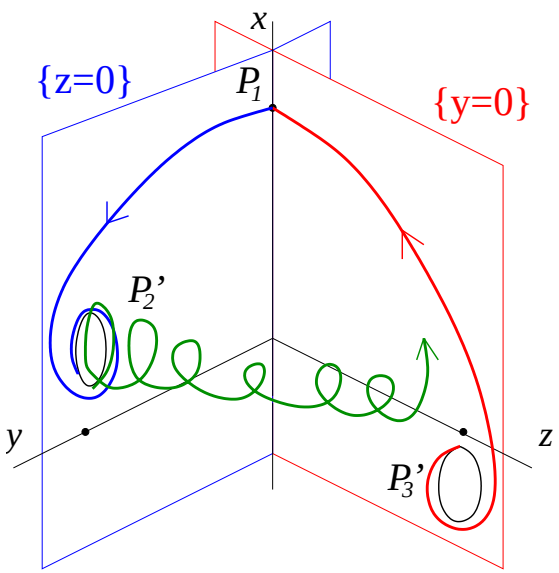

Figure 3.1: A schematic diagram of the snap shot at time $t = 0$ of the unstable manifolds of P_1 (blue), P_2' (green) and P_3' (red). The black closed curves denote P_2' and P_3'. Connections between P_1 and P_2', as well as P_1 and P_3', lie on the invariant planes $\{z = 0\}$ and $\{y = 0\}$, respectively. Since $P_2' \in \{z = 0, x \geq 0\}$ and $P_3' \in \{y = 0, x \leq 0\}$, the unstable manifold of P_2' will not have transversal intersections with the stable manifold of P_3'.

Therefore,

$$\begin{aligned} x(t) &= \gamma\left(e^{et}\frac{e^{e\pi/\omega}}{1-e^{e\pi/\omega}}\int_t^{t+\pi/\omega} e^{-e\tau} f(2\omega\tau)d\tau\right) \\ &= \gamma\left(\frac{1}{e^{-e\pi/\omega}-1}\int_0^{\pi/\omega} e^{-e\tau} f(2\omega(t+\tau))d\tau\right). \end{aligned}$$

The connections from P_1 to P_2' and from P_3' to P_1 exist due to the persistence of the supporting planes $\{z = 0\}$ and $\{y = 0\}$. In contrast, the invariant plane $\{x = 0\}$ and the connection between $P_2(0, 1, 0)$ and $P_3(0, 0, 1)$ are destroyed by the forcing term. In fact, there is no connection between P_2' and P_3' because the solutions starting at an initial point in $\{x = 0\}$ will only flow into $\{x > 0\}$. See Figure 3.1 for a schematic description.

In the absence of the perturbation, the unstable manifolds of P_i's are 2-dimensional objects if we put them in the extended (x, y, z, t) space. Since P_i's are hyperbolic,

the dimension of their unstable manifolds is not changed by adding a small periodic perturbation. In other words, the unstable manifolds of P_i's depicted in the Figure 3.1 are actually 2-dimensional in the extended space.

To analyze the global dynamics near a cycle is normally difficult. In general, the Poincaré map method is a good way to begin investigating it.

3.3 The construction of the Poincaré Map

Let the two cross sections near $P_1 = (1, 0, 0)$ be $H_1^{in} = \{(x, y, z) : |x - 1| \leq h, 0 \leq y \leq h, z = h\}$ and $H_1^{out} = \{(x, y, z) : |x - 1| \leq h, y = h, 0 \leq z \leq h\}$, where h is a small constant, and define the cross sections near $P_2 = (0, 1, 0)$ and $P_3 = (0, 0, 1)$ in similar ways, see Figure 3.2.

Note that the radial eigenvalues of P_1, P_2 and P_3 are identity. Therefore, for small enough c and e with $1 > c > e > 0$, the trajectories close to the original heteroclinic cycle will visit these cross sections in turn. Hence, we will always assume that c and e are small enough in the following calculation to ensure the intersections of the trajectory and the cross sections.

Local maps can be constructed by integrating the linearized systems near P_1, P_2 and P_3, while global maps can be estimated by C^1-diffeomorphisms between neighborhoods of the P_j. We calculate not only the point where an orbit hits each cross section at each step but also the time that the orbit spends between hits. Although the time spent on global parts of Poincaré map is relatively small compared with the time spent near P_j, especially when γ is small, we will not ignore it throughout our calculation because it could be large compared with the period $\frac{2\pi}{\omega}$ of the perturbation function f, i.e. when ω is large. The time spent on the global parts will be denoted by three constants δ_1, δ_2 and δ_3.

At each stage, we compute leading order and $O(\gamma)$ terms in the local and global

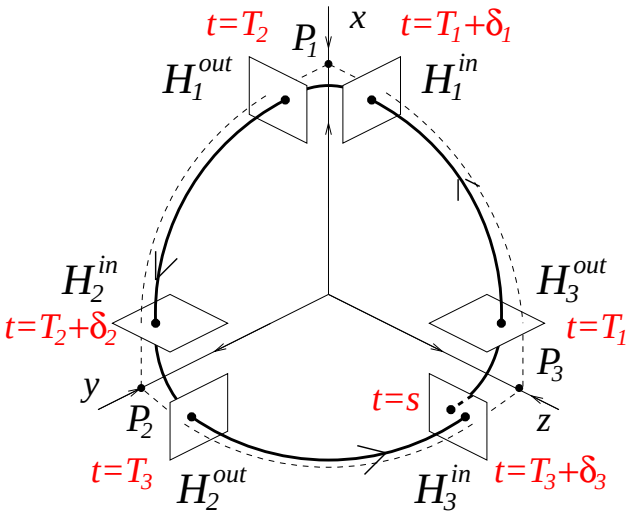

Figure 3.2: The cross sections of the cycle and the time when a trajectory near the heteroclinic cycle hits the cross sections.

maps. For notational convenience, variables without suffix will be treated as depending only on time t. Variables with suffix, corresponding to values of the variables on a cross-section, will be treated as functions of γ.

3.3.1 $H_3^{in} \to H_3^{out}$

First of all, we derive the local map from H_3^{in} to H_3^{out}. Let $(x_1, h, z_1) \in H_3^{in}$, near P_3, as the initial point of a specific orbit at the initial time $t = s$ and suppose that this orbit intersects H_3^{out} at (h, y_2, z_2) at time $t = T_1(\gamma)$.

Since the flow is close to P_3, we will write $z(t) = 1+w(t)$ and denote $z_1 = 1+w_1$.

In this case, the dynamics is subject to the linearized system

$$\begin{cases} \dot{x} &= ex + \gamma f(2\omega t) \\ \dot{y} &= -cy \\ \dot{z} &= \dot{w} = -w - (1+c)x + (e-1)y \end{cases}$$

Integrating this system from H_3^{in} to H_3^{out}, we get

$$\begin{cases} h &= x_1 \mathrm{e}^{e(T_1-s)}\left(1+\gamma\frac{1}{x_1}\int_s^{T_1}\mathrm{e}^{-e(\tau-s)}f(2\omega\tau)d\tau\right) \\ y_2 &= h\mathrm{e}^{-c(T_1-s)} \\ w_2 &= w_1\mathrm{e}^{-(T_1-s)}\left(1+\frac{1}{w_1}\int_s^{T_1}\mathrm{e}^{\tau-s}(-(1+c)x(\tau)+(e-1)y(\tau))d\tau\right) \end{cases} \tag{3.3}$$

From the first equation of (3.3), it is clear that

$$T_1(0) = s + \log\left(\frac{h}{x_1}\right)^{1/e}. \tag{3.4}$$

Differentiating the first equation of (3.3) with respect to γ and setting $\gamma = 0$, we get

$$0 = e\mathrm{e}^{e(-s+T_1(0))}x_1T_1'(0) + \mathrm{e}^{e(-s+T_1(0))}\int_s^{T_1(0)}\mathrm{e}^{-e(-s+\tau)}f(2\omega\tau)d\tau,$$

which implies

$$T_1'(0) = -x_1^{-1}\frac{1}{e}\int_s^{T_1(0)}\mathrm{e}^{-e(\tau-s)}f(2\omega\tau)d\tau. \tag{3.5}$$

Hence,

$$T_1(\gamma) = s + \log\left(\frac{h}{x_1}\right)^{1/e} - \gamma\left[x_1^{-1}\frac{1}{e}\int_s^{T_1(0)}\mathrm{e}^{-e(\tau-s)}f(2\omega\tau)d\tau\right] + O(\gamma^2).$$

Similarly, from the second equation of (3.3), we can easily verify that $y_2\mid_{\gamma=0} = h\left(\frac{h}{x_1}\right)^{-c/e}$ and

$$\begin{aligned} y_2'(0) &= h\mathrm{e}^{-c(T_1(0)-s)}(-cT_1'(0)) \\ &= x_1^{-1+c/e}\tfrac{c}{e}h^{1-c/e}\int_s^{T_1(0)}\mathrm{e}^{-e(\tau-s)}f(2\omega\tau)d\tau. \end{aligned} \tag{3.6}$$

Therefore,

$$y_2(\gamma) = h^{1-c/e}x_1^{c/e} + \gamma\left[x_1^{-1+c/e}\tfrac{c}{e}h^{1-c/e}\int_s^{T_1(0)}\mathrm{e}^{-e(\tau-s)}f(2\omega\tau)d\tau\right] + O(\gamma^2).$$

To derive $w_2(\gamma)$, we first note that, (integration by parts)

$$\begin{aligned} \int_s^{T_1(\gamma)}\mathrm{e}^{\tau-s}x(\tau)d\tau &= \mathrm{e}^{\tau-s}x(\tau)\mid_s^{T_1(\gamma)} - \int_s^{T_1(\gamma)}\mathrm{e}^{\tau-s}\dot{x}(\tau)d\tau \\ &= \mathrm{e}^{T_1(\gamma)-s}h - x_1 - \int_s^{T_1(\gamma)}e\mathrm{e}^{\tau-s}x(\tau)d\tau - \gamma\int_s^{T_1(\gamma)}\mathrm{e}^{\tau-s}f(2\omega\tau)d\tau, \end{aligned}$$

and,

$$\begin{aligned}\int_s^{T_1(\gamma)} \mathrm{e}^{\tau-s} y(\tau)d\tau &= \mathrm{e}^{\tau-s} y(\tau)\,|_s^{T_1(\gamma)} - \int_s^{T_1(\gamma)} \mathrm{e}^{\tau-s}\dot{y}(\tau)d\tau \\ &= \mathrm{e}^{T_1(\gamma)-s} y_2(\gamma) - h + c\int_s^{T_1(\gamma)} \mathrm{e}^{\tau-s} y(\tau)d\tau.\end{aligned}$$

These imply that

$$\begin{aligned}\int_s^{T_1(\gamma)} \mathrm{e}^{\tau-s} x(\tau)d\tau &= \tfrac{1}{1+e}\left(\mathrm{e}^{T_1(\gamma)-s}h - x_1 - \gamma\int_s^{T_1(\gamma)} \mathrm{e}^{\tau-s} f(2\omega\tau)d\tau\right), \\ \int_s^{T_1(\gamma)} \mathrm{e}^{\tau-s} y(\tau)d\tau &= \tfrac{1}{1-c}\left(\mathrm{e}^{T_1(\gamma)-s} y_2(\gamma) - h\right).\end{aligned}$$

So,

$$\begin{aligned}w_2(\gamma) &= \mathrm{e}^{-(T_1(\gamma)-s)}\left[w_1 - \tfrac{1+c}{1+e}\left(\mathrm{e}^{T_1(\gamma)-s}h - x_1 - \gamma\int_s^{T_1(\gamma)} \mathrm{e}^{\tau-s} f(2\omega\tau)d\tau\right)\right. \\ &\quad \left. + \tfrac{e-1}{1-c}\left(\mathrm{e}^{T_1(\gamma)-s} y_2(\gamma) - h\right)\right], \\ w_2(0) &= (\tfrac{h}{x_1})^{-1/e}\left[w_1 - \tfrac{1+c}{1+e}\left((\tfrac{h}{x_1})^{1/e}h - x_1\right) + \tfrac{e-1}{1-c}\left((\tfrac{h}{x_1})^{1/e-c/e}h - h\right)\right] \\ &\approx -\tfrac{1+c}{1+e}h,\end{aligned}$$

and,

$$\begin{aligned}w_2'(0) &= -\mathrm{e}^{s-T_1(0)}\left[w_1 - \tfrac{1+c}{1+e}(\mathrm{e}^{-s+T_1(0)}h - x_1) - \tfrac{1-e}{1-c}(-h + \mathrm{e}^{-s+T_1(0)} y_2(0))\right] T_1'(0) \\ &\quad + \mathrm{e}^{s-T_1(0)}\left[-\tfrac{1+c}{1+e}\left(-\int_s^{T_1(0)} \mathrm{e}^{-s+\tau} f(2\omega\tau)d\tau + \mathrm{e}^{-s+T_1(0)}hT_1'(0)\right)\right. \\ &\quad \left. - \tfrac{1-e}{1-c}\left(\mathrm{e}^{-s+T_1(0)} y_2(0)T_1'(0) + \mathrm{e}^{-s+T_1(0)} y_2'(0)\right)\right]\end{aligned} \tag{3.7}$$

Note that the terms involving $y_2(0)$ and $\mathrm{e}^{-s+T_1(0)}h$ are cancelled out, and x_1 and w_1 in the first bracket can be ignored since they are far smaller than h for small enough γ. Hence, only three terms are left in (3.7).

$$w_2'(0) \approx -\mathrm{e}^{s-T_1(0)}\frac{1-e}{1-c}hT_1'(0) - \frac{1-e}{1-c}y_2'(0) + \frac{1+c}{1+e}h^{-1/e}x_1^{1/e}\int_s^{T_1(0)} \mathrm{e}^{-s+\tau} f(2\omega\tau)d\tau$$

By (3.4) and (3.6), the first term in the last equation is

$$-\left(\frac{h}{x_1}\right)^{-1/e}\frac{1-e}{1-c}hT_1'(0),$$

while the second term is

$$\frac{1-e}{1-c}h\left(\frac{h}{x_1}\right)^{c/e}(-c)T_1'(0),$$

which is far larger than the first term since $c/e > 1$ and $x_1 \ll 1$. It follows that

$$\begin{aligned} w_2'(0) &\approx -x_1^{-1+c/e}\tfrac{c(1-e)}{e(1-c)}h^{1-c/e}\int_s^{T_1(0)} \mathrm{e}^{-e(\tau-s)} f(2\omega\tau)d\tau \\ &\quad +\tfrac{1+c}{1+e}h^{-1/e}x_1^{1/e}\int_s^{T_1(0)} \mathrm{e}^{-s+\tau} f(2\omega\tau)d\tau. \end{aligned}$$

Therefore,

$$\begin{cases} T_1(\gamma) &= s + \log(\frac{h}{x_1})^{1/e} - \gamma\left[x_1^{-1}\frac{1}{e}\int_s^{T_1(0)} \mathrm{e}^{-e(\tau-s)} f(2\omega\tau)d\tau\right] + O(\gamma^2) \\ y_2(\gamma) &= h^{1-c/e}x_1^{c/e} + \gamma\left[x_1^{-1+c/e}\frac{c}{e}h^{1-c/e}\int_s^{T_1(0)} \mathrm{e}^{-e(\tau-s)} f(2\omega\tau)d\tau\right] + O(\gamma^2) \\ z_2(\gamma) &= 1 - \tfrac{1+c}{1+e}h + \gamma\Big[-x_1^{-1+c/e}\tfrac{c(1-e)}{e(1-c)}h^{1-c/e}\int_s^{T_1(0)} \mathrm{e}^{-e(\tau-s)} f(2\omega\tau)d\tau \\ &\quad +x_1^{1/e}\tfrac{1+c}{1+e}h^{-1/e}\int_s^{T_1(0)} \mathrm{e}^{-s+\tau} f(2\omega\tau)d\tau\Big] + O(\gamma^2). \end{cases} \tag{3.8}$$

3.3.2 $H_3^{out} \to H_1^{in}$

Now we consider the first of the global maps.

Suppose that the unstable manifold of P_3' intersects H_3^{out} and H_1^{in} at $(h, 0, \zeta_2(t,\gamma))$ and $(\xi_3(t,\gamma), 0, h)$, respectively (See Figure 3.1). For simplicity, we use ζ_2 and ξ_3 to denote $\zeta_2(t,\gamma)$ and $\xi_3(t,\gamma)$, and ζ_{20}, ξ_{30} to denote $\zeta_2(T_1(0),0)$ and $\xi_3(T_1(0),0)$. The same notation will be used in all the following.

We expand the diffeomorphism between H_3^{out} and H_1^{in} near the point $(h, 0, \zeta_2(T_1(\gamma),\gamma))$ and suppose that the flow starting at $(h, 0, \zeta_2(t_1,\gamma))$ takes the time δ_1 to arrive at $(\xi_3(t_2,\gamma), 0, h)$.

The first order Taylor estimate gives us the linearised map $(h, y_2, z_2) \to (x_3, y_3, h)$:

$$\begin{cases} x_3 &\approx \xi_3(T_1(\gamma)+\delta_1,\gamma) + A_{11}(T_1(\gamma),\gamma)y_2 + A_{12}(T_1(\gamma),\gamma)(z_2 - \zeta_2(T_1(\gamma),\gamma)) \\ y_3 &\approx B_{11}(T_1(\gamma),\gamma)y_2 \end{cases},$$

where A_{11}, A_{12} and B_{11} are smooth functions of $T_1(\gamma)$ and γ which do not vanish for all small enough γ generically, and δ_1 denotes the time spent from H_3^{out} to H_1^{in}. Here, we denote $A_{110} = A_{11}(T_1(0),0)$, $A_{120} = A_{12}(T_1(0),0)$ and $B_{110} = B_{11}(T_1(0),0)$.

Substituting (3.8) into this gives

$$\begin{aligned} x_3 &= \xi_{30} + A_{110}h^{1-c/e}x_1^{c/e} + A_{120}(1 - \tfrac{1+c}{1+e}h - \zeta_{20}) \\ &\quad + \Big[\tfrac{\partial \xi_3}{\partial \gamma}(T_1(0)+\delta_1, 0) + \tfrac{\partial A_{11}}{\partial \gamma}(T_1(0),0)h^{1-c/e}x_1^{c/e} + \tfrac{\partial A_{12}}{\partial \gamma}(T_1(0),0)\Big(1 - \tfrac{1+c}{1+e}h - \zeta_{20}\Big) \\ &\quad - A_{120}\tfrac{\partial \zeta_2}{\partial \gamma}(T_1(0),0) - A_{120}x_1^{-1+c/e}\tfrac{c(1-e)}{e(1-c)}h^{1-c/e}\int_s^{T_1(0)} \mathrm{e}^{-e(\tau-s)} f(2\omega\tau)d\tau \\ &\quad + A_{120}x_1^{1/e}\tfrac{1+c}{1+e}h^{-1/e}\int_s^{T_1(0)} \mathrm{e}^{-s+\tau} f(2\omega\tau)d\tau\Big]\gamma + O(\gamma^2) \end{aligned} \tag{3.9}$$

and

$$\begin{aligned} y_3 &= B_{110}h^{1-c/e}x_1^{c/e} + \Big[\Big(\tfrac{\partial B_{11}}{\partial t}(T_1(0),0)T_1'(0) + \tfrac{\partial B_{11}}{\partial \gamma}(T_1(0),0)\Big)h^{1-c/e}x_1^{c/e} \\ &\quad + B_{110}x_1^{-1+c/e}\tfrac{c}{e}h^{1-c/e}\int_s^{T_1(0)} \mathrm{e}^{-e(\tau-s)} f(2\omega\tau)d\tau\Big]\gamma + O(\gamma^2) \end{aligned} \tag{3.10}$$

Here, we use the fact that

$$\begin{aligned} \xi_3(T_1(\gamma)+\delta_1, \gamma) &= \xi_{30} + \Big[\tfrac{\partial \xi_3}{\partial t}(T_1(0)+\delta_1, 0)T_1'(0) + \tfrac{\partial \xi_3}{\partial \gamma}(T_1(0)+\delta_1, 0)\Big]\gamma \\ &= \xi_{30} + \tfrac{\partial \xi_3}{\partial \gamma}(T_1(0)+\delta_1, 0)\gamma, \end{aligned}$$

since $\frac{\partial \xi_3}{\partial t}(T_1(0)+\delta_1, 0) = \lim_{\delta\to 0}\frac{\xi_3(T_1(0)+\delta+\delta_1,0)-\xi_3(T_1(0)+\delta_1,0)}{\delta} = 0$, and the same fashion for the other similar terms.

The $x_1^{c/e}$ terms in (3.9) can be ignored since $c/e > 1$ and $x_1 \ll 1$. As for (3.10), by (3.5), we need to compare the size of $x_1^{c/e}$ and $x_1^{-1+c/e}\int_s^{T_1(0)} \mathrm{e}^{-e(\tau-s)} f(2\omega\tau)d\tau$. Since

$$\begin{aligned} \int_s^{T_1(0)} \mathrm{e}^{-e(\tau-s)} f(2\omega\tau)d\tau &\geq \int_s^{s+1} \mathrm{e}^{-e(\tau-s)} f(2\omega\tau)d\tau \\ &\geq \mathrm{e}^{-e}\int_s^{s+1} f(2\omega\tau)d\tau \gg x_1, \end{aligned}$$

for small enough γ, the $x_1^{c/e}$ term in (3.10) can be ignored. Putting all the constant terms together, we then have

$$\begin{cases} x_3 = A_{130} + \Big[A_{140} - A_{120}x_1^{-1+c/e}\tfrac{c(1-e)}{e(1-c)}h^{1-c/e}\int_s^{T_1(0)} \mathrm{e}^{-e(\tau-s)} f(2\omega\tau)d\tau \\ \qquad + A_{120}x_1^{1/e}\tfrac{1+c}{1+e}h^{-1/e}\int_s^{T_1(0)} \mathrm{e}^{-s+\tau} f(2\omega\tau)d\tau\Big]\gamma + O(\gamma^2) \\ y_3 = B_{110}h^{1-c/e}x_1^{c/e} + B_{110}\Big[x_1^{-1+c/e}\tfrac{c}{e}h^{1-c/e}\int_s^{T_1(0)} \mathrm{e}^{-e(\tau-s)} f(2\omega\tau)d\tau\Big]\gamma + O(\gamma^2) \end{cases} \tag{3.11}$$

where A_{120}, A_{130}, A_{140} and B_{110} are constant.

At this point, the time is $T_1(\gamma) + \delta_1$.

3.3.3 $H_1^{in} \to H_1^{out}$

From this section on, we will omit most of the details and only describe the main ideas of the calculation.

Let $x(t) = 1 + u(t)$, $x_3 = 1 + u_3$ and $x_4 = 1 + u_4$, where $y_3, u_3 \sim O(\gamma)$. As the flow passes into the vicinity of the fixed point $P_1(1, 0, 0)$, the dynamics of the system is given to leading order in γ by the linearized system

$$\begin{cases} \dot{x} &= \dot{u} = -u - (1+c)y + (e-1)z \\ \dot{y} &= ey \\ \dot{z} &= -cz \end{cases}$$

Integrating it from H_1^{in} to H_1^{out} we then get the following map from H_3^{in} to H_1^{out} up to order γ:

$$\begin{cases} T_2(\gamma) &= s + \delta_1 + \log(B_{110}^{-1} h^{1+c/e} x_1^{-1-c/e})^{1/e} - \gamma \left[x_1^{-1} \frac{e+c}{e^2} \int_s^{T_1(0)} \mathrm{e}^{-e(\tau-s)} f(2\omega\tau) d\tau \right] \\ z_4(\gamma) &= h^{1-c^2/e^2} B_{110}^{c/e} x_1^{c^2/e^2} + \gamma \left[x_1^{-1+c^2/e^2} B_{110}^{c/e} h^{1-c^2/e^2} \frac{c^2}{e^2} \int_s^{T_1(0)} \mathrm{e}^{-e(\tau-s)} f(2\omega\tau) d\tau \right] \\ x_4(\gamma) &= 1 - \frac{1+c}{1+e} h + \gamma \left[x_1^{-1+c^2/e^2} \frac{c^2(1-e)}{e^2(1-c)} B_{110}^{c/e} h^{1-c^2/e^2} \int_s^{T_1(0)} \mathrm{e}^{-e(\tau-s)} f(2\omega\tau) d\tau \right] \end{cases} . \tag{3.12}$$

3.3.4 $H_1^{out} \to H_2^{in}$

Suppose that the unstable manifold of P_1 intersects H_1^{out} and H_2^{in} at $(\xi_4(t,\gamma), h, 0)$ and $(h, \eta_5(t,\gamma), 0)$, where ξ_4 and η_5 are smooth functions of t and γ as before, then the linearised map $(x_4, h, z_4) \to (h, y_5, z_5)$ is

$$\begin{cases} y_5 &= \eta_5(T_2(\gamma) + \delta_2, \gamma) + A_{21}(T_2(\gamma), \gamma)(x_4(\gamma) - \xi_4(T_2(\gamma), \gamma)) + A_{22}(T_2(\gamma), \gamma) z_4(\gamma) \\ & \quad + O(\gamma^2) \\ z_5 &= B_{22}(T_2(\gamma), \gamma) z_4(\gamma) + O(\gamma^2) \end{cases} ,$$

for some coefficients A_{21}, A_{22} and B_{22} which do not vanish for all small enough $\gamma = 0$ generically. Here δ_2 denotes the time spent from $H_1^{out} \to H_2^{in}$.

Substituting (3.12) into the above expressions we obtain

$$\begin{cases} y_5(\gamma) &= \eta_{50} + A_{210}(x_4(0) - \xi_{40}) + A_{220}z_4(0) \\ &\quad +\gamma\left[\frac{\partial \eta_5}{\partial \gamma}(T_2(0)+\delta_2,0) + \frac{\partial A_{21}}{\partial \gamma}(T_2(0),0)(x_4(0)-\xi_{40}) + A_{210}(x_4'(0)\right. \\ &\quad \left. -\frac{\partial \xi_4}{\partial \gamma}(T_2(0),0)) + A_{220}z_4'(0) + \frac{\partial A_{22}}{\partial \gamma}(T_2(0),0)z_4(0)\right] + O(\gamma^2) \\ &= A_{230} + \gamma\,[A_{24}(T_2(0),0) \\ &\quad +x_1^{-1+c^2/e^2}A_{250}B_{110}^{c/e}h^{1-c^2/e^2}\tfrac{c^2}{e^2}\int_s^{T_1(0)} \mathrm{e}^{-e(\tau-s)}f(2\omega\tau)d\tau\Big] + O(\gamma^2) \\ z_5(\gamma) &= B_{220}B_{110}^{c/e}h^{1-c^2/e^2}x_1^{c^2/e^2} + \gamma\left[\frac{\partial B_{22}}{\partial \gamma}(T_2(0),0)z_4(0) + B_{220}z_4'(0)\right] + O(\gamma^2) \\ &= B_{220}B_{110}^{c/e}h^{1-c^2/e^2}x_1^{c^2/e^2} \\ &\quad +\gamma\left[x_1^{-1+c^2/e^2}B_{220}B_{110}^{c/e}h^{1-c^2/e^2}\tfrac{c^2}{e^2}\int_s^{T_1(0)} \mathrm{e}^{-e(\tau-s)}f(2\omega\tau)d\tau\right] + O(\gamma^2). \end{cases} \tag{3.13}$$

At this point, the time is $t = T_2(\gamma) + \delta_2$.

3.3.5 $H_2^{in} \to H_2^{out}$

Let $y(t) = 1 + v(t), y_5 = 1 + v_5$ and $y_6 = 1 + v_6$. Consider the linearized system near P_2

$$\begin{cases} \dot{x} &= -cx + f(2\omega t)\gamma \\ \dot{y} &= \dot{v} = -v + (e-1)x - (c+1)z \\ \dot{z} &= ez \end{cases}$$

As in the previous sections, we integrate this linearised system to derive

$$\begin{cases} T_3(\gamma) &= s+\delta_1+\delta_2+\log(B_{220}^{-1}B_{110}^{-1-c/e}h^{1+c/e+c^2/e^2}x_1^{-1-c/e-c^2/e^2})^{1/e} \\ &\quad -\gamma\left[x_1^{-1}\frac{e^2+ce+c^2}{e^3}\int_s^{T_1(0)}\mathrm{e}^{-e(\tau-s)}f(2\omega\tau)d\tau\right]+O(\gamma^2) \\ x_6(\gamma) &= h^{1-c^3/e^3}B_{220}^{c/e}B_{110}^{c^2/e^2}x_1^{c^3/e^3} \\ &\quad +\gamma\left[\mathrm{e}^{-c(T_3(0)-T_2(0)-\delta_2)}\int_{T_2(0)+\delta_2}^{T_3(0)}\mathrm{e}^{c(\tau-T_2(0)-\delta_2)}f(2\omega\tau)d\tau\right]+O(\gamma^2) \\ y_6(\gamma) &= 1-\frac{1+c}{1+e}h+\frac{1-e}{1-c}\gamma\left[\mathrm{e}^{-(T_3(0)-T_2(0)-\delta_2)}\int_{T_2(0)+\delta_2}^{T_3(0)}\mathrm{e}^{\tau-T_2(0)-\delta_2}f(2\omega\tau)d\tau\right. \\ &\quad \left.-\mathrm{e}^{-c(T_3(0)-T_2(0)-\delta_2)}\int_{T_2(0)+\delta_2}^{T_3(0)}\mathrm{e}^{c(\tau-T_2(0)-\delta_2)}f(2\omega\tau)d\tau\right]+O(\gamma^2). \end{cases} \tag{3.14}$$

3.3.6 $H_2^{out} \to H_3^{in}$

We suppose that the unstable manifold of P_2' intersects H_2^{out} and H_3^{in} at $(\xi_6(t,\gamma),$ $\eta_6(t,\gamma),\ h)$ and $(\xi_7(t,\gamma), h, \zeta_7(t,\gamma))$. Note that the forms of these two intersection points are a little bit different from the previous ones due to the loss of the invariant plane $\{x=0\}$.

Then the map $(x_6, y_6, h) \to (x_7, h, y_7)$ takes the leading-order form

$$\begin{cases} x_7 &= \xi_7(T_3(\gamma)+\delta_3,\gamma)+A_{31}(T_3(\gamma),\gamma)(x_6(\gamma)-\xi_6(T_3(\gamma),\gamma)) \\ &\quad +A_{32}(T_3(\gamma),\gamma)(y_6(\gamma)-\eta_6(T_3(\gamma),\gamma))+O(\gamma^2) \\ z_7 &= \zeta_7(T_3(\gamma)+\delta_3,\gamma)+B_{31}(T_3(\gamma),\gamma)(x_6(\gamma)-\xi_6(T_3(\gamma),\gamma)) \\ &\quad +B_{32}(T_3(\gamma),\gamma)(y_6(\gamma)-\eta_6(T_3(\gamma),\gamma))+O(\gamma^2) \end{cases},$$

where A_{31}, A_{32}, B_{31} and B_{32}, as before, are smooth functions of $T_3(\gamma)$ and γ which do not vanish for all small enough γ generically, and δ_3 is the time spent from H_2^{out} to H_3^{in}.

Substituting (3.14) into these expressions we obtain

$$\begin{aligned} x_7(\gamma) &= \mu x_1^{c^3/e^3}+\xi_7(T_3(\gamma)+\delta_3,\gamma)-A_{310}\xi_6(T_3(\gamma),\gamma) \\ &\quad +\gamma\left[A_{310}\mathrm{e}^{-c(T_3(0)-T_2(0)-\delta_2)}\int_{T_2(0)+\delta_2}^{T_3(0)}\mathrm{e}^{c(\tau-T_2(0)-\delta_2)}f(2\omega\tau)d\tau\right. \\ &\quad \left.+\frac{\partial A_{32}}{\partial\gamma}(1-\frac{1+c}{1+e}h-\eta_{60})\right], \end{aligned} \tag{3.15}$$

where μ is a constant which depends only on f.

Since ξ_6 and ξ_7 are the x-coordinates of the intersections of the unstable manifold of P_2' with the cross sections H_2^{out} and H_3^{in}, respectively, by taking h small enough, we estimate ξ_6 and ξ_7 as affine maps of $x_{P_2'}$ and $x_{P_3'}$, where $x_{P_2'}$ and $x_{P_3'}$ denote the x-coordinates of P_2' and P_3', respectively. By the same way as we did in Lemma 3.2.1, it is easy to derive that

$$x_{P_2'} = \gamma \frac{1}{e^{c\pi/\omega} - 1} \int_0^{\pi/\omega} e^{c\tau} f(2\omega(t+\tau)) d\tau,$$

and

$$x_{P_3'} = \gamma \frac{1}{e^{-e\pi/\omega} - 1} \int_0^{\pi/\omega} e^{-e\tau} f(2\omega(t+\tau)) d\tau.$$

Therefore,

$$\xi_6(t,\gamma) = \lambda_1 + \gamma\lambda_2 \frac{1}{e^{c\pi/\omega} - 1} \int_0^{\pi/\omega} e^{c\tau} f(2\omega(t+\tau)) d\tau, \tag{3.16}$$

$$\xi_7(t,\gamma) = \lambda_3\gamma + \gamma\lambda_4 \frac{1}{e^{-e\pi/\omega} - 1} \int_0^{\pi/\omega} e^{-e\tau} f(2\omega(t+\tau)) d\tau, \tag{3.17}$$

where $\lambda_1, \lambda_2, \lambda_3$ and λ_4 are constants.

Substituting (3.16) and (3.17)) into (3.15), we have

$$\begin{aligned} x_7(\gamma) \;=\; & \mu x_1^{c^3/e^3} \\ & \gamma \Big[\mu_1 + \mu_2 e^{-c(T_3(0)-T_2(0)-\delta_2)} \int_{T_2(0)+\delta_2}^{T_3(0)} e^{c(\tau - T_2(0) - \delta_2)} f(2\omega\tau) d\tau \\ & -\mu_4 \tfrac{1}{e^{c\pi/\omega}-1} \int_0^{\pi/\omega} e^{c\tau} f(2\omega(T_3(\gamma)+\tau)) d\tau \\ & -\mu_5 \tfrac{1}{e^{-e\pi/\omega}-1} \int_0^{\pi/\omega} e^{-e\tau} f(2\omega(T_3(\gamma)+\delta_3+\tau)) d\tau \Big] \end{aligned}.$$

As for z_7, since it is not related to z_1, there is no need to calculate it.

Note that the expression for $x_7(\gamma)$ depends on $T_3(\gamma)$ which in turn is given in (3.14) in terms of x_1 and s, so we have a map $(x_1, s) \to (x_7, T_3 + \delta_3)$ which is our Poincaré map, in the form $(x,t) \to (\overline{x}, \overline{t}) = F(x,t) = (f_1(x,t), f_2(x,t)) =$

$(f_1(x,t), t + T(x,t))$, and

$$\begin{cases} f_1(x,t) &= \mu x^d + \gamma\left[\mu_1 + \mu_2 L_1(x,t) - \mu_4 G_1(x,t) - \mu_5 G_2(x,t)\right] + O(\gamma^2) \\ f_2(x,t) &= t + \mu_3 - \xi \log x - \gamma\xi L_2(x,t)x^{-1} + O(\gamma^2) \end{cases}, \tag{3.18}$$

where $\xi = \frac{e^2+ce+c^2}{e^3}$, $d = c^3/e^3$, μ and $\mu_i's$ are constants, $T(x,t)$ is the time necessary for a point (x,t) to complete one iterate, and

$$L_1(x,t) = \mathrm{e}^{-c(T_3(0)-T_2(0)-\delta_2)} \int_{T_2(0)+\delta}^{T_3(0)} \mathrm{e}^{c(\tau-T_2(0)-\delta_2)} f(2\omega\tau)d\tau, \tag{3.19}$$

$$L_2(x,t) = \int_t^{T_1(0)} \mathrm{e}^{-e(\tau-t)} f(2\omega\tau)d\tau, \tag{3.20}$$

$$G_1(x,t) = \frac{1}{\mathrm{e}^{c\pi/\omega}-1} \int_0^{\pi/\omega} \mathrm{e}^{c\tau} f(2\omega(T_3(\gamma)+\tau))d\tau, \tag{3.21}$$

$$G_2(x,t) = \frac{1}{\mathrm{e}^{-e\pi/\omega}-1} \int_0^{\pi/\omega} \mathrm{e}^{-e\tau} f(2\omega(T_3(\gamma)+\delta_3+\tau))d\tau. \tag{3.22}$$

Remark 3.3.1 *Note that for, $\gamma = 0$, system (3.18) is reduced to the Poincaré map of the unperturbed ODE system. In this case, $f_1(x,t) = \mu_1 x^d$ is a one dimensional map depending only on x and under repeated iteration, x tends to 0 since $d = c^3/e^3 > 1$. In other words, the heteroclinic cycle in the unperturbed system is asymptotically stable if $d > 1$. This is consistent with [43]. Moreover, this leads to the divergence of the return time $T(x,t) = \mu_3 - \xi \log x$ in each iteration, which is a characteristic feature of trajectories near a stable heteroclinic cycle.*

In the following chapters, we will mainly restrict our consideration to the same system as [18] where $f(2\omega t) = \sin^2(\omega t)$:

$$\begin{cases} \dot{x} &= x(1-(x+y+z)-cy+ez) + \gamma(1-x)\sin^2(\omega t) \\ \dot{y} &= y(1-(x+y+z)-cz+ex) \\ \dot{z} &= z(1-(x+y+z)-cx+ey) \end{cases}, \tag{3.23}$$

In this case, our Poincaré map becomes

$$\begin{cases} f_1(x,t) &= \mu x^d + \gamma\,[\mu_1 + \mu_2(-a_1\cos(2\omega g) - b_1\sin(2\omega g)) \\ & \quad -\mu_4(-a_1\cos(2\omega(\overline{t}-\delta_3)) - b_1\sin(2\omega(\overline{t}-\delta_3))) \\ & \quad -\mu_5(-a_2\cos(2\omega\overline{t}) - b_2\sin(2\omega\overline{t}))] + O(\gamma^2) \\ f_2(x,t) &= t + \mu_3 - \xi\log(x) - \gamma\frac{\xi}{2e}[1 - a_2\cos(2\omega t) + b_2\sin(2\omega t)]x^{-1} + O(\gamma^2) \end{cases}, \tag{3.24}$$

where $a_1 = \frac{c^2}{c^2+4\omega^2}$, $b_1 = \frac{2c\omega}{c^2+4\omega^2}$, $a_2 = \frac{e^2}{e^2+4\omega^2}$, $b_2 = \frac{2e\omega}{e^2+4\omega^2}$, $g = t + \mu_3 - \xi\log(x)$, μ, μ_i's and δ_3 are constant.

Remark 3.3.2 *The Poincaré map here is slightly different from the one we have published in [18] and has both a sounder mathematical basis and a better agreement with our numerical results (see later).*

Remark 3.3.3 *The form of the (3.24) can be divided into two parts which are due to (i) the mean of the perturbation function ,and (ii) the oscillation of the perturbation function. More precisely, if we write the perturbation function $f(2\omega t)$ as the form $A+(f(2\omega t)-A)$ where $A = \frac{1}{2\pi}\int_0^{2\pi} f(t)dt$ denotes its mean and $f(2\omega t)-A$ is its oscillation part, then the integrals in (3.19), (3.20), (3.21) and (3.22) can be also wrote in the form of their means plus oscillation parts. It follows that if we take the perturbation function as $(1-x)(\delta(f(2\omega t) - A) + \gamma A)$ where $f(2\omega t) = \sin^2(\omega t)$, then the Poincaré map is of the form*

$$\begin{cases} f_1(x,t) &= \mu x^d + \gamma\mu_1 \\ & \quad +\delta\,[\mu_2(-a_1\cos(2\omega g) - b_1\sin(2\omega g)) \\ & \quad -\mu_4(-a_1\cos(2\omega(\overline{t}-\delta_3)) - b_1\sin(2\omega(\overline{t}-\delta_3))) \\ & \quad -\mu_5(-a_2\cos(2\omega\overline{t}) - b_2\sin(2\omega\overline{t}))] + O(\gamma^2) \\ f_2(x,t) &= t + \mu_3 - \xi\log(x) \\ & \quad -\frac{\xi}{2e}\left[\gamma - \delta\left(a_2\cos(2\omega t) - b_2\sin(2\omega t)\right)\right]x^{-1} + O(\gamma^2) \end{cases}. \tag{3.25}$$

We will discuss the dynamics of the system with this general perturbation in section 4.6.

To make the Poincaré map (3.24) well-defined, we need to check if there exists an open set V in H_3^{in} such that $F(V) \subseteq V$. In section 4.2, the asymptotic order of x is discussed. In the two cases we are going to analyse in chapter 4, $O(\hat{x})$ could be larger than or around γ depending on the size of d, where $\hat{x}$ satisfies $\hat{x} = \hat{x}^d + \gamma$. It follows that the asymptotic order of x is around $O(\hat{x})$ or $O(\gamma)$. Therefore, the Poincaré map (3.24) is well-defined, at least, in the discussions in the next chapter.

3.4 Comparison with Afraimovich et al's result

V. S. Afraimovich et al.[3] also calculate the Poincaré map for a similar system

$$\begin{aligned} \dot{x} &= x(1-(x+y+z)-cy+ez)+\gamma g_1(t) \\ \dot{y} &= y(1-(x+y+z)-cz+ex)+\gamma g_2(t) \\ \dot{z} &= z(1-(x+y+z)-cx+ey)+\gamma g_3(t) \end{aligned},$$

wher g_1, g_2 and g_3 are periodic functions. In the case $g_1(t) = \sin^2 t$, $g_2(t) = g_3(t) \equiv 0$, the system is similar to our system (3.23) with $\omega = 1$. They proposed a map as a model of their Poincaré map:

$$\begin{cases} \bar{x} = A(Bx+\gamma(1+a\sin t))^d \\ \bar{t} = t + \bar{\omega} - \eta \log(Bx+\gamma(1+a\sin t)), (mod\ 2\pi) \end{cases}, \tag{3.26}$$

where $\eta = \xi = \frac{e^2+ce+c^2}{e^3}$ and a is a parameter.

In their calculation of the local maps, the time-dependent terms are ignored. This results in incorrectness, especially in the case d large. Intuitively, the time a trajectory spent in the local maps is much larger than that in the global maps for large d. Therefore, the periodic forcing term should affect the local maps more than the global ones.

By letting $x = y^d$, we are able to transform the x equation of (3.26) into a similar form as our Poincaré map (3.24):

$$\bar{y} = A^{1/d}\left(By^d + \gamma(1+a\sin t)\right).$$

Taylor expanding the second equation of (3.26), we have

$$\begin{aligned}\bar{t} &= t + \bar{\omega} - \eta \log(By^d + \gamma(1 + a\sin t)) \\ &= t + \bar{\omega} - \eta\left[\log(By^d) + \gamma B^{-1}(1 + a\sin t)y^{-d}\right] \\ &= t + \tilde{\omega} - \eta d \log y + \gamma\eta B^{-1}(1 + a\sin t)y^{-d}.\end{aligned}$$

For the case $a = 0$, by (3.26), $x \sim O(\gamma^d)$ and, hence, $y \sim O(\gamma)$. Therefore, since $\eta = \xi$, the spending time $T = \bar{t} - t$ of their map for the case $a = 0$ is

$$T \approx C - \xi d \log \gamma,$$

for some constant C. However, for large d, we show in section 4.4.1 that the spending time for $a = 0$ should be

$$T \approx C_1 - \xi \log \gamma,$$

where C_1 is a constant, which is a contradiction. In other words, even though we can turn the x equation of their map (3.26) into the form as our map (3.24), the t equation of their map is still incorrect.

In addition, consider the time-averaged function of the first equation of their map

$$\bar{x} = A(Bx + \gamma)^d,$$

and our map

$$\bar{x} = \mu x^d + \mu_1 \gamma.$$

There is a substantial difference between these two when d is large. In this case, the attracting fixed points of these two maps appear at different scalings: $x \sim O(\gamma^d)$ and $x \sim O(\gamma)$, respectively. For example, take $c = 0.25, e = 0.2$ (i.e. $d \approx 2$) and $\gamma = 10^{-6}$, numerical simulation of the original ODE system (3.23) shows that the time-average of x is around 10^{-5}, which can be obtained easily in our map by suitable parameters μ and μ_1. Moreover, μ and μ_1 can be constant

even though γ is changed for fixed c and e. This should be always true because μ and μ_1 depend only on c, e and the time-average of the perturbation function. In contrast, the constant A in their map is actually not a constant but a function of γ. Nevertheless, the two maps are equivalent if d near 1 for a fixed γ. We will discuss this issue in more detail at the beginning of the next chapter.

Accordingly, Afraimovich's map is not correct for large d. In contrast, we will show in the next chapter that our Poincaré map (3.24) is capable to simulate the original ODE system (3.23) numerically, as well as give explanations of how these complex dynamics arise analytically for d near 1 or large.

3.5 Two assumptions on the parameters

In this section, we state two assumptions on the parameters in our map (3.24) which we use to capture the intrinsic nature of the ODE system (3.23).

Firstly, because there exist small intervals of t in which $\sin^2(\omega t)$ is close to 0, a typical orbit of (3.23) will in general attracted by the original heteroclinic cycle within these intervals. Thus, we make the first assumption on the parameters μ_1, μ_2, μ_4 and μ_5 in (3.24) as:

(A.1) *μ_1, μ_2, μ_4 and μ_5 are assumed to make the perturbation part of the first equation of (3.24) near* 0 *in some small intervals of* t.

Secondly, it is quite natural to assume that the returning time is always positive:

(A.2) *μ_3 is large enough that $f_2(x,t) > t$ for all (x,t).*

Clearly, (A.2) is actually not important for the dynamics of our map as replacing μ_3 by $\mu_3 + \frac{k\pi}{\omega}$ for any integer k will not make any difference. But to make the return time well-defined, we will assume (A.2) to be ture.

Most of our analytic work in the next chapter is not based on these assumptions

except for the results in section 4.4.2 where we use (A.1) only for simplifying the Poincaré map. However, bearing them in mind will help us to find a suitable sets of parameters to match accurately our 2D map system with the original ODE system.

Remark 3.5.1 *Recall that the existence of the parameter δ_3 is due to that the time spent on the global maps for a trajectory might be large when comparing to the period of the perturbation function. In other words, when the forcing frequency ω is large, δ_3 could be important. Nevertheless, since $\omega < 0.5$ in the following numerical simulations, we always take δ_3 to be 0 for simulations.*

3.6 Discussion

In this chapter, we have presented a systematic method to calculate the Poincaré map for a heteroclinic system with periodic forcing. The whole calculation is divided into two parts: local maps and global maps. Local maps are those maps near equilibrium points and are computed from the linearized systems. We estimate the global maps, which are the maps between neighbourhoods of the equilibrium points, by means of the unstable manifolds of P_1', P_2' and P_3'.

Because of the time-dependent perturbation, the linearized systems near the P_is become non-autonomous. By including the time-dependent term through all steps in the calculation, we obtain a better Poincaré map than the one Afraimovich et al. have. In their local maps, the time-dependent effects are ignored for simplicity. However, a typical trajectory in a heteroclinic system spends far more time near equilibrium points than between them. Therefore, the time-dependent perturbation should affect the dynamics of the local maps more than the global maps and so it is essential to include this.

Although the perturbation term only acts on the x-coordinate in our ODE sys-

tem (3.23), the whole calculation can be carried out in the same way for the general case and the result should be of the same form as (3.18). An example will be shown in section 5.3.3 where we add three perturbation functions on each coordinate.

Moreover, the perturbation term $\gamma(1-x)f(2\omega t)$ can be replaced by $\gamma f(2\omega t)$ without affecting the Poincaré map. Through the derivation of the Poincaré map, we can see that only the local maps $H_3^{in} \to H_3^{out}$ and $H_2^{in} \to H_2^{out}$ involve the perturbation term. In these two cases, however, the x in the perturbation term can be ignored due to $x \sim O(\gamma)$. We will derive the Poincaré map of a similar system with such perturbation terms $\gamma(\phi_1(2\omega t), \phi_2(2\omega t), \phi_3(2\omega t))$ in section 5.3 where the result shows that the map takes the same form as (3.18).

Chapter 4

Analysis of the Poincaré Map

4.1 Introduction

In the previous chapter we considered the dynamics of the following system (1.3) of ODEs:

$$\begin{cases} \dot{x} &= x(1-(x+y+z)-cy+ez)+\gamma(1-x)f(2\omega t) \\ \dot{y} &= y(1-(x+y+z)-cz+ex) \\ \dot{z} &= z(1-(x+y+z)-cx+ey) \end{cases},$$

wher $f(2\omega t)$ is a periodic function. We showed that the dynamics for the case $f(2\omega t) = \sin^2(\omega t)$ could be reduced to the following 2D map (3.24) in the limit of small forcing amplitude γ:

$$\begin{cases} f_1(x,t) &= \mu x^d + \gamma\,[\mu_1 + \mu_2(-a_1\cos(2\omega g) - b_1\sin(2\omega g)) \\ & \quad -\mu_4(-a_1\cos(2\omega(\overline{t}-\delta_3)) - b_1\sin(2\omega(\overline{t}-\delta_3))) \\ & \quad -\mu_5(-a_2\cos(2\omega\overline{t}) - b_2\sin(2\omega\overline{t}))] + O(\gamma^2) \\ f_2(x,t) &= t + \mu_3 - \xi\log(x) - \gamma\frac{\xi}{2e}[1 - a_2\cos(2\omega t) + b_2\sin(2\omega t)]x^{-1} + O(\gamma^2) \end{cases}, \tag{4.1}$$

where $a_1 = \frac{c^2}{c^2+4\omega^2}$, $b_1 = \frac{2c\omega}{c^2+4\omega^2}$, $a_2 = \frac{e^2}{e^2+4\omega^2}$, $b_2 = \frac{2e\omega}{e^2+4\omega^2}$, $g = t + \mu_3 - \xi\log(x)$, μ, μ_i's and δ_3 are constant

In this chapter, we will show that this 2D map capture the dynamics of the ODEs across a wide range of forcing frequencies ω and both close to, and far from, the resonant bifurcation in the unforced case (i.e. values of the eigenvalue ratio c/e near unity, and greater than unity). We also discuss the dynamics of the 2D map (3.24) and show how it may be understood in various different asymptotic limits where it displays distinct dynamical behaviour.

Firstly, we discuss the asymptotic order of x in section 4.2 in which we show that both the order of x in the map system (3.24) and the ODE system (1.3) are relative to the size of d. Specifically, this order is at least approximately around $O(\gamma)$. Our results show that there is some limitation for the Poincaré map obtained by Afraimovich et al. in [3] to well-approximate the ODE system they studied, and the analytic results they proved for the map are in fact irrelevant to the ODE system since one assumption they made in all the proofs is $x \sim O(\gamma^d)$.

By section 4.2, the order of x in the map system (3.24) are different in two cases: ϵ near 0 and ϵ large, where $\epsilon = d - 1$. We discuss these two cases in the following two sections. In section 4.3, we proved that the dynamics of the system (3.24) in the case ϵ near 0 are equivalent to the dynamics of a forced damped pendulumn with torque. In contrast, circle map dynamics can be observed in the system (3.24) in the case ϵ large. We prove in section 4.4 that the system (3.24) is equivalent to an invertible circle map for ω large and a non-invertible circle map for ω near 0. As for the case where ω is of intermediate size, we are unable to proceed any analytic study due to the complicated form of the system (3.24). Nevertheless, we use 0-1 test to prove numerically that the transition from non-invertible to invertible circle map when increasing ω do exist and the 'chaotic'-like regions for large enough ω are not chaotic.

The effect of varying γ will be discussed in section 4.5 in which we found that, in some sense, the bifurcation structure when varying γ is similar to that

when varying ω.

It is hope that the Poincaré map (3.24) of the ODE system (1.3) for the case $f(2\omega t) = \sin^2(\omega t)$ can be served as a model map to describe the dynamics of the system (1.3) for general periodic functions $f(2\omega t)$. However, the function $\gamma \sin^2(\omega t)$ has the feature that its mean and the amplitude are of the same order. It then arises a question that if the results we obtain in the first few sections in this chapter are still ture for the case when the function $\gamma f(2\omega t)$ does not possess this feature. We will vary the mean and amplitude of the perturbation function separately in section 4.6 to get a more general model map and discuss its bifurcation structure in detail.

The chapter closes with a discussion in section 4.7.

4.2 The asymptotic order of x

In this section, we first define d and γ in a more careful way, and then investigate how important the x^d term is for different d.

Firstly, consider the average function $l(x) = x^d + \gamma$ of the first equation of (3.24)

$$\begin{aligned} f_1(x,t) &= \mu x^d + \gamma\,[\mu_1 + \mu_2(-a_1\cos(2\omega g) - b_1\sin(2\omega g)) \\ &\quad -\mu_4(-a_1\cos(2\omega(\bar{t}-\delta_3)) - b_1\sin(2\omega(\bar{t}-\delta_3))) \\ &\quad -\mu_5(-a_2\cos(2\omega\bar{t}) - b_2\sin(2\omega\bar{t}))] + O(\gamma^2) \end{aligned} .$$

Here, for simplicity, we set parameters $\mu = \mu_1 = 1$. Nevertheless, the result we demonstrate in this section can be extended to the general μ and μ_1 without any difficulty.

Because we are interested in periodic solutions of the system, we assume that our d and γ are such that $l(x) = x$ has at least one solution. To do this, note that $l'(x_m) = 1$ for $x_m = (\frac{1}{1+\epsilon})^{1/\epsilon}$, where $\epsilon = d - 1$. Since $l(0) = \gamma > 0$, if $l(x_m) \leq x_m$,

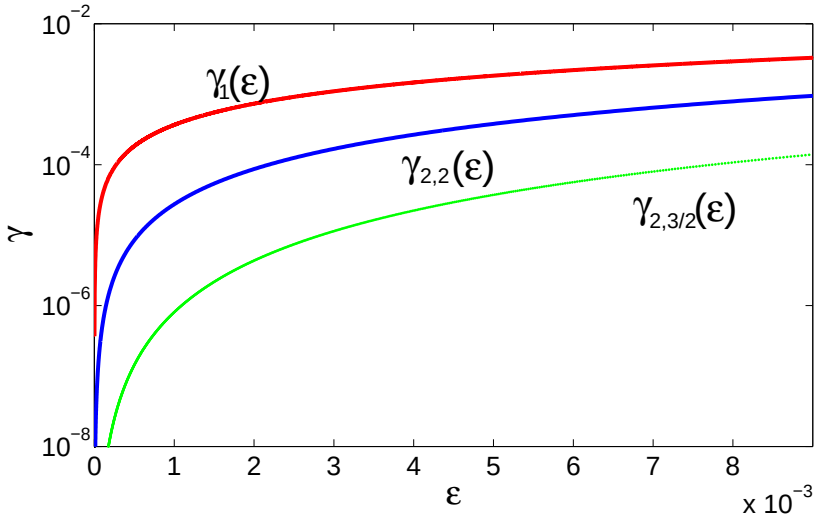

Figure 4.1: The region Φ_p is between two curves: $\gamma = \gamma_1(\epsilon)$ and $\gamma = \gamma_{2,p}(\epsilon)$. $\hat{x}$ exists if (ϵ, γ) is below the curve $\gamma = \gamma_1(\epsilon)$. The curve $\gamma = \gamma_{2,p}(\epsilon)$, by definition, is the points of (ϵ, γ) where $\hat{x} = \gamma^{1/p}$. Here, we display two cases for $p = 2$ (blue) and $p = 3/2$ (green).

i.e. $\gamma \leq x_m - x_m^{1+\epsilon}$, then $l(x) = x$ has at least one solution. In other words, for each $\epsilon > 0$, there exists a curve $\gamma_1(\epsilon) = \left(\frac{1}{1+\epsilon}\right)^{1/\epsilon} - \left(\frac{1}{1+\epsilon}\right)^{(1+\epsilon)/\epsilon}$ such that if $\gamma \leq \gamma_1(\epsilon)$, then $l(x) = x$ has a solution. Denote the solution smaller than x_m as $\hat{x}$.

The asymptotic size of $\hat{x}$ can also be estimated. Fix a constant $p > 1$. Then $\hat{x} = \gamma^{1/p}$ if and only if $\epsilon = \epsilon_p(\gamma) = \frac{p\log(\gamma^{1/p}-\gamma)}{\log\gamma} - 1$. Since $\epsilon_p(\gamma)$ is a strictly monotonically increasing function of $\gamma > 0$, by the inverse function theorem, there exists a function $\gamma_{2,p}(\epsilon)$ such that $\hat{x} = \gamma^{1/p}$ if and only if $\gamma = \gamma_{2,p}(\epsilon)$. See Figure 4.1. Therefore, if $(\epsilon, \gamma) \in \Phi_p = \{(\epsilon, \gamma) : \gamma_{2,p}(\epsilon) \leq \gamma \leq \gamma_1(\epsilon)\}$, then $\gamma^{1/p} \leq \hat{x} \leq x_m$. It follows that, by suitably choosing ϵ and γ, $\hat{x}$ could be close to $O(\gamma)$ or asymptotically far larger than γ and this implies that x^d can either be neglected or not, respectively, in the system (3.24).

In most of our later numerical simulations, we normally fix $e = 0.2$ and $\gamma =$

10^{-6} and consider two typical cases: $c = 0.2001$ and $c = 0.25$. Upper and lower bounds on $\hat{x}$ can be found by means of linear estimation. See Figure (4.2). More precisely, consider the line L_1 in the $(x, l(x))$ plane joining two points $(0, \gamma)$ and $(x_m, x_m^d + \gamma)$. It intersects $y = x$ at the point $(\frac{x_m}{x_m - x_m^d}\gamma, \frac{x_m}{x_m - x_m^d}\gamma)$. Since L_1 is larger than $l(x)$ between 0 and x_m, it follows that $\hat{x} \leq \frac{x_m}{x_m - x_m^d}\gamma$. Similarly, consider the line L_2 which is tangent to $l(x)$ at $(\gamma, \gamma^d + \gamma)$. Since $\gamma < \hat{x}$, the intersection of L_2 and $y = x$, which is $\left(1 + \frac{\gamma^\epsilon}{1-(1+\epsilon)\gamma^\epsilon}\right)\gamma$, is also smaller than $\hat{x}$. In short,

$$\left(1 + \frac{\gamma^\epsilon}{1-(1+\epsilon)\gamma^\epsilon}\right)\gamma \leq \hat{x} \leq \frac{x_m}{x_m - x_m^d}\gamma.$$

Figure (4.2) shows the upper and lower bounds of $\hat{x}^d$ for fixed $e = 0.2$ and $\gamma = 10^{-6}$. Since the first equation of our Poincaré map and its average map are only differed by an oscillation of order γ, it turns out that the x^d term plays an important role when c near e. However, it can be ignored if c is near 0.25.

Now consider Afraimovich's system (3.26)

$$\begin{cases} \bar{x} = A(Bx + \gamma(1 + a\sin t))^d \\ \bar{t} = t + \bar{\omega} - \eta\log(Bx + \gamma(1 + a\sin t))(mod\ 2\pi) \end{cases}.$$

By using the 'Annulus Principle', they prove the following theorem ([3]):

Theorem 4.2.1 *If $d > 1$, $\gamma \ll 1$ and $0 < a < 1/(\sqrt{1+\eta^2})$, then there is an invariant closed curve as the maximal attractor $x(t)$ for equation (3.26).*

Throughout their proof, the estimate $x = O(\gamma^d)$ is crucially important to make the theorem valid. However, this estimate is only true when γ is small enough for a fixed d, or when d is large enough for a fixed γ. For example, take $a = 0.02, d = 1.0028, \eta = 20, A = 1, B = 1$ and $\gamma = 10^{-6}$. In this case, bistable dynamics can be observed although the condition $0 < a < 1/(\sqrt{1+\eta^2})$ is satisfied. Therefore, Theorem 4.2.1 is true only if $(\gamma, d) \in \{(\gamma, d) : d > d_0(\gamma)\}$ for some function $d_0(\gamma)$.

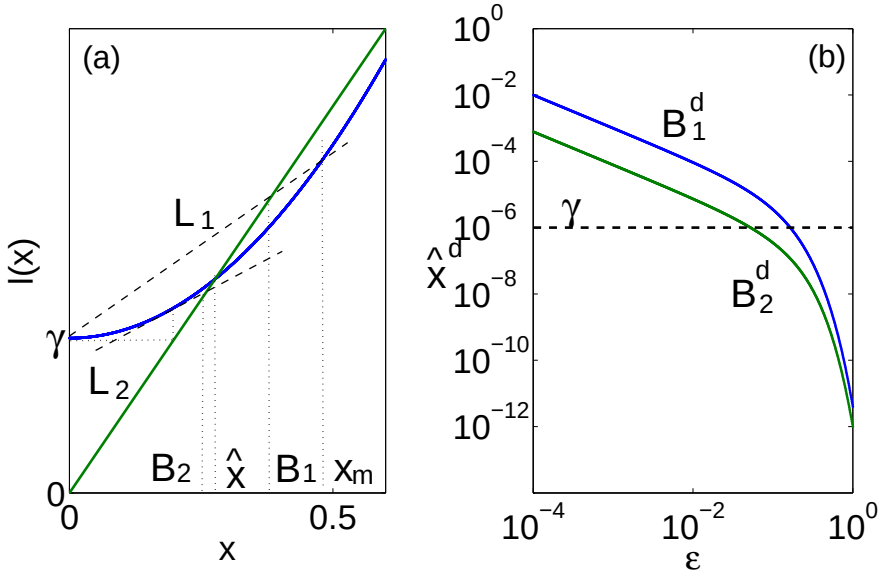

Figure 4.2: (a) The schematic diagram shown how we find the upper (B_1) and lower (B_2) bound of $\hat{x}$. The blue curve is the graph of $y = l(x)$ and the green line is the diagonal line $y = x$. (b) The upper (blue) and lower (green) bound of $\hat{x}^d$ for $e = 0.2$ and $\gamma = 10^{-6}$. We plot both axes in *log*-scale. The figure shows that, for ϵ small, as is the case c/e near 1, $O(\hat{x}^d) \gg \gamma$. In contrast, $\hat{x}^d$ is far smaller than γ when ϵ is large, i.e. c/e large, and hence can be ignored in the map.

For our system, it is clear that x will never be asymptotically $O(\gamma^d)$ as $\gamma \to 0$. This constrains the application of the 'Annulus Principle' to prove the existence of an invariant closed curve as the maximal attractor although numerical simulations suggest that this is always true for at least small enough ω and for d near 1 for a fixed γ. Nevertheless, we have proved this fact in Theorem 4.3.2.

Overall, Afraimovich et al. derived a Poincaré map (3.26) for a heteroclinic system with periodic perturbations which is, in fact, only valid for c/e near 1. However, their analytic study of this map is ture only when c/e large. Consequently, the analytic results they obtained for the map (3.26) is irrelevant to the

original ODE system.

In the following two sections, we investigate in the bifurcation structure of system (3.24) when varying the forcing frequency ω. Therefore, d and γ will be fixed. The term 'ϵ near 0' means that, for a given γ, ϵ is small enough such that the term x^d can not be omitted in our Poincaré map (3.24), i.e. $\hat{x} \gg \gamma$. In contrast, we say that we are in the case 'ϵ large' if, for a given γ, ϵ is large enough that x^d can be ignored without changing the bifurcation structure. In this case, $\hat{x} \sim \gamma$. Note that these actual values of ϵ all depend on γ.

4.3 ϵ near 0

In this section, instead of analysing the complicated Poincaré map (3.24), we consider a simple map as a model to explain the dynamics of (3.24). This model map demonstrates numerically similar dynamics as the ODE system (3.23) with the benefit of being analytically tractable.

The results in the last seciton show that $\mu x^d + \gamma\mu_1$ terms will dominate the first equation of (3.24) when ϵ is close enough to 0 and x is near $\hat{x}$. In this case, $O(\hat{x}) \gg \gamma$ and the coefficients $a_1 \approx a_2$. The remaining terms of this equation can be considered as small sine perturbation of $\hat{x}$. Therefore, a possible model to replace the first equation of (3.24) is

$$\bar{x} = \mu x^d + \gamma\mu_1 \left(1 + \sqrt{a_2}\sin(2\omega t)\right).$$

As for the second equation of (3.24), we hope that our model map can keep the features of the Poincaré map (3.24) both in the cases of $\gamma = 0$, when there exists a $\log x$ term, and $\gamma > 0$, when a periodic perturbation adding into it. Hence,

$$\bar{t} = t + \mu_3 - \xi \log \bar{x},$$

could be the simplest way to describe the t-dynamics. In other words, if we define a new γ as the original $\mu_1\gamma$, our model map then takes the form

$$\begin{cases} \bar{x} &= \mu x^d + \gamma\left(1 + \sqrt{a_2}\sin(2\omega t)\right) \\ \bar{t} &= t + \mu_3 - \xi \log \bar{x} \end{cases} . \tag{4.2}$$

This model map contains all the terms we know must be there in the absence of external forcing, and incorporates a generic time-periodic term in the simplest way possible, allowing frequency locking to arise.

The numerical integration of the ODE system and the iteration of our 2D model map (4.2) when varying ω, in the case: c=0.2001, e=0.2 and $\gamma = 10^{-6}$, agree well near $\hat{x}$ as shown in Figure 4.3. Here, we set $\mu = 1, \mu_2 = 20$ and $\mu_3 = 27$, i.e. the γ in (4.2) is $2 \cdot 10^{-5}$. Although the end points of the frequency-locking intervals are not the same, the main global features of the dynamics in these two systems are essentially identical. We observe that, in the map, orbits are attracted either to an invariant curve or to a fixed point, and both may be stable simultaneously. The corresponding dynamics for the ODE system is the existence of a stable invariant torus or periodic orbit which again may both be stable at the same time. Moreover, these attractors occur in a regular pattern as ω increasing.

The periodic orbits occur in frequency-locking intervals can be identified by considering a plot of the return period $T = \bar{t} - t$ against ω. Numerically, at least, it appears that the only possible period of a periodic orbit in the ODE system (3.23), as well as in the model map (4.2), is $k\pi/\omega$, for some $k \in \mathbb{Z}$. In other words, the curves in Figure 4.4 lie on hyperbolas $T(\omega) = k\pi/\omega$ indexed by k. This results in the relationship $\omega/\omega' = k/2$, where $\omega' = 2\pi/T$ is the frequency of the periodic orbit.

In the rest of this section, we will consider system (4.2) as a model to demonstrate the dynamics of the ODE system (3.23) for the case ϵ near 0. We will give a detailed analysis near the end and the centre of the frequency locking intervals

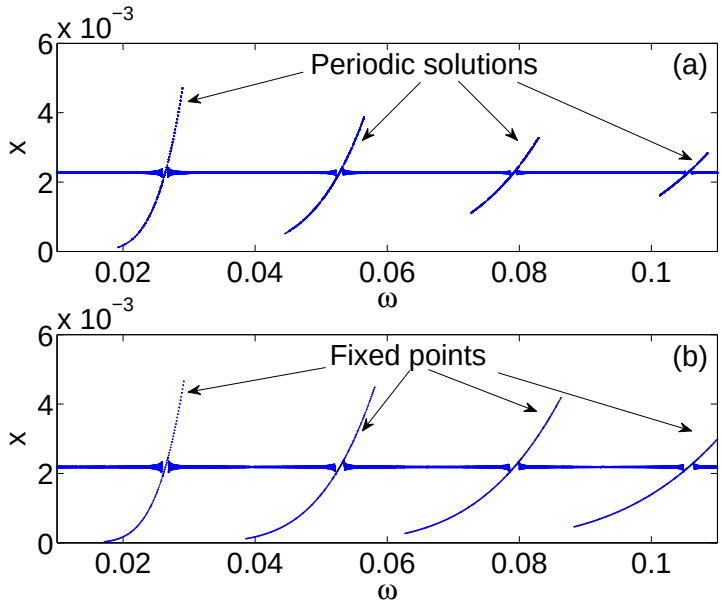

Figure 4.3: (a) The dynamics of the ODE system (3.23) for $c = 0.2001$, $e = 0.2$ and $\gamma = 10^{-6}$. We plot the x-coordinates of the points of two typical trajectories on the cross section H_3^{in} for each fixed ω. The curves in the figure display the existence of periodic solutions of the system. Bistability occurs in both ends of all these curves. The rest parts of the figure, which all sit near $\hat{x} \approx 2.2 \cdot 10^{-3}$, demonstrate complex dynamics with $|x - \hat{x}| \sim O(\gamma)$. (b) A similar dynamics can be observed by iterating our modle map (4.2). Here, $\gamma = 2 \cdot 10^{-5}$, $\mu = 1$ and $\mu_3 = 27$ and the curves in the figure display the existence of fixed points.

for small ω. In the case $\omega \to \infty$, the dynamics are the same as the dynamics when ϵ is large. We will leave this case to be studied later in section 4.4.1.

4.3.1 Local bifurcations of the system

In this section, we analyze the bifurcation structure of the system near the end of the frequency locking intervals.

Fixed k. Clearly, a fixed point $(x, t) = (x(\omega), t(\omega))$ exists at a fixed ω in the

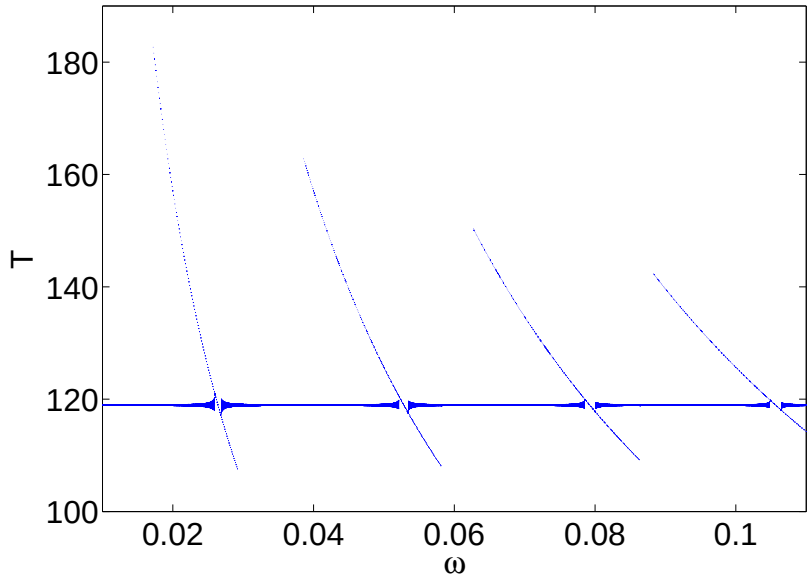

Figure 4.4: The $T-\omega$ plot for the system (4.2) for $c = 0.2001$, $e = 0.2$, $\mu = 1, \mu_3 = 27$ and $\gamma = 2 \cdot 10^{-5}$. The curves, where periodic solutions exist (compared to figure 4.3), all lie on hyperbolas indexed by k.

system (4.2) if only if

$$\begin{cases} x &= \mu x^d + \gamma(1 + \sqrt{a_2}\sin(2\omega t)) \\ \mu_3 - \xi \log x &= k\pi/\omega \end{cases}, \tag{4.3}$$

i.e. $x(\omega) = e^{(\mu_3 - k\pi/\omega)/\xi}$. Let ω_k^- be the left end of the k^{th} frequency-locking interval in ω. Since $x(\omega)$ is a monotone increasing function of ω and

$$\lim_{\omega\to 0} x(\omega) < x \in \{x : x = \mu x^d + \gamma(1 + \sqrt{a_2}\sin(2\omega t)), \text{for some } t\} < \lim_{\omega\to\infty} x(\omega),$$

ω_k^- can be defined as the smallest ω such that $x(\omega)$ satisfies the first equation of (4.3) for some t. In this case, $\sin(2\omega t)$ must take value -1 since $x(\omega_k^-)$ is the minimum. As a resutl, $t(\omega_k^-) = \frac{3\pi}{4\omega_k^-}$.

As soon as ω is slightly larger than ω_k^-, $x(\omega) > x(\omega_k^-)$ and then there exist two

$t(\omega)$, one larger and one smaller than $t(\omega_k^-)$ such that $(x(\omega), t(\omega))$ are fixed points for (4.2).

The stability of these fixed points can be easily verified. The Jacobian of system (4.2) is

$$\begin{pmatrix} d\mu x^{d-1} & 2\omega\sqrt{a_2}\cos(2\omega t)\gamma \\ -\frac{\xi}{x}d\mu x^{d-1} & 1-\frac{\xi}{x}2\omega\sqrt{a_2}\cos(2\omega t)\gamma \end{pmatrix},$$

which has two eigenvalues:

$$\lambda_1 = 1 - 2\frac{\xi}{x}\omega\sqrt{a_2}\cos(2\omega t)\gamma - \frac{d\mu x^{d-1}\frac{\xi}{x}2\omega\sqrt{a_2}\cos(2\omega t)\gamma}{1-d\mu x^{d-1}-\frac{\xi}{x}2\omega\sqrt{a_2}\cos(2\omega t)\gamma}$$

and

$$\lambda_2 = d\mu x^{d-1} + \frac{d\mu x^{d-1}\frac{\xi}{x}2\omega\sqrt{a_2}\cos(2\omega t)\gamma}{1-d\mu x^{d-1}-\frac{\xi}{x}2\omega\sqrt{a_2}\cos(2\omega t)\gamma}.$$

When $\omega = \omega_k^-$, i.e. $t = t(\omega_k^-)$, the two eigenvalues are $\lambda_2 = d\mu x^{d-1}$, which is smaller than 1, and $\lambda_1 = 1$. The first eigenvalue turns out to be smaller than 1 if $t(\omega) > t(\omega_k^-)$ and greater than 1 otherwise, while the second one is always a positive number which is smaller than 1 if ω is closed enough to ω_k^-. Accordingly, we have proved the following proposition.

Proposition 4.3.1 *System (4.2) undergoes a saddle-node bifurcation when ω passes through ω_k^- and a stable fixed point occurs near $(x(\omega_k^-), t(\omega_k^-))$ after that.*

The same argument applies to the right end ω_k^+ of the k^{th} frequency-locking interval in ω where another saddle-node bifurcation occurs and the fixed point disappear. These saddle-node bifurcations correspond to the ends of the segments of curves in Figure 4.3 and 4.4.

From Figure 4.3, it appears that there exists an invariant set near $x = 0.0022$. As $x(\omega)$ increases when ω increases for a fixed k, the question arises as to how the dynamics of the system change when the stable fixed point $(x(\omega), t(\omega))$ passes near the invariant set. We analyse this situation in the next section.

4.3.2 Global bifurcations of the system

We now turn to investigating the dynamics near the centre of the k^{th} frequency-locking window. As shown in Figure 4.5, a stable fixed point $(x(\omega), t(\omega))$ moves from below to above the invariant curve when ω increases. In between, a global bifurcation occurs and the stable fixed point dominates the whole dynamics. We will show that the phenomena which happen here are just like the bifurcation which occur in the well-known forced damped pendulum.

Let $(\hat{x}, \omega_k)$ satisfy

$$\begin{cases} \hat{x} &= \mu\hat{x}^d + \gamma \\ \mu_3 - \xi \log \hat{x} &= \frac{k\pi}{\omega_k} \end{cases}.$$

Clearly, $\omega_k = \frac{k\pi}{\mu_3 - \xi \log \hat{x}} \approx \frac{k\pi}{\mu_3 - 3/e \log \hat{x}}$ since $\xi = \frac{1}{e}(1 + c/e + c^2/e^2) \approx 3/e$ for $\epsilon \ll 1$.

Consider points (x, ω) near $(\hat{x}, \omega_k)$. We define the new variables (y, λ) by letting $x_n = \hat{x}(1 + y_n)$ and $\mu_3\omega - \frac{3\omega}{e} \log \hat{x} = k\pi + \frac{3\omega_k}{e}\lambda$, and we consider $|y|$ and $|\lambda|$ to be small. We also define $s_n = 2\omega t_n$ and substitute into (4.2). Then

$$\begin{aligned} \bar{x} = x_{n+1} = \hat{x}(1 + y_{n+1}) &= \mu\hat{x}^d(1 + y_n)^d + \gamma(1 + \sqrt{a_2}\sin s_n) \\ &= (\hat{x} - \gamma)(1 + dy_n + O(y_n^2)) + \gamma(1 + \sqrt{a_2}\sin s_n) \\ &= (\hat{x} - \gamma)(1 + y_n) + (\hat{x} - \gamma)\left(\epsilon y_n + O(y_n^2)\right) \\ &\quad + \gamma(1 + \sqrt{a_2}\sin s_n) \end{aligned}$$

Since $|x_n - \hat{x}| \sim O(\gamma)$, we have $|y_n| \sim O(\hat{x}^{-1}\gamma)$. Therefore, $|\hat{x}y_n| \sim O(\gamma)$ and $|\hat{x}y_n^2| \sim O(\hat{x}^{-1}\gamma^2)$. It then follows that

$$\begin{aligned} \bar{x} &= (\hat{x} - \gamma)(1 + y_n) + \gamma(1 + \sqrt{a_2}\sin s_n) + O(\epsilon\gamma) + O(\hat{x}^{-1}\gamma^2) \\ &\approx (\hat{x} - \gamma)(1 + y_n) + \gamma(1 + \sqrt{a_2}\sin s_n) \end{aligned},$$

for small enough ϵ and for some p such that $\gamma^{1/p} \leq \hat{x}$. This implies

$$y_{n+1} - y_n = \gamma\hat{x}^{-1}(-y_n + \sqrt{a_2}\sin s_n).$$

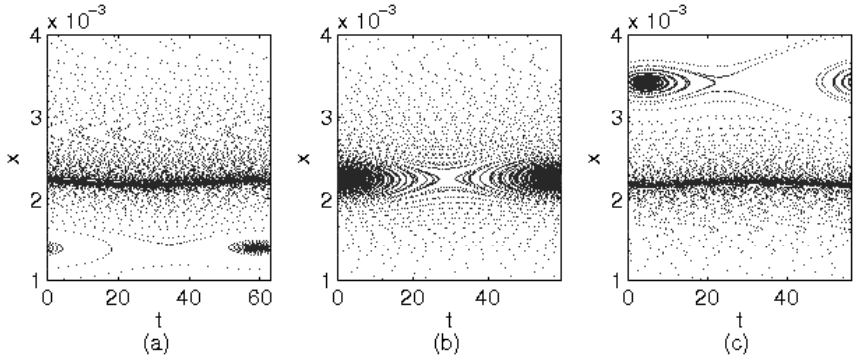

Figure 4.5: The dynamics of the system (4.2) at (a) $\omega = 0.05$, (b) $\omega = 0.053$ and (c) $\omega = 0.056$, for $c = 0.2001$, $e = 0.2$, $\mu_3 = 27$ and $\gamma = 2 \cdot 10^{-5}$. We plot all the transient points of five initial points to find their asymptotic attractors. Figure (a) and (c) show that the stable fixed point exists alongside the invariant curve. As ω increasing, the stable fixed point moves from below the invariant curve, before it intersects and destroys the invariant curve as shown in figure (b), toward above the invariant curve, which reappears for large enough ω. (For schematic diagrams of these three scenarios, see Figure 4.6 (b), (d) and (f).)

As for the s_n terms, using (4.2) we obtain

$$\begin{aligned} 2\omega(\bar{t} - t) = s_{n+1} - s_n &= 2\omega\mu_3 - \tfrac{6\omega}{e}(\log \hat{x} + \log(1 + y_{n+1})) \\ &= 2\omega\mu_3 - \tfrac{6\omega}{e}(\log \hat{x} + y_{n+1}) + O(y_{n+1}^2) \cdot \\ &\approx \tfrac{6\omega_k}{e}\lambda - \tfrac{6\omega}{e}y_{n+1} \end{aligned}$$

Therefore,

$$\begin{cases} \frac{y_{n+1}-y_n}{\hat{x}^{-1}\gamma} &= -y_n + \sqrt{a_2}\sin s_n \\ \frac{s_{n+1}-s_n}{\hat{x}^{-1}\gamma} &= \frac{6\omega_k}{e\hat{x}^{-1}\gamma}(\lambda - \frac{\omega}{\omega_k}y_{n+1}) \end{cases} .$$

Since $\gamma^{1/p} \le \hat{x} \le x_m$ for some fixed $p > 1$, we have $\hat{x}^{-1}\gamma \to 0$ if $(\epsilon, \gamma) \to 0$ within Φ_p (see section 4.2). Hence, the last system above can then be well

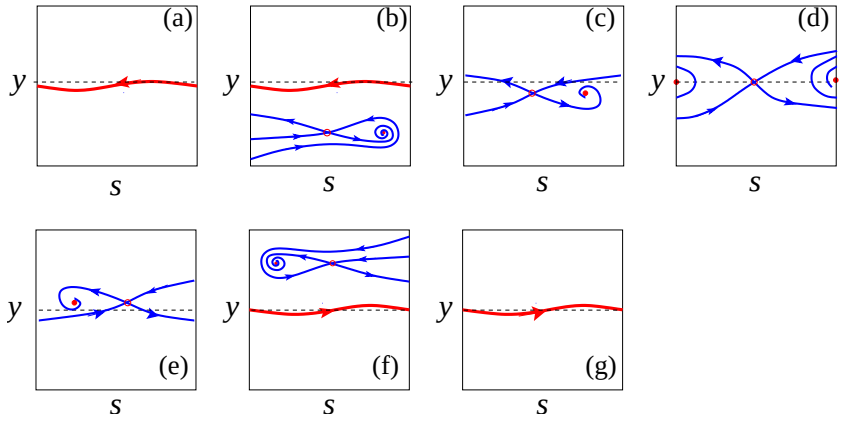

Figure 4.6: The schematic diagram depicted seven scenarios of the attractor(s) of the system (4.2) and (4.7) for the cases $\lambda < 0$ ((a), (b) and (c)), $\lambda = 0$ ((d)), and $\lambda > 0$ ((e), (f) and (g)). The red points denote the fixed points: one stable (solid) and another one unstable. The one-dimensional invariant curve is also coloured in red if it exists. The blue curves are the stable and unstable manifold of the unstable fixed points. The dashed line denotes $y = 0$. As ω increases, i.e. λ moves from negative to positive, a pair of fixed points appear through a saddle-node bifurcation ((a)→(b)); the system then undergoes a global bifurcation (as is shown in (c)) when the invariant curve disappear; the fixed points then move from below to above the line $y = 0$ ((c),(d) and (e)); another global bifurcation happens (as is shown in (e)) and the invariant curve reappears; this pair of fixed points then disappear through another saddle-node bifurcation ((f)→(g)).

approximated by the continuou-time dynamical system

$$\begin{cases} \dot{y} &= -y + \sqrt{a_2}\sin s \\ \dot{s} &= \eta^2(\lambda - \frac{\omega}{\omega_k}y) \end{cases}, \tag{4.4}$$

where $\eta^2 = 6\omega_k/(e\hat{x}^{-1}\gamma)$ is a parameter.

Figure 4.7 displays that the ODE system (4.4) does possess similar dynamics as the map system (4.2) near ω_k. Here, we take $\omega_k = 0.053$ and $\hat{x} = 2.2 \cdot 10^{-3}$, for the case $c = 0.2001$, $e = 0.2$, $\mu_3 = 27$ and $\gamma = 2 \cdot 10^{-5}$. The parameters η and λ are computed according to their definitions.

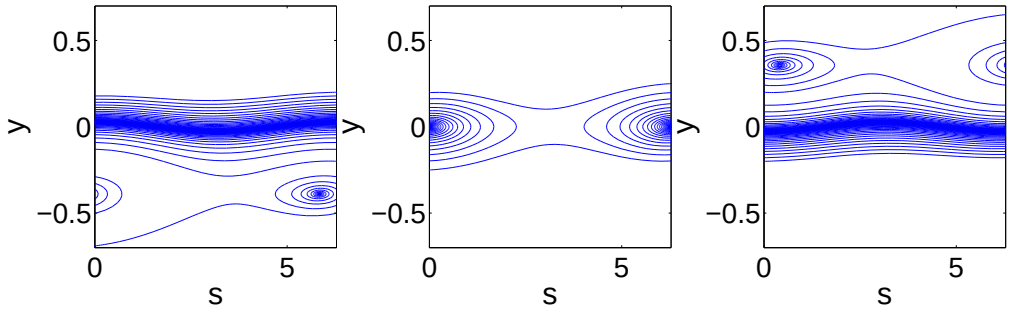

Figure 4.7: The dynamics of the system (4.4) at (a) $\omega = 0.05$ ($\lambda = -0.3725$), (b) $\omega = 0.053$ ($\lambda = 0$) and (c) $\omega = 0.056$ ($\lambda = 0.3725$), for $c = 0.2001$, $e = 0.2$, $\mu_3 = 27$ and $\gamma = 2 \cdot 10^{-5}$. We take $\omega_k = 0.053$ and $\hat{x} = 2.2 \cdot 10^{-3}$. The curves are the transients of three initial points and the fixed points are $y = \frac{\omega_k}{\omega}\lambda$. Comparing to figure 4.5, the ODE system (4.4) demonstrates similar dynamics as the map system (4.2) near ω_k. (For schematic diagrams of these three scenarios, see Figure 4.6 (b), (d) and (f).)

Combining the two equations in (4.4), we obtain

$$\begin{aligned} \ddot{s} &= -\eta^2 \tfrac{\omega}{\omega_k}\dot{y} \\ &= \eta^2 \tfrac{\omega}{\omega_k} y - \eta^2 \tfrac{\omega}{\omega_k}\sqrt{a_2}\sin s \\ &= -\dot{s} + \eta^2\lambda - \eta^2 \tfrac{\omega}{\omega_k}\sqrt{a_2}\sin s \end{aligned} \quad .$$

After rescaling time derivatives by $d/dt \to \eta d/dt$ and s by $s \to (\omega/\omega_k)\sqrt{a_2}s$, we obtain the canonical equation for a damped pendulum with constant torque:

$$\ddot{s} + \eta^{-1}\dot{s} + \sin s = \frac{\omega_k}{\omega}\sqrt{a_2}^{-1}\lambda. \tag{4.5}$$

Physically, the $\eta^{-1}\dot{s}$ term corresponds to linear friction: oscillations are strongly damped when η is small. The $\sqrt{a_2}^{-1}\lambda$ term corresponds to a constant applied torque.

The dynamics of equation (4.5) are quite simple and have been fully investigated ([15, 35, 6]). If $|\frac{\omega_k}{\omega}\sqrt{a_2}^{-1}\lambda| > 1$, the only invariant set is a stable periodic

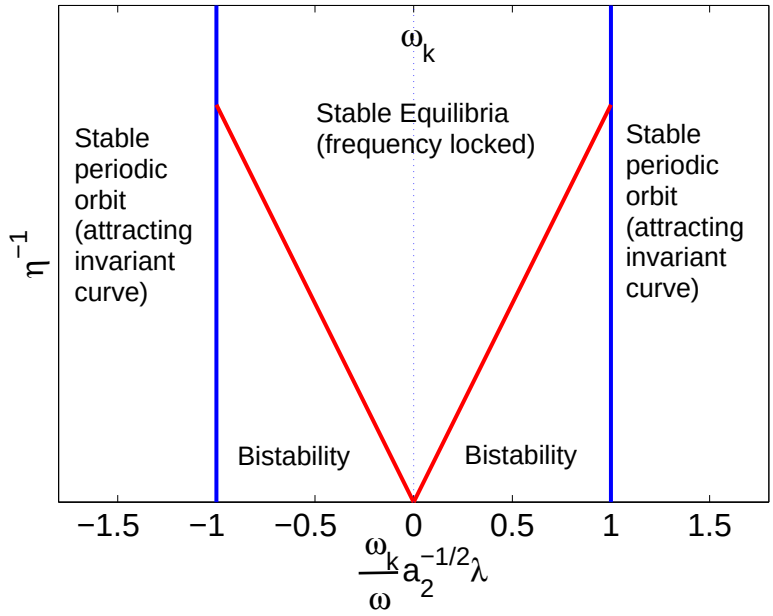

Figure 4.8: The bifurcation diagram of the forced pendulumn with torque (4.5) which is equivalent to our Poincaré map (4.2 for ϵ small enough. . In our map (4.2), the centre of the k^{th} frequency-locking interval in ω is denoted by ω_k, η is a constant and λ is relative to $|\omega - \omega_k|$. As ω moves away from ω_k, we expect to see the changes of the dynamics from frequency-locked only to bistability and then to an attracting invariant curve only.

orbit. If $|\frac{\omega_k}{\omega}\sqrt{a_2}^{-1}\lambda| < 1$ and η^{-1} is large, then only equilibria exist. However, bistability may occur when $|\frac{\omega_k}{\omega}\sqrt{a_2}^{-1}\lambda| < 1$ and η^{-1} is small. In this case, the stable equilibria and periodic orbit coexist. See Figure 4.8 for the bifurcation diagram of (4.5).

We now use this analysis to explain the dynamics of system (4.2) for small ϵ. Firstly, note that $\eta^{-1} \to 0$ as $\hat{x}^{-1}\gamma \to 0$. In other words, (4.2) can be well approximated by the ODE equation (4.5) for small enough η^{-1}. Therefore, as ω moves away from ω_k, i.e. $\frac{\omega_k}{\omega}\sqrt{a_2}^{-1}\lambda$ moves away from 0, the dynamics of the system (4.2) will also change from only frequency-locking to bistability, and then

to having only a stable invariant curve, as was shown in Figure 4.6.

Therefore, we have proved the following proposition:

Proposition 4.3.2 *The dynamics of the system (4.2) are equivalent to the dynamics of a damped pendulum with constant torque (4.5) near the centres of each of the frequency-locking intervals when the parameters ϵ and γ are both sufficiently small as long as $(\epsilon, \gamma) \in \Phi_p$ for some $p > 1$.*

4.3.3 The dynamics for ω near 0

As was shown in 4.3.2, a one-dimensional attractor exists near the center of each frequency-locking intervals except when the fixed point attractor dominate the whole dynamics. However, we are not sure if this is always the case for general ω although our numerical simulation suggests that this one-dimensional attractor always exists for all ω. In this section, we prove the existence of this one-dimensional attractor for ω small enough.

We first prove a similar theorem analogous to Afraimovich's Theorem 4.2.1 which provides a sufficient condition for the existence of an invariant curve as the maximal attractor for their map (3.26). As we have discussed in section 4.2, their result is only valid for $x \sim O(\gamma^d)$, which is irrelevant to the original ODE system. Nevertheless, this is also true for the case $x \gg O(\gamma^d)$, i.e. d near 1.

Consider the following system $(\overline{x}, \overline{\theta}) = F(x, \theta)$ defined by:

$$\begin{cases} \overline{x} &= \mu x^d + \gamma(1 + a \sin\theta) \\ \overline{\theta} &= \theta + \tilde{\omega} - \tilde{\eta} \log \overline{x}. \end{cases} \tag{4.6}$$

Fix γ. Recall that $\hat{x}$ satisfies the equation $\hat{x} = \mu \hat{x}^d + \gamma$ and suppose $\hat{x}$ is of order $\gamma^{1/p}$ for some $p > 1$, which is sufficiently large such that $\hat{x} \gg r$. This can be done by letting d be close enough to 1. We begin by proving that

$$D = \left\{ (x, \theta) : 0 < \hat{x} - \frac{2a}{1 - d\mu\hat{x}^{d-1}}\gamma \leq x \leq \hat{x} + \frac{2a}{1 - d\mu\hat{x}^{d-1}}\gamma,\ 0 \leq \theta \leq 2\pi \right\} \tag{4.7}$$

is an invariant region for F.

Lemma 4.3.1 *D is an invariant region for F.*

Proof: Denote $\bar{A} = \frac{2a}{1-d\mu\hat{x}^{d-1}}$. If $(x,\theta) \in D$, then, by Taylor expanding the first term of the following inequality,

$$\begin{aligned}
\bar{x} &\leq \mu(\hat{x} + \bar{A}\gamma)^d + \gamma(1 + a\sin\theta) \\
&= \mu\hat{x}^d + \gamma d\mu\hat{x}^{d-1}\bar{A} + \gamma + \gamma a\sin\theta + O(\gamma^2) \\
&= \hat{x} + \gamma d\mu\hat{x}^{d-1}\bar{A} + \gamma a\sin\theta + O(\gamma^2) \\
&\leq \hat{x} + \gamma(d\mu\hat{x}^{d-1}\bar{A} + a) + O(\gamma^2) \\
&= \hat{x} + \gamma\frac{a+ad\mu\hat{x}^{d-1}}{1-d\mu\hat{x}^{d-1}} + O(\gamma^2) \\
&< \hat{x} + \bar{A}\gamma + O(\gamma^2),
\end{aligned}$$

since $d\mu\hat{x}^{d-1} < d\mu x_m^{d-1} = 1$ by the definition of x_m in section 4.2. Similarly, $\hat{x} - \bar{A}\gamma$ provides a lower bound for $\bar{x}$ of F in D since

$$\begin{aligned}
\bar{x} &\geq \mu(\hat{x} - \bar{A}\gamma)^d + \gamma(1 + a\sin\theta) \\
&= \mu\hat{x}^d - \gamma d\mu\hat{x}^{d-1}\bar{A} + \gamma + \gamma a\sin\theta + O(\gamma^2) \\
&= \hat{x} - \gamma d\mu\hat{x}^{d-1}\bar{A} + \gamma a\sin\theta + O(\gamma^2) \\
&\geq \hat{x} - \gamma(d\mu\hat{x}^{d-1}A + a) + O(\gamma^2) \\
&= \hat{x} - \gamma\frac{a+ad\mu\hat{x}^{d-1}}{1-d\mu\hat{x}^{d-1}} + O(\gamma^2) \\
&> \hat{x} - \bar{A}\gamma + O(\gamma^2).
\end{aligned}$$

Hence, D is an invariant region for F. ■

This lemma implies the existence of an attractor for F in D. However, we cannot at the moment identify what it looks like. The 'Annulus Principle' provides sufficient conditions for F to possess an invariant closed curve as its maximal attractor. Here, the maximal attractor of F in D is defined to be $\cap_{n=1}^{\infty} F^n(D)$.

Theorem 4.3.1 *("Annulus Principle" [2]) Let $\Psi : (x,\theta) \longrightarrow (\bar{x},\bar{\theta}), x \in \mathbb{R}^n, \theta \in \mathbb{R}^m$, be a map of the form*

$$\bar{x} = f(x,\theta),\ \bar{\theta} = \theta + g(x,\theta)\ (mod\ 2\pi),$$

where f, g are differentiable functions which are 2π-periodic in $\theta = (\theta_1, \ldots, \theta_m)$. Assume that Ψ maps an annulus $D = \{(x, \theta) : |x| \leq r_0\}$, $r_0 > 0$, into its interior. Introduce the following norms of vectors or matrices in D: $\|\cdot\| = \sup_{(x,\theta)\in D} |\cdot|$, where $|\cdot|$ is the Euclidean norm. If

$$(a) \quad \|(I + g_\theta)^{-1}\| < \infty,$$

$$(b) \quad \|f_x\| < 1,$$

$$(c) \quad 1 - \|(I + g_\theta)^{-1}\| \cdot \|f_x\| > 2\sqrt{\|(I + g_\theta)^{-1}\|^2 \cdot \|g_x\| \cdot \|f_\theta\|},$$

$$(d) \quad 1 + \|(I + g_\theta)^{-1}\| \cdot \|f_x\| < 2\|(I + g_\theta)^{-1}\|,$$

where I is the $m \times m$ identity matrix and subscripts indicate differentiation with respect to the corresponding variables, then the maximal attractor in D is an invariant m-dimensional torus which is the graph of some function $x = h(\theta)$, where h is $2\pi-$periodic in θ, and is smooth.

Now, we are ready to prove the following theorem:

Theorem 4.3.2 *Suppose d and γ take values so that $\hat{x} \gg \gamma$. Then there exists a constant δ, depending on d and γ, such that if $\tilde{\eta}a < \delta$ and $a < \frac{(x_m - \hat{x})(1 - d\mu\hat{x}^{d-1})}{2\gamma}$, then there exists an invariant closed curve as the maximal attractor for F in D.*

Recall that x_m is defined to satisfy $d\mu x_m^{d-1} = 1$.

Proof: Within and only within this proof, let $f(x, \theta) = \mu x^d + (1 + a\sin\theta)\gamma$, $g(x, \theta) = \tilde{\omega} - \tilde{\eta}\log\overline{x}$, $M = \hat{x} + \frac{2a}{1 - d\mu\hat{x}^{d-1}}\gamma$ and $m = \hat{x} - \frac{2a}{1 - d\mu\hat{x}^{d-1}}\gamma$. Since $a < \frac{(x_m - \hat{x})(1 - d\mu\hat{x}^{d-1})}{2\gamma}$, $M < x_m$.

Let $(x, \theta) \in D$. We proceed to check each of the conditions (a)-(d) in turn.

(a)

$$|g_\theta| = \left| -\frac{\tilde{\eta}a\cos\theta\gamma}{\mu x^d + (1 + a\sin\theta)\gamma} \right|.$$

It is easy to prove that for each fixed x, the maximal value of the right hand side in this last equality when varying θ is

$$\frac{\tilde{\eta}a\gamma}{\sqrt{(\mu x^d + r)^2 - a^2\gamma^2}},$$

which is smaller than 1 for $\tilde{\eta}a$ small enough. In this case,

$$\|(1+g_\theta)^{-1}\| = \frac{1}{1-\frac{\tilde{\eta}a\gamma}{\sqrt{(\mu m^d+r)^2-a^2\gamma^2}}} < \infty$$

is always satisfied.

(b) $\|f_x\| = \|d\mu x^{d-1}\| = d\mu M^{d-1} < d\mu x_m^{d-1} = 1$ since $\hat{x}$ is smaller than x_m and $d\mu x_m^{d-1} = 1$ by the definition of $\hat{x}$ and x_m in section 4.2.

(c) $\|g_x\| = \|-\tilde{\eta}\frac{d\mu x^{d-1}}{\mu x^d+\gamma(1+a\sin\theta)}\| < \tilde{\eta}\frac{d\mu M^{d-1}}{m}$ since $\mu x^d+\gamma(1+a\sin\theta) > m$ by Lemma 4.3.1 and $\|f_\theta\| = a\gamma$. By letting $\tilde{\eta}a \to 0$, $\|(1+g_\theta)^{-1}\|$ will tend to 1 and $\|g_x\|\|f_\theta\|$ will tend to 0. Thus, the third condition of the 'Annulus Principle' is clearly true.

(d) Since $\|(1+g_\theta)^{-1}\|(2-\|f_x\|) \to 2-\|f_x\| > 1$ as $\tilde{\eta}a \to 0$, the fourth condition is also valid.

Hence, the conditions of Theorem 4.3.1 are met in our case, for $\tilde{\eta}a$ sufficiently small, so we are done.■

Theorem 4.3.2 completes the case which is not considered by Afraimovich in the proof of Theorem 4.2.1 in [3]. More precisely, recall that Afraimovich's map (3.26):

$$\begin{cases} \bar{x} = A(Bx+\gamma(1+a\sin t))^d \\ \bar{t} = t+\bar{\omega}-\eta\log(Bx+\gamma(1+a\sin t)) \ (mod\ 2\pi) \end{cases}.$$

They prove that for the case if $x \sim O(\gamma^d)$, i.e. d is large, there exists an invariant curve as a maximal attractor for the system (3.26) if the conditions in Theorem 4.2.1 are satisfied. For the case d near 1, the first equation of this map is

$$\begin{aligned} \bar{x} &= A\left[(Bx)^d+\gamma d(Bx)^{d-1}(1+a\sin t)+O(\gamma^2)\right] \\ &\approx AB^dx^d+\gamma(1+a\sin t)+O(\gamma^2) \end{aligned},$$

for $|d-1|$ small enough, while the second equation of this map is

$$\begin{aligned} \bar{t} &= t+\bar{\omega}-\tfrac{\eta}{d}(\log\bar{x}-\log A) \\ &= t+\tilde{\omega}-\tilde{\eta}\log\bar{x}. \end{aligned}$$

In other words, Afraimovich's map (3.26) is equivalent to the map (4.6) when d is near 1. It follows that, by Theorem 4.3.2, if the corresponding conditions are satisfied, then their map (3.26) also has an invariant curve as its maximal attractor for d near 1.

In our case, $\theta = 2\omega t$, $a = \sqrt{a_2}$ and $\eta = 2\omega\xi$. Note that the definition of the invariant set D in (4.7) depends on ω. Nevertheless, since $\sqrt{a_2} \nearrow 1$ as $\omega \searrow 0$, we can always find an uniform invariant set D_0, which is independent of ω, by replacing a by 1. Then, because both $\eta a = 2\omega\xi\sqrt{a_2}$ and a tend to 0 as $\omega \to 0$, we have

Corollary 4.3.1 *Suppose d and γ are such that $\hat{x} \gg \gamma$. Then there exists an ω_0, depending on d and γ, such that if $\omega < \omega_0$, then system (4.2) has an invariant closed curve as its maximal attractor in D_0.*

4.4 ϵ large

For large enough ϵ, by the results in section 4.2, x^d becomes far smaller than γ. In this case, the whole dynamics of the first equation of (3.24) depends on all the terms except x^d. Therefore, our Poincaré map can be further approximated by dropping the x^d term to take

$$\begin{cases} \bar{x} = f_1(x,t) = \gamma[\mu_1 + \mu_2(-a_1\cos(2\omega g) - b_1\sin(2\omega g)) \\ \qquad\qquad -\mu_4(-a_1\cos(2\omega(\bar{t}-\delta_3)) - b_1\sin(2\omega(\bar{t}-\delta_3))) \\ \qquad\qquad -\mu_5(-a_2\cos(2\omega\bar{t}) - b_2\sin(2\omega\bar{t}))] + O(\gamma^2) \\ \bar{t} = f_2(x,t) = g - \gamma\frac{\xi}{2e}[1 - a_2\cos(2\omega t) + b_2\sin(2\omega t)]x^{-1} + O(\gamma^2) \end{cases}, \quad (4.8)$$

where $g = t + \mu_3 - \xi\log x$.

This system is far more complicated than the system (4.2) and firstly we will deal with two extreme cases: $\omega \gg 1$ (section 4.4.1) and $\omega \ll 1$ (section 4.4.2).

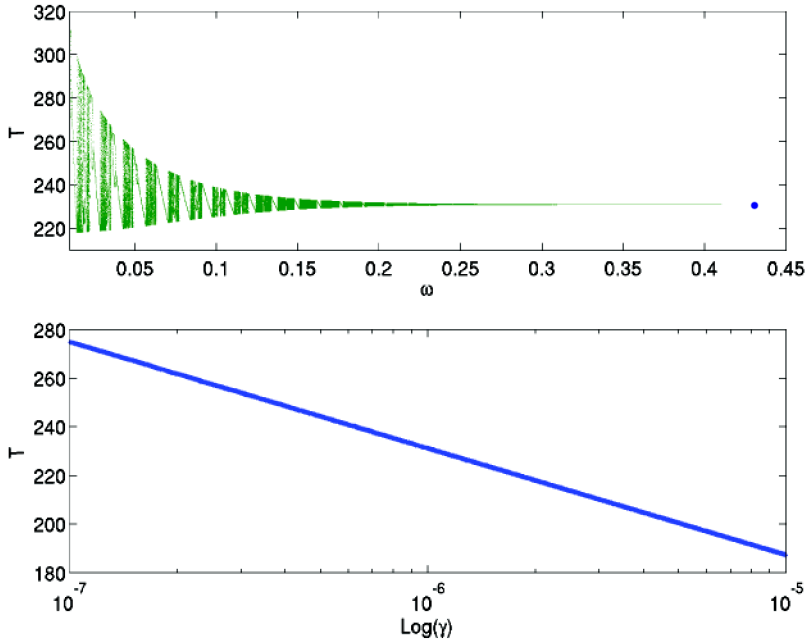

Figure 4.9: The dynamics when $\omega \to \infty$. The upper subplot shows that the ODEs system tends to the averaged one (a blue dot on the right end). The linear relationship between period T and $\log \gamma$ is displayed on the lower subplot. The slope of this line is equal to ξ. The graphs are plotted for parameter values $c = 0.25, e = 0.2$ and $\gamma = 10^{-6}$.

In general, both cases provide circle map dynamics. Numerical results will be displayed in section 4.4.3 for the case of intermediate values of ω, where detailed analytical study is not possible.

4.4.1 The dynamics for large ω

From the first equation of (4.8), we see that $|x_n - \mu_1\gamma| \sim O(\gamma^2)$ as $\omega \to \infty$. The second equation of (4.8) indicates that the limit of the spending time of the map,

$T_n = t_{n+1} - t_n$, will be

$$\begin{aligned} T &= \mu_3 - \xi \log(\mu_1\gamma + O(\gamma^2)) - \gamma\tfrac{\xi}{2e}\tfrac{1}{\mu_1\gamma+O(\gamma^2)} + O(\gamma^2) \\ &= \mu_3 - \tfrac{\xi}{2e\mu_1} - \xi\log(\mu_1\gamma) + O(\gamma) \\ &= C_1 - \xi\log\gamma + O(\gamma), \end{aligned}$$

where $C_1 = \mu_3 - \frac{\xi}{2e\mu_1} - \xi\log\mu_1$ is a constant.

In the limit $\omega \to \infty$, we expect that the forcing term of our ODE system (3.23) can be replaced by the averaged one $\frac{1}{2}(1-x)\gamma$. In fact, the differences between the Poincaré maps of the ODE systems for the perturbation function $\frac{1}{2}$ and $\sin^2(\omega t)$ are those terms in (4.8) with sin and cos which tend to 0 as $\omega \to \infty$.

Note that the above argument is also valid for the case ϵ near 0. But now, $\hat{x}$ becomes the asymptotic attractor for the $x-$dynamics as $\omega \to \infty$. Therefore, we have proved the following proposition

Proposition 4.4.1 *The dynamics of the system (3.23) will tend to the averaged one as $\omega \to \infty$. For a given γ, if ϵ is large enough, then the period of the attracting periodic orbit $T \approx C_1 - \xi\log\gamma$ for some constant C_1.*

The computational results also confirm this fact, (see Figure 4.9), and they also demonstrate the linear relationship between T and $\log\gamma$ for large ω. The slope takes the value ξ which provides another independent confirmation of the analytic reduction carried out in Chapter 3.

Taking ω large enough such that $a_1 \approx a_2 \sim O(\gamma)$, then $x \approx \mu_1\gamma$. Substituting this into the second equation of (4.8), we have

$$\begin{aligned} \bar{t} &= t + \mu_3 - \xi\log(\mu_1\gamma) - \tfrac{\xi}{2e\mu_1}(1 - \sqrt{a_2}\sin(2\omega t)) \\ &= t + \nu + \tfrac{\xi\sqrt{a_2}}{2e\mu_1}\sin(2\omega t) \end{aligned},$$

where $\nu = \mu_3 - \xi\log(\mu_1\gamma) - \frac{\xi}{2e\mu_1}$. Let $s = \frac{\omega}{\pi}t$, then

$$\begin{aligned} \bar{s} &= s + \tfrac{\omega}{\pi}\nu + \tfrac{\xi\omega\sqrt{a_2}}{2\pi e\mu_1}\sin(2\pi s) \\ &\approx s + \tfrac{\omega}{\pi}\nu + \tfrac{\xi}{4\pi\mu_1}\sin(2\pi s) \end{aligned}, \tag{4.9}$$

since $\sqrt{a_2} \approx \frac{e}{2\omega}$ when $\omega \gg 1$. (4.9) is actually the canonical family of the circle maps

$$\bar{\theta} = \theta + \alpha + \frac{\beta}{2\pi}\sin(2\pi\theta),$$

which are invertible if $\beta < 1$ and noninvertible if $\beta > 1$ as discussed in section 2.3.2. Comparing to this, we see that letting ω tend to ∞ in our map (4.9) is equivalent to letting α tend to ∞ and fixing $\beta = \frac{\xi}{2\mu_1}$ in the canonical family of the circle maps. Therefore, we have proved the following proposition:

Proposition 4.4.2 *For large enough ω, there exists a constant μ_0 near $\xi/2$ such that (i) if $\mu_1 > \mu_0$, system (3.24) is equivalent to the canonical family of invertible circle map; (ii) if $\mu_1 < \mu_0$, it is equivalent to the noninvertible ones.*

In conclusion, the map (4.8) is roughly a periodic oscillator for ω near ∞. However, in detail, it still demonstrates a rather complicated dynamics as that of the canonical circle map.

4.4.2 The dynamics for ω near 0

In this section, we consider the other limiting case, $\omega \to 0$. In this case, $a_1 \approx a_2$ and $b_1 \approx b_2$. The map (4.8) can then be further simplified to the form

$$\begin{cases} f_1(x,t) &\approx \mu_1\gamma + \Big(\mu_2\sqrt{a_1}\sin(2\omega g + \theta) + \mu_4\sqrt{a_1}\sin(2\omega(\bar{t} - \delta_3) + \theta) \\ &\quad + \mu_5\sqrt{a_1}\sin(2\omega\bar{t} + \theta)\Big) \\ f_2(x,t) &\approx t + \mu_3 - \xi\log(x) - \frac{\xi}{2e}(1 - \sqrt{a_1}\cos(2\omega t))x^{-1}\gamma, \end{cases} \tag{4.10}$$

where $\theta = \tan^{-1}\frac{a_1}{b_1} \approx \tan^{-1}\frac{a_2}{b_2} \approx \frac{\pi}{2}$.

We will take μ_5 near $-\mu_1$ to satisfy the assumption (A.1), and drop the μ_2 and μ_4 terms for simplicity. In other words, we are looking at the dynamics in the parameter space where μ_2 and μ_4 near 0. In this case, $x = \mu_1\gamma(1 - \sqrt{a_1}\cos(2\omega t))$

is clearly an invariant curve for the system. Therefore, substituting this expression for $x(t)$ into (4.10), the whole dynamics can be represented by a one-dimensional map

$$\bar{t} = h(t) = t + \nu - \xi \log(1 - \sqrt{a_1}\cos(2\omega t)),$$

where $\nu = \mu_3 - \xi \log(\mu_1 \gamma) - \frac{\xi}{2e\mu_1}$.

Let $s = \omega t/\pi$ to normalize the effect of ω, the last equation then becomes

$$\bar{s} = h(s) = s + \frac{\omega}{\pi}\nu - \frac{\omega}{\pi}\xi \log(1 - \sqrt{a_1}\cos(2\pi s)). \tag{4.11}$$

Numerical simulation shows that the dynamics of (4.11) fit the dynamics of the original ODE system (3.23) very well. See Figure 4.10. Here, we take $\nu = 232$. A sequence of periodic windows with period n, for $n = 2, 3, 4, ...$, can be easily observed when we track ω down to 0.

Equation (4.11) is the lift of a degree 1 circle map defining on $[0, 1)$ and, because $\sqrt{a_1}$ is near 1, this map will never be a homeomorphism for all $\omega > 0$. More precisely, the equation $h'(s) = 1 + \frac{2\omega\xi\sqrt{a_1}\sin(2\pi s)}{1-\sqrt{a_1}\cos(2\pi s)} = 0$ has at least one solution for all ω because the upper bound of the absolute value of the last term is $\frac{2\omega\xi\sqrt{a_1}}{\sqrt{1-a_1}} = c/e + (c/e)^2 + (c/e)^3$ which is larger than 3 since $c/e > 1$.

As we have mentioned in section 2.3.2, this kind of maps can demonstrate more complicated dynamics than their homeomorphism counterparts as they can possess rotation intervals instead of rotation numbers. Figure 4.11 shows the rotation intervals of the map (4.11) which indicate the positions where the system (4.11) has infinitely many periodic solutions. Recall that the rotation interval is defined by $\rho(f) = [\rho(f_-),\ \rho(f_+)]$, where $f_-(s)$ is the largest monotone function which is smaller than $f(s)$ and $f_+(s)$ is the smallest monotone function which is larger than $f(s)$. The definition of $\rho(f)$ is, as usual, the set of all possible rotation

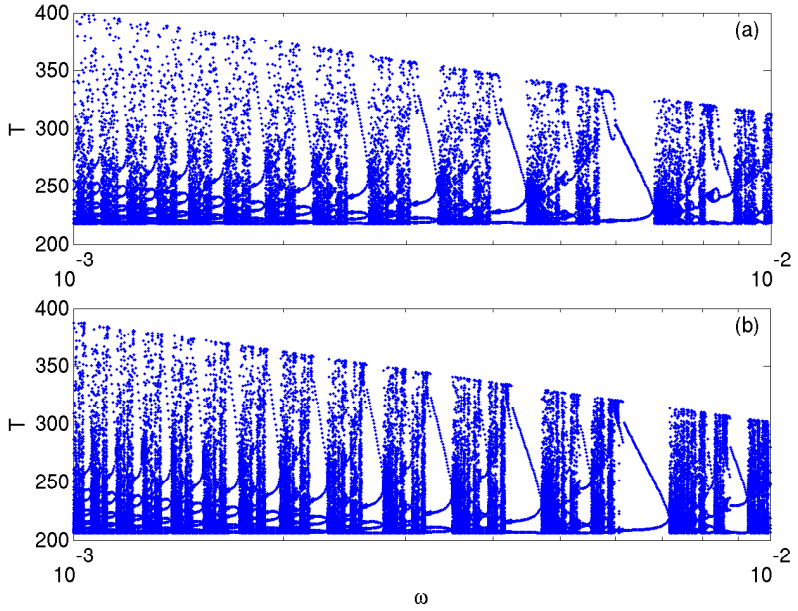

Figure 4.10: The dynamics of (a) the ODE system (3.23) and (b) the map (4.11) for $\omega \in [10^{-3}, 10^{-2}]$. Here we set the ω-axis to be log-scaled. In both the ODE system and the map, we can see that period-2, period-3,..., periodic solutions exist when ω decreases toward 0. Each period-k solution appears due to a saddle-node bifurcation and then disappears through a sequence of period-doubling cascade. This is an indication that both systems can demonstrate chaotic dynamics in some intervals of ω.

numbers:

$$\rho(f, x) = \lim_{n\to\infty} \frac{f^n(x) - x}{n},$$

for different initial points x. Since f_- and f_+ are monotone, $\rho(f_-)$ and $\rho(f_+)$ are not sets but two single values. Figure 4.11 is plotted by calculating numerically the rotation numbers of f_- and f_+ for each ω.

By R.S. MacKay and C. Tressers' result [49], a non-trivial rotation interval of f implies topological chaos. As a result, system (4.11) has chaotic dynamics at those ω where it has a non-trivial rotation interval. Note that this identification

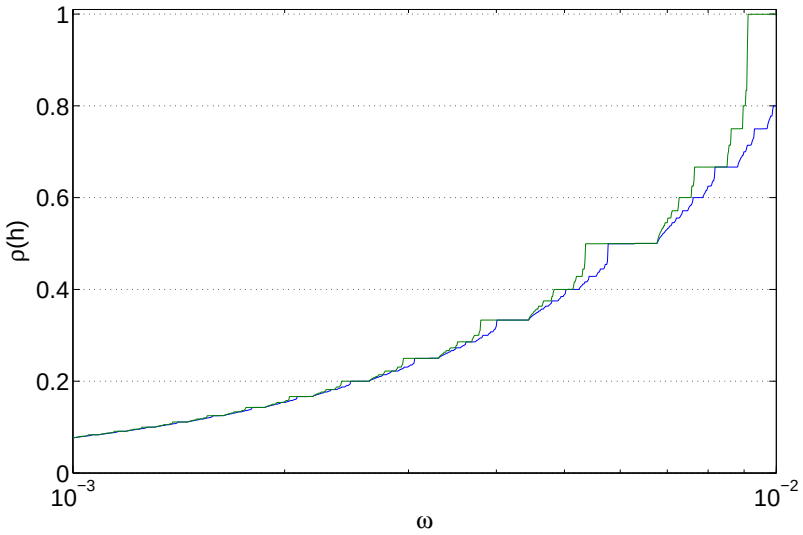

Figure 4.11: Rotation intervals of the map (4.11). Here we set the ω-axis to be log −scaled. For each ω, we plot the maximum (green) and minimum (blue) of all possible rotation numbers of the map (4.11). The existence of a rotation interval for some ω indicates the existence of infinitely many periodic solutions of the system for this ω.

doesn't give the whole intervals in ω where system (4.11) has chaotic dynamics. As we have displayed in section 2.3.2, R.S. MacKay and C. Tresser [49] also proved that there exist maps with frequency-locking but topological chaotic dynamics. Therefore, there might be some intervals in ω where system (4.11) is frequency-locked but chaotic.

Comparing Figure 4.10 and 4.11, we can see that the period-n solutions are located at thoses ω where $\rho(f_-) = \rho(f_+)$. Also, we can note that, the interval where period-n periodic solutions exist in Figure 4.11 is larger than in Figure 4.10. This is due to the fact that period-doubling doesn't change the rotation number. In the following, we gives a first-order estimate for these intervals.

To derive the boundaries of the regions where period-n solutions exist, we first consider a general circle map $\phi(s) = s + \alpha + \beta p(s)$, where $p(s)$ is a periodic

function with $p(s+1) = p(s)$. It is clear that a period n solution exists when $\alpha = 1/n$ and $\beta = 0$. Therefore, for β small enough, we can Taylor expand $\alpha = 1/n + a\beta + b\beta^2 + O(\beta^3)$. By induction,

$$\phi^n(s) = s + n\alpha + \beta(\sum_{k=0}^{n-1} p(\phi^k(s))).$$

Substituting the expansion of α into the equation $\phi^n(s) = s + 1$, we have

$$a = -\frac{1}{n}\sum_{k=0}^{n-1} p(s + \frac{k}{n})$$

and

$$b = -\frac{1}{n}\sum_{k=1}^{n-1} p'(s + \frac{k}{n})\left(a + \sum_{l=1}^{k} p(s + \frac{l-1}{n})\right).$$

In our case, $\alpha = \frac{\omega}{\pi}\nu$, $\beta = \frac{\omega}{\pi}\xi$ and $p(s) = -\log(1 - \sqrt{a_1}\cos(2\pi s))$ where $a_1 = \frac{c^2}{c^2+4\omega^2}$. Consider the first order estimate of the region of (α,β) where a period-n solution exists

$$\frac{\omega}{\pi}\nu = \frac{1}{n} + \frac{1}{n}\sum_{k=0}^{n-1}\log(1 - \sqrt{a_1}\cos(2\pi(s + \frac{k}{n})))\frac{\omega}{\pi}\xi,$$

and let M_n and m_n be the maximum and minimum of $\sum_{k=0}^{n-1}\log(1 - \sqrt{a_1}\cos(2\pi(s + \frac{k}{n})))$, respectively. Then

$$m_n \le \left(\frac{\omega}{\pi}\nu - \frac{1}{n}\right)\frac{n\pi}{\omega\xi} \le M_n,$$

which implies

$$\frac{\pi}{n\nu - m_n\xi} \le \omega \le \frac{\pi}{n\nu - M_n\xi}.$$

Therefore, the first order estimate of the interval in ω where a period-n solution exists is

$$\left[\frac{\pi}{n\nu - m_n\xi}, \frac{\pi}{n\nu - M_n\xi}\right].$$

This sequence of periodic intervals is actually an infinite sequence as ω tends to 0 if the only parameter ν is taken to satisfy $\nu > \xi \log 2$. More precisely, since

$$h^n(s) = s + \frac{n\omega}{\pi}\nu - \frac{\omega}{\pi}\xi \sum_{k=0}^{n-1} \log(1 - \sqrt{a_1}\cos(2\pi h^k(s))),$$

we have

$$\frac{n\omega}{\pi}\nu - \frac{n\omega}{\pi}\xi \log(1 + \sqrt{a_1}) \leq h^n(s) - s \leq \frac{n\omega}{\pi}\nu - \frac{n\omega}{\pi}\xi \log(1 - \sqrt{a_1}).$$

If $\nu > \xi \log 2$, then the lower bound of $h^n(s) - s$ is greater than 1 for large enough n and for a fixed ω since

$$\frac{n\omega}{\pi}\nu - \frac{n\omega}{\pi}\xi \log(1 + \sqrt{a_1}) > \frac{n\omega}{\pi}\xi \left(\log 2 - \log(1 + \sqrt{a_1})\right) > 0,$$

Note that, for a fixed ω, $h^n(s) - s$ are bounded smooth periodic functions of s for all n. Therefore, if we consider the sequences of the graphs $\Gamma_{n,\omega} : \{(s, h^n(s) - s)\}$, for each ω, there exists a n_ω such that if $n > n_\omega$, then the graph $\Gamma_{n,\omega}$ is above the horizontal line $\bar{L} : \{(s, 1)\}$. In addition, it is easy to see that the upper bound of $h^n(s) - s$ tends to 0 as $\omega \to 0$. In other words, those $\Gamma_{n,\omega}$ which are above the horizontal line $\bar{L}$ will eventually intersect it if we decrease ω. Since $h^n(s) - s$ is smooth, it follows that, for each fixed n, period-n solutions of (4.11) appear through a saddle-node bifurcation and disappear through another saddle-node bifurcation as ω decreases.

Hence, we have proved

Proposition 4.4.3 *For each $n \in \mathbb{N}$, if $\nu > \xi \log 2$, then there exists an interval of ω within which a period-n orbit appears for the system (4.11).*

The period-n interval can only ensure us the existence of a period-n solution. However, the occurrence of a rotation interval can be viewed as a synonymous of chaos since it indicates the existence of infinitely many periodic orbit of different periods.

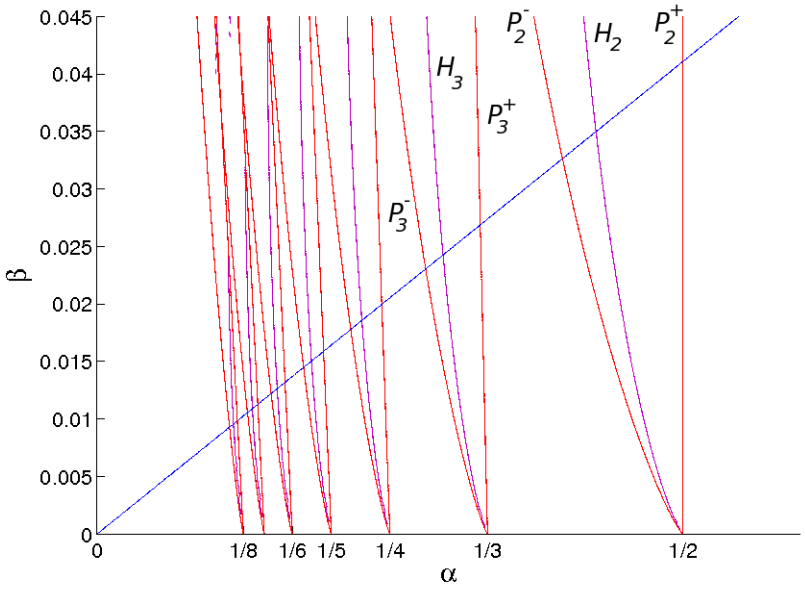

Figure 4.12: The boundaries of the Arnol'd tongues (P_n^- and P_n^+, red) and the homoclinic bifurcation curves (H_n, purple) of the map (4.11). The blue line is the points where $(\alpha,\beta) = (\frac{\omega}{\pi}\nu, \frac{\omega}{\pi}\xi)$, which is the case of (4.11). When letting ω down to 0, we are following the blue line down to the origin point. For each fixed β, if $P_n^- \le \alpha \le P_n^+$, then there exists a period-n solution. If $P_n^- \le \alpha \le H_n$, then the system has infinitely many periodic solutions including period-n due to the homoclinic bifurcation occuring at H_n.

Figure 4.12 is the bifurcation diagram of the map (4.11). The blue line denotes the points where $(\alpha,\beta) = (\frac{\omega}{\pi}\nu, \frac{\omega}{\pi}\xi)$. For each fixed ω, we have a normal Arnold's tongue picture for the map $\bar{s} = s + \alpha - \beta\log(1 - \sqrt{a_1}\cos(2\pi s))$. So for a given value of $\beta = \frac{\omega}{\pi}\xi$, we can record those α where the bifurcations occur. The red and purple curves then show the values of α where we have saddle-node (P_n^+ and P_n^-) and homoclinic bifurcations (H_n), respectively. Specifically, these P_n^+'s, P_n^-'s and H_n's are functions of β. Recall that a homoclinic cycle exists after a homoclinic bifurcation and, as we have discussed in section 2.3.2, this homoclinic cycle gives chaotic dynamics. As ω moves toward 0, we move down on the blue line and

we expect a period-n solution to occur if $\alpha \in [P_n^-,\ P_n^+]$ before the homoclinic bifurcation, after which infinitely many periodic solutions appear and coexist when $\alpha \in [P_n^-,\ H_n]$. This period-n solution then disappear when passing through the other end P_n^- of period-n region.

All in all, system (3.24) displays noninvertible circle map dynamics for ω small enough and the parameters $\mu_2, \mu_4 \approx 0$ and $\mu_5 \approx -\mu_1$. The sequence of period-n intervals always exists for every $n \in \mathbb{N}$ if μ_1 and μ_3 satisfy $\mu_3 - \xi \log(\mu_1\gamma) - \frac{\xi}{2e\mu_1} > \xi \log 2$.

4.4.3 The dynamics for intermediate values of ω

Within our Poincaré map (4.8), the dynamics are decided by two main terms coming from the derivation of local and global maps. Recall that the terms containing ωg come from local maps while those containing $\omega\bar{t}$ from global ones. When the forcing frequency ω is very small, the effect of perturbation on local map is expected to fade out because of longer spending time. In this sense, taking μ_2 to be near 0 in section 4.4.2 becomes reasonable.

As ω increasing, the dynamics of (4.8) are also affected more and more by the local terms. In other words, local and global terms compete to each other for the dynamics of (4.8) and we cannot reduce the form of our Poincaré map further. Therefore, we will only display numerical results for the dynamics of (4.8).

The numerical integration of the ODE system and the iteration of our 2D Poincaré map, in the case : $c = 0.25$, $e = 0.2$ and $\gamma = 10^{-6}$, agree very well as shown in Figure 4.13. Here, we set $\mu_1 = 9.6$, $\mu_2 = 0.3$, $\mu_3 = 17$, $\mu_4 = 26.4$ and $\mu_5 = -35.7$.

The main features of the dynamics of the ODEs system as well as the Poincaré map system are a sequence of frequency-locking areas with chaotic regions in between. At the ends of the frequency-locking intervals, the periodic orbit un-

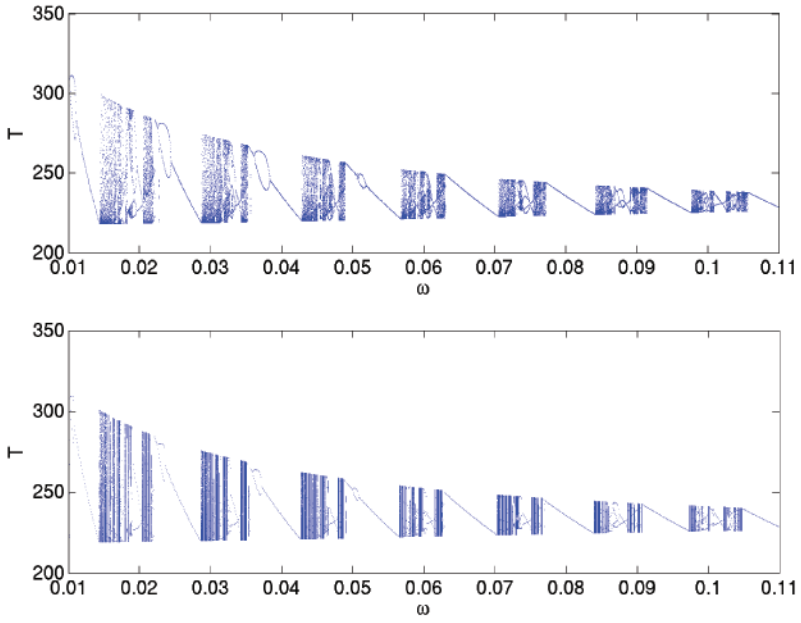

Figure 4.13: Frequency locking windows for the ODEs system (upper) and Poincaré map (lower) when $c = 0.25$, $e = 0.2$ and $\gamma = 10^{-6}$. The parameters in the Poincaré map are: $\mu_1 = 9.6$, $\mu_2 = 0.3$, $\mu_3 = 17$, $\mu_4 = 26.4$ and $\mu_5 = -35.7$.

dergoes a saddle-node bifurcation and then disappears. Figure 4.14 confirms this assertion. Denote t_n mod π/ω as t_n for simplicity. We plot t_{n+1} against t_n for fixed $\omega = 0.0428$, $c = 0.25$ and $e = 0.2$ (other parameters are the same as those in Figure 4.13).

Note also that the bistability phenomenon, which happens when d near 1, disappear. This is due to the saddle-node bifurcations, which result in the occurrence of equilibrium points, all occuring at the maxima and minima of the invariant curves when c/e is large enough. More precisely, suppose $x = h(t)$ is the invariant curve of the system and denote $x(\omega)$ is the fixed point of (4.8) if it exists. Then for those d large enough, $\max_t h(t)$ at $\omega_k^+ = x(\omega_k^+)$ and $\min_t h(t)$ at $\omega_k^- = x(\omega_k^-)$, where ω_k^+, ω_k^- are the end points of the k^{th} frequency-locking interval of ω. In contrast,

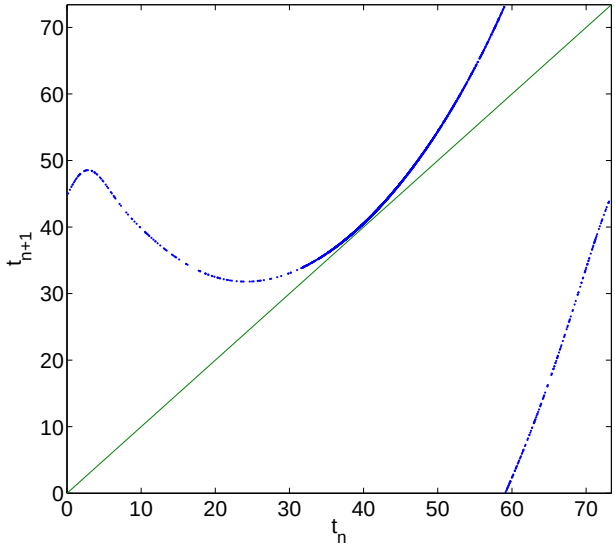

Figure 4.14: Circle-map-like dynamics. We plot t_{n+1} against t_n for fixed $\omega = 0.0428$ $e = 0.2$ and $c = 0.25$.

the invariant curve is around $\hat{x} + O(\gamma)$ which is far away from $x(\omega_k^+)$ and $x(\omega_k^-)$ in the case d near 1.

Although the disappearance of the bistability looks just like the result of increasing η^{-1} in the forced damped pendulum system (4.5), we emphasize that the period-doubling bifurcations, which happen in some frequency-locking intervals of ω with lower index k, are not captured by (4.5).

A better way to explain this is through circle maps. In section 4.4.1 and 4.4.2, we have shown that our Poincaré map is equivalent to two families of circle maps: $\bar{s} = s + \frac{\omega}{\pi}\nu + \frac{\xi}{4\pi\mu_1}\sin(2\pi s)$ for large ω, and $\bar{s} = s + \frac{\omega}{\pi}\nu - \frac{\omega}{\pi}\xi\log(1 - \sqrt{a_1}\cos(2\pi s))$ for ω near 0. It turns out there might be a transition between these two families when we vary ω from near 0 to near ∞.

In our numerical simulation, μ_1 is 9.6 which is slightly larger than $\xi/2$. By Theorem 4.4.2, this indicates that, for large enough ω, the dynamics of our Poincaré

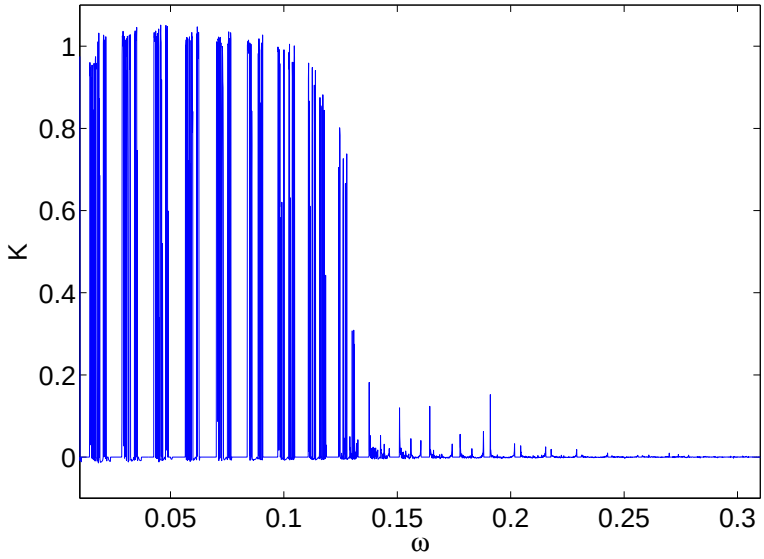

Figure 4.15: 0-1 test result computed by regression method for $c = 0.25$, $e = 0.2$ and $\gamma = 10^{-6}$.

map is equivalent to the canonical family of invertible circle maps

$$\bar{s} = s + \frac{\omega}{\pi}\nu + \frac{b}{2\pi}\sin(2\pi s), \tag{4.12}$$

where $b < 1$. Therefore, for large enough ω, our Poincaré map will turn, from a noninvertible circle map, into a near invertible or invertible canonical circle map. In other words, the period-doubling bifurcations which can be seen in some frequency-locking windows (see Figure 4.13) must eventually disappear as ω increases.

From this point of view, the regions that we have called 'chaotic' in the last few paragraphs might not be actually chaotic, especially for large ω. Indeed, almost all maps of the family (4.12) with $b < 1$ possess periodic dynamics except for values of ω in a set of measure near 0, for ω between two frequency-locking intervals. It is well-known that the canonical circle maps (4.12) in the invertible

case cannot produce chaotic dynamics. In contrast, since chaotic dynamics are a common phenomenon for a family of noninvertible circle maps, it follows that our Poincaré maps are expected to demonstrate truly chaotic dynamics for small ω.

The '0-1 test' has been implemented to confirm this assertion numerically. Recall from section 2.4 in Chapter 2 that the 0-1 test distinguishes between regular and chaotic dynamics in a deterministic system. If the asymptotic growth rate K of a time series of data is 1, the test proves the occurrence of chaotic dynamics. In contrast, the test returns $K = 0$ if the underlying dynamics is regular (i.e. periodic or quasiperiodic). Figure 4.15 shows that the dynamics are always regular for large enough ω even in the 'chaotic' regions. Here, for each ω, we use regression method for 9,000 data points and take $n = 900$. K is defined to be the median of K_ϖ for 100 $\varpi \in (0, \pi)$. For the definitions of notations, please refer to section 2.4.

4.5 The effect of varying γ

So far, we have presented a thorough study on the dynamics of the system (3.23) for different d and fixed γ. In this section, we discuss the effect of changing γ for a fixed d.

In section 4.2, the order of the time-averaged system was shown to depend on a combination of d and γ. Nevertheless, changing d will never be the same as changing γ. This is because changes in d affect the unstable manifolds of the equilibrium points in the unperturbed system and hence affect all the unknown parameters in Poincaré map (3.24).

Firstly, we consider the case when ϵ is large. Figure 4.16 displays the bifurcation structure of the ODE system and shows how it scales with γ for $c = 0.25$ and $e = 0.2$. The figures for each value of γ are quite similar except that more period-doubling bifurcations occur for smaller γ. We explain why this happens in

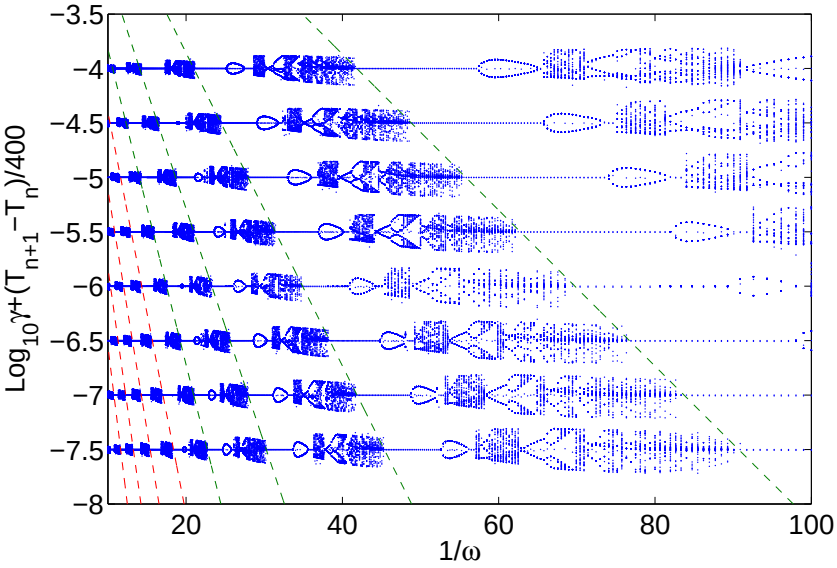

Figure 4.16: Bifurcation structure of the ODE system and its scaling with γ for $c = 0.25$ and $e = 0.2$. The ends of the k^{th} frequency-locking intervals are located on the gree dashed curves and the red dashed lines which are defined by (4.13) and (4.14), respectively.

the following paragraph.

Recall that, for ω small enough, the system is equivalent to a non-invertible circle map (4.11):

$$\bar{s} = h(s) = s + \frac{\omega}{\pi}\nu - \frac{\omega}{\pi}\xi \log(1 - \sqrt{a_1}\cos(2\pi s)),$$

where $\nu = \mu_3 - \xi \log(\mu_1\gamma) - \frac{\xi}{2e\mu_1}$. Suppose ω_* is such that the ODE system can be well-approximated by (4.11), and that period-doubling bifurcations happen in all the frequency-locking intervals for which $0 < \omega < \omega_*$. Note that the term $-\frac{\omega_*}{\pi}\xi \log(1 - \sqrt{a_1}\cos(2\pi s))$ will not be affected if we change γ. Therefore, by decreasing γ, we are only increasing $\frac{\omega_*}{\pi}\nu$ and hence including more and more frequency-locking intervals of ω within $\omega < \omega_*$.

Also, by (4.11), we can notice that the ends ω_k^+, ω_k^- of the k^{th} frequency-locking

intervals in ω all satisfy

$$\frac{\omega_k^{\pm}}{\pi}\nu - \frac{\omega_k^{\pm}}{\pi}\xi \log(1 \pm \sqrt{a_1}) = k,$$

which implies

$$\log\gamma = -\frac{\pi k}{\xi\omega_k^{\pm}} + \frac{\mu_3}{\xi} - \frac{1}{2e\mu_1} - \log(\mu_1(1 \pm \sqrt{a_1})), \tag{4.13}$$

where $k = 1, 2, ...,$ is small enough such that the ODE system is equivalent to the non-invertible circle map (4.11). We denote these curves in Figure 4.16 by green dashed curves. These curves can be replaced by straight lines

$$\log\gamma = -\left(\frac{\pi}{\xi}k \pm \frac{1}{4\mu_1}\right)\frac{1}{\omega_k^{\pm}} + \frac{\mu_3}{\xi} - \frac{1}{2e\mu_1} - \log\mu_1, \tag{4.14}$$

for large enough ω where the ODE system is equivalent to the invertible circle map (4.9)

$$\bar{s} = s + \frac{\omega}{\pi}\nu + \frac{\xi}{4\pi\mu_1}\sin(2\pi s).$$

The red dashed lines display good match in Figure 4.16.

Figure 4.16 also demonstrates an interesting phenomenon. If we fix ω and let γ decrease, we will trace out a similar bifurcation structure as we observe in the usual case of fixing γ and increasing ω. In other words, for a fixed periodic perturbation, changing the strength of the forcing term will produce a sequence of isolated intervals where periodic attractors exist, with complex dynamics between them. This has implications for a coupled heteroclinic system because in this situation of coupled heteroclinic cycles, the effective frequency of the forcing term is unknown and all we can do is to control the forcing strength through the coupling coefficient.

In the case ϵ near 0, the ODE system near the centre of k^{th} frequency-locking interval of ω is equivalent to the forced damped pendulum (4.5):

$$\ddot{s} + \eta^{-1}\dot{s} + \sin s = \frac{\omega_k}{\omega}\sqrt{a_2}^{-1}\lambda,$$

where $\eta^{-1} = \sqrt{\frac{e\gamma}{6\hat{x}\omega_k}}$. By section 4.2, we have to be very careful in letting γ decrease. If γ is too small, the average $\hat{x}$ of x will become $O(\gamma)$ and thus the ODE system cannot be well estimated by (4.5). Therefore, we consider only large enough γ such that the ODE system remains equivalent to (4.5). In this case, decreasing γ makes intervals in ω in which we have only frequency-locking (and no bistability) smaller because η^{-1} is also decreasing. However, the whole bifurcation structure remains qualitatively unchanged.

4.6 Comparison with a periodic system perturbed by a periodic forcing

Consider a more general perturbation in the form $(1-x)(\delta(f(2\omega t)-A)+\gamma A)$ where δ and γ are independent parameters, and $A = \frac{1}{2\pi}\int_0^{2\pi} f(t)dt$. Then the system (1.3) becomes

$$\begin{cases} \dot{x} &= x(1-(x+y+z)-cy+ez)+(1-x)(\delta(f(2\omega t)-A)+\gamma A) \\ \dot{y} &= y(1-(x+y+z)-cz+ex) \\ \dot{z} &= z(1-(x+y+z)-cx+ey) \end{cases} . \quad (4.15)$$

For $\delta = \gamma$, we recover the original system (1.3). The independent parameters δ and γ enable us to vary the amplitude and mean of the perturbation function separately. As the mean and amplitude of the perturbation function $\gamma(1-x)\sin^2(\omega t)$ are the same, the analysis we have done so far can be only served as a model for a heteroclinic system with such kind of perturbation. By separating the mean and amplitude of the perturbation function, we obtain the benefit of being able to understand the dynamics of a heteroclinic system with a general periodic perturbation function. In this section, we will show how the dynamics of the system (4.15) changes as we move from the case $\delta \ll \gamma$ to the case $\delta = \gamma$. To keep the biological meaning of (4.15), the case $\delta > \gamma$ will not be discussed.

Firstly, we prove that there exists a periodic attractor for $\delta = 0$:

$$\begin{cases} \dot{x} &= x(1-(x+y+z)-cy+ez)+\gamma(1-x)A \\ \dot{y} &= y(1-(x+y+z)-cz+ex) \\ \dot{z} &= z(1-(x+y+z)-cx+ey) \end{cases} . \tag{4.16}$$

There is no need to derive the Poincaré map of this system step by step again since we need only to refer back to the general expression for the Poincaré map given by (3.18). Substituting A into it, we get

$$\begin{aligned} L_1(x,t) &= \mathrm{e}^{-c(T_3(0)-T_2(0)} \int_{T_2(0)}^{T_3(0)} \mathrm{e}^{c(\tau-T_2(0))} A d\tau \\ &= A/c(1-\mathrm{e}^{-c(T_3(0)-T_2(0))}) = \nu_1 - \nu_2 x^d, \end{aligned}$$

where ν_1 and ν_2 are constants, and,

$$L_2(x,t) = \int_t^{T_1(0)} \mathrm{e}^{-e(\tau-t)} A d\tau = \frac{A}{e}\left(\frac{x}{h}-1\right).$$

Since the unstable manifold of P_2' is time-independent in this case, $G_1(x,t)$ and $G_2(x,t)$ give two constants. Therefore, the Poincaré map of the system (4.16) is of the form

$$\begin{cases} f_1(x,t) &= \mu x^d + [\nu_3 + \nu_4 x^d]\gamma + O(\gamma^2) \\ &= \mu x^d + \nu_3 \gamma + O(\gamma^{1+d}) \\ f_2(x,t) &= t + \mu_3 - \xi \log x + \frac{\xi A}{e}(1/h - x)\gamma \\ &= t + \mu_3 - \xi \log x + O(\gamma) \end{cases} . \tag{4.17}$$

where ν_3 and ν_4 are constants.

Clearly, there is an attracting fixed point x_0 for γ small enough for the first equation of (4.17) since $d > 1$. This implies the existence of a periodic attractor for the corresponding system (4.16). Moreover, the period of this periodic solution is approximately $\mu_3 - \xi \log x_0$.

Therefore, in some sense, system (4.15) for which $\delta \neq 0$ is merely a periodic oscillator perturbed by a periodic function.

In the following, we take $f(2\omega t) = \sin^2(\omega t)$. As we have shown in Remark 3.3.3, the Poincaré map of system (4.15) with $f(2\omega t) = \sin^2(\omega t)$ is:

$$\begin{cases} \bar{x} = f_1(x,t) = \mu x^d + \gamma\mu_1 \\ \qquad\qquad +\delta\left[\mu_2(-a_1\cos(2\omega g) - b_1\sin(2\omega g))\right. \\ \qquad\qquad -\mu_4(-a_1\cos(2\omega(\bar{t}-\delta_3)) - b_1\sin(2\omega(\bar{t}-\delta_3))) \\ \qquad\qquad \left.-\mu_5(-a_2\cos(2\omega\bar{t}) - b_2\sin(2\omega\bar{t}))\right] + O(\gamma^2) \\ \bar{t} = f_2(x,t) = t + \mu_3 - \xi\log(x) \\ \qquad\qquad -\frac{\xi}{2e}\left[\gamma - \delta\left(a_2\cos(2\omega t) + b_2\sin(2\omega t)\right)\right]x^{-1} + O(\gamma^2) \end{cases} \tag{4.18}$$

In the case when ϵ is large and ω is near 0, the first equation of this map (4.18) can be reduced further, by assuming μ_2 and μ_4 to be near 0 and μ_5 to be near $-\mu_1$ and noting that x^d term can be ignored as we did in section 4.4.2, into:

$$\bar{x} = f_1(x,t) = \mu_1(\gamma - \delta\sqrt{a_1}\cos(2\omega\bar{t})).$$

So, $x = \mu_1(\gamma - \delta\sqrt{a_1}\cos(2\omega\bar{t}))$ is an invariant curve for the system. Substituting this expression for $x(t)$ into the second equation of (4.18) and letting $s = \omega t/\pi$, this map can then be represented by a one-dimensional map:

$$\bar{s} = h(s) = s + \frac{\omega}{\pi}\nu - \frac{\omega}{\pi}\xi\log(1 - \gamma^{-1}\delta\sqrt{a_1}\cos(2\pi s)), \tag{4.19}$$

where $\nu = \mu_3 - \xi\log(\mu_1\gamma) - \frac{\xi}{2e\mu_1}$. Since $h'(s) = 1 + \frac{2\omega\xi\gamma^{-1}\delta\sqrt{a_1}\sin(2\pi s)}{1-\gamma^{-1}\delta\sqrt{a_1}\cos(2\pi s)}$, (4.19) is invertible if and only if $h'(s) = 0$ has no real solutions, which is true if and only if $(\gamma^{-1}\delta)^2 < \frac{c^2+4\omega^2}{c^2+4\omega^2c^2\xi^2}$. Note that $\frac{c^2+4\omega^2}{c^2+4\omega^2c^2\xi^2} \nearrow 1$ as $\omega \searrow 0$. Therefore, (4.19) is invertible over the whole range of ω for which it applies if $\gamma^{-1}\delta$ is small enough. Moreover, if $\delta \ll \gamma$, (4.19) is very close to the rigid rotation $\bar{s} = s + \frac{\omega}{\pi}\nu$ and hence we expect that all the period-k intervals have widths that tend to zero as $\delta \to 0$; thus they will be very difficult to observe in numerical simulations.

In the case $\gamma^{-1}\delta$ near 1, (4.19) remains invertible for all small enough ω but becomes non-invertible at large ω. This is always the case until $\gamma^{-1}\delta = 1$, at which

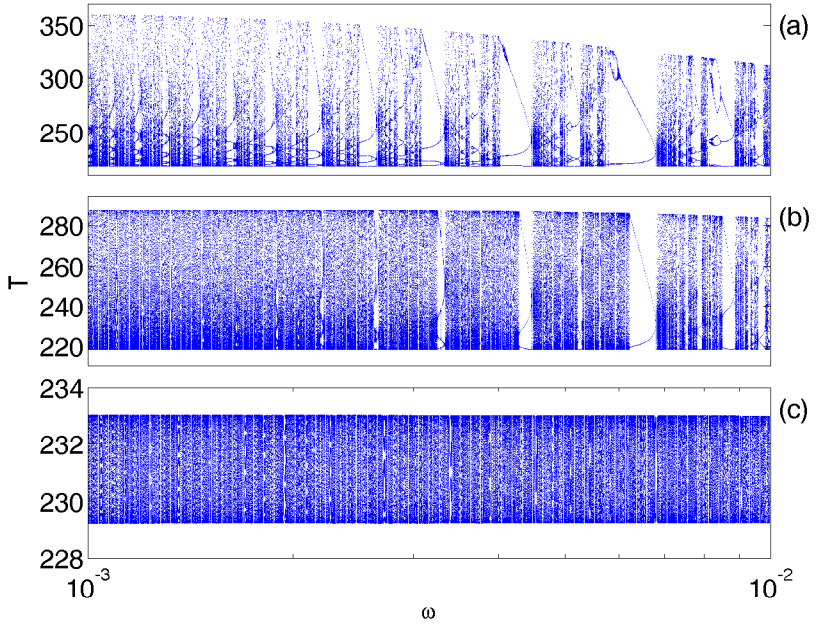

Figure 4.17: The transition of the dynamics of (4.15). Here we compare the dynamics for a fixed $\gamma = 10^{-6}$ with different δ: (a) $\delta = 9.99\times10^{-7} = 0.999\gamma$, (b) $\delta = 9.5\times10^{-7} = 0.95\gamma$ and (c) $\delta = 10^{-7} = 0.1\gamma$. The ω-coordinate is in *log*-scale.

point it becomes non-invertible for all valid ω. This is consistent with the results we proved in section 4.4.2.

Figure 4.17(c) shows that the dynamics of the ODE system (4.15) for ω near 0 are almost the same as a rigid rotation for $\delta \ll \gamma$. The dynamics appears to be periodic or quasiperiodic for all ω. As we increase δ, the widths of the period-k intervals increase, and they can be clearly observed, as shown in Figure 4.17(b). Compared to Figure 4.10, period-doubling bifurcations appear in some, but not all, period-k intervals of ω for $\delta = 9.99 \times 10^{-7}$ and $\gamma = 10^{-6}$. This indicates that the dynamics of (4.15) here correspond to the non-invertible circle map case.

By a similar argument as we did in section 4.4.1, we discuss the case ω large and ϵ large as follows. Taking ω large enough such that $a_1 \approx a_2 \sim O(\gamma)$, then

the first equation of the Poincaré map (4.18) gives $x \approx \mu_1\gamma$ since x^d term can be ignored in this case. Substituting this into the second equation of (4.18), we have

$$\bar{t} = t + \nu + \gamma^{-1}\delta\frac{\xi\sqrt{a_2}}{2e\mu_1}\sin(2\omega t),$$

where $\nu = \mu_3 - \xi\log(\mu_1\gamma) - \frac{\xi}{2e\mu_1}$. Since $\sqrt{a_2} \approx \frac{e}{2\omega}$, by letting $s = \frac{\omega}{\pi}t$, the last equation then becomes

$$\bar{s} \approx s + \frac{\omega}{\pi}\nu + \frac{\xi}{4\pi\mu_1}\gamma^{-1}\delta\sin(2\pi s),$$

Clearly, it is always an invertible circle map for any fixed μ_1 if δ is small enough.

Figure 4.18 shows the regions where the ODEs system (4.15) is equivalent to an invertible or non-invertible circle map. The green line is the case when $\gamma = \delta$, which has been studied in previous sections. As was showed in Proposition 4.4.2, for large enough μ_2 and ω, the case $\gamma = \delta$ provides invertible-circle-map dynamics. This implies that the blue curve C_2 will eventually intersect the green line. However, this is not the case if μ_2 is not large enough. As it stands, we are not sure if the two blue curves intersect or not for small enough $\gamma^{-1}\delta$.

For the case of ϵ near 0, by the same way as we did in section 4.3.2, the Poincaré map (4.18) now takes the form

$$\begin{cases} \bar{x} &= \mu x^d + \mu_1\left[\gamma + \delta(-a_2\cos(2\omega t) + b_2\sin(2\omega t))\right] \\ \bar{t} &= t + \mu_3 - \xi\log\bar{x} \end{cases},$$

which can be reduced, by defining a new γ and μ_3, into

$$\begin{cases} \bar{x} &= \mu x^d + \gamma\left(1 + \gamma^{-1}\delta\sqrt{a_2}\sin(2\omega t)\right) \\ \bar{t} &= t + \mu_3 - \xi\log\bar{x} \end{cases},$$

Clearly, the analysis in section 4.3.2 for the dynamics near the centre of the k-th frequency-locking interval can be proceeded directly by only replacing $\sqrt{a_2}$

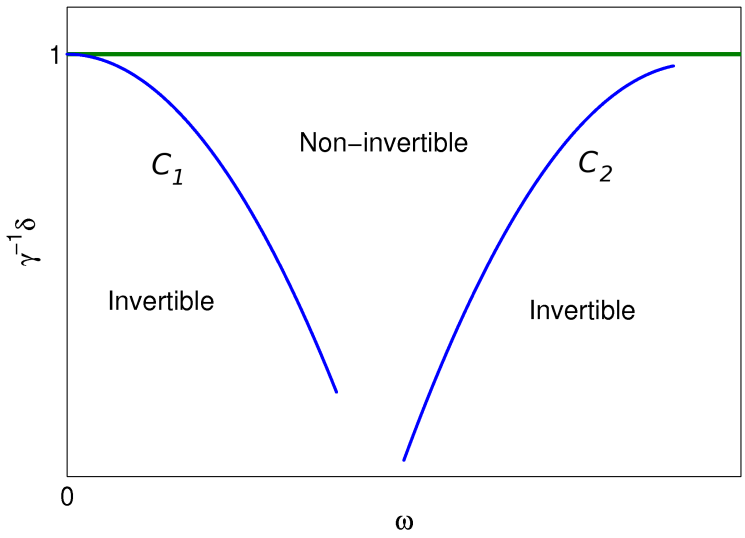

Figure 4.18: The schematic diagram depicted the regions where the 2 parameter ODEs system (4.15) is equivalent to an invertible or non-invertible circle map for ϵ large.

with $\gamma^{-1}\delta\sqrt{a_2}$. Therefore, system (4.15) is equivalent to the forced damped pendulum with torque:

$$\ddot{s} + \eta^{-1}\dot{s} + \sin s = \gamma\delta^{-1}\frac{\omega_k}{\omega}\sqrt{a_2}^{-1}\lambda, \tag{4.20}$$

where $\eta^2 = \frac{6\omega_k\hat{x}}{e\gamma}$. Referring to Figure 4.8, the only attractor of (4.20) is a stable periodic orbit if $|\lambda| > \gamma^{-1}\delta\frac{\omega}{\omega_k}\sqrt{a_2}$, and a stable equilibrium exists otherwise. Therefore, what we observe in the $\omega - T$ figure of system (4.15) when decreasing δ is only the shrinking of the frequency-locking intervals and the decreasing of the amplitude of the invariant curve.

4.7 Discussion

In this chapter, we have presented analytic studies of the dynamics of the Poincaré map of a G-H system perturbed by a periodic function. The frequency

ω of the perturbation function is varied continuously in order to examine the bifurcation structure of the system. The results also provide explanations of the frequency-locking phenomena in the original ODEs system reported by Rabinovich *et al* [63].

We first notice that the order of the time-averaged map depends on both γ and c for a fixed e. Therefore, to make the problem in the same scale, we have to adjust c when letting γ tend to 0. This argument was not found in the work done by Afraimovich *et al.* Moreover, we can now identify two different cases in which the maps can be reduced into two different forms and the dynamics they demonstrates are two different types of oscillators weakly perturbed by another oscillator.

More precisely, we call the case 'ϵ near 0' if, for a given γ, ϵ is small enough such that x^d term plays an important role for the dynamics of our Poincaré map. In this case, we observe stable equilibrium points and stable 1-dimensional invariant curves dominate the dynamics in turns when varying ω. There are overlappings of these two scenarios where bistability occur. We have proved that the model map, which demonstrates similar dynamics as the original ODE system, is basically equivalent to a damped pendulum with constant torque near the centres of each frequency-locking intervals.

As for the case where ϵ is large enough that x^d term doesn't affect the dynamics, bistability disappears. What we can see is a sequence of frequency-locking intervals of ω with chaotic-like windows in between; see the $\omega - T$ plot in Figure 4.13. We have proved that the map (or the original ODE system) is now equivalent to circle maps. These circle maps could be invertible or non-invertible depending on the size of ω and the parameters in the map. Therefore, for large enough ω and parameters, the chaotic-like windows are actually not chaotic but periodic or quasi-periodic. However, for some intervals of small ω, the system does demon-

strates topological chaos. This is supported by strong numerical evidence from (i) 0-1 test and (ii) the calculation of rotation intervals.

We have also demonstrated that the G-H system perturbed by a general class of periodic functions $(1-x)(\delta(f(2\omega t)-A)+\gamma A)$ can be regarded as an oscillator perturbed by a periodic function. As we have shown previously for the special case $\gamma = \delta$ in section 4.3 and 4.4, there are intrinsic differences between the case ϵ near 0 and ϵ large for all $0 < \delta < \gamma$. For the case ϵ near 0, there is no major difference in the dynamics between the case $\gamma = \delta$ and $\delta < \gamma$. However, if ϵ large and $\delta < \gamma$, the system is equivalent to an invertible, non-invertible and then invertible circle map when ω increasing from 0 to ∞. The results here can be considered as good descriptions in general for the dynamics of a heteroclinic system perturbed by a periodic function.

A well analytic study for ω of intermediate size is still needed. The difficulty comes from the fact that ω is now the same order of c and e and hence we are unable to reduce the Poincaré map into a simpler form.

Chapter 5

Symmetric Solutions in Coupled Cell Systems

5.1 Introduction

It is well known that symmetric periodic solutions could exist in a system with symmetry. For example, the **SO**(2)-equivariant differential equation

$$\begin{cases} \dot{x} &= (1-(x^2+y^2))x - y \\ \dot{y} &= (1-(x^2+y^2))y + x \end{cases}$$

has a periodic solution $x(t) = \cos t$, $y(t) = \sin t$ with **SO**(2)-symmetry. However, symmetry in a system doesn't generically imply that every solution is symmetric. Note that if $\dot{x} = f(x)$ is Γ-equivariant and the action of Γ on $\mathbb{R}^n$ is irreducible then $f(0) = 0$. So the solution $x(t) = 0$ is Γ-equivariant, i.e. in this case there is always at least one Γ-symmetric solution trajectory.

Spatially symmetric periodic solutions in a symmetric system possess temporal symmetry automatically [28]. More precisely, suppose $\dot{x} = f(x)$ is a Γ-equivariant system, where Γ is a symmetry group, and $x(t)$ is a T-periodic solution of it. If $\gamma \in \Gamma$ is a symmetry of $x(t)$, then $\gamma x(t)$ and $x(t)$ must be identical,

i.e. $\gamma\{x(t)\} = \{x(t)\}$. By the uniqueness of solutions of ODE system, there exists $\theta_\gamma \in \mathbf{S}^1 = [0, T]$ such that $\gamma x(t + \theta_\gamma) = x(t)$. In other words, $(\gamma, \theta_\gamma) \in \Gamma \times \mathbf{S}^1$ is a spatio-temporal symmetry of the periodic solution $x(t)$. We denote the group of all spatio-temporal symmetries of $x(t)$ by $\Sigma_{x(t)}$.

It is clear that the map $(\gamma, \theta_\gamma) \to \gamma$ is an isomorphism from $\Sigma_{x(t)}$ to H, where

$$H = \{\gamma \in \Gamma : \gamma\{x(t)\} = \{x(t)\}\}.$$

In other words, H is the group of all spatio-temporal symmetries of $x(t)$. We call a symmetry γ of $x(t)$ a spatial symmetry if $\theta_\gamma = 0$ and let

$$K = \{\gamma \in \Gamma : \gamma x(t) = x(t)\ ,\ \forall t\}$$

be the group of all spatial symmetries of $x(t)$. In the case $K = \{1\}$, we call the periodic solution trivial. For example, $x(t) = (\epsilon \sin t, \epsilon \sin t, \epsilon \sin t, \epsilon \sin t)$ is a trivial periodic solution of the system

$$\dot{x_i} = \epsilon \cos t, \text{ for } i = 1, ..., 4,$$

which is a Z_4-symmetric (cyclically symmetric) system

$$\dot{x_i} = 0, \text{ for } i = 1, ..., 4,$$

perturbed by periodic functions $\epsilon \cos t$.

The following theorem, due to P-L. Buono and M. Golubitsky, characterizes possible spatio-temporal symmetry of periodic solutions of a Γ-equivariant system.

Theorem 5.1.1 *([28]) Let Γ be a finite group acting on $\mathbb{R}^n$. There is a periodic solution to some Γ-equivariant system of ODEs on $\mathbb{R}^n$ with spatial symmetries K and spatio-temporal symmetries H if and only if*
(a) H/K is cyclic,

(b) K is an isotropy subgroup,

(c) dim Fix(K)≥ 2. If dim Fix(K)=2, then either H = K or H = N(K),

(d) H fixes a connected component of Fix(K)\L_K.

Moreover, when these conditions hold, hyperbolic asymptotically stable limit cycles with the desired symmetry exist.

We are not going to discuss this theorem in detail. Nevertheless, according to this theorem, it is necessary that H/K is cyclic for a periodic solution to have a spatio-temporal symmetry. In this sense, we will only consider periodic solutions of Z_n-symmetric systems in this chapter, where Z_n is the cyclic group generated by $\sigma : (x_1, ..., x_n) \to (x_n, x_1, ..., x_{n-1})$.

In a system containing a robust heteroclinic cycle which is stable, we can produce an attracting periodic solution either by adding perturbation terms to break the parts of the symmetry group which lead to the existence of the fixed point subspaces which support the connections, or by coupling the system with another one. In the second case, we expect that synchronization could occur and the ratio of frequencies of two heteroclinic cycling subsystems could be rational. The question then arises: in a system with symmetry, what is the general form of the ratio of frequencies between two oscillating subsystems if they are symmetric?

M. Tachikawa in [74] considered an ecological system consisting of two replicator equations coupled diffusively. Of these two replicator equations, one has a heteroclinic cycle attractor and the other one has a limit cycle attractor. In his paper, frequency-locking intervals with specific ratios of frequencies can be observed numerically when varying the strength of coupling. The author explained graphically that these specific ratios come from the existence of symmetric periodic solutions. In this chapter, we investigate analytically the possible ratios for symmetric periodic solutions.

Instead of studying coupled systems directly, we firstly consider a single sys-

tem with periodic perturbations. This is similar to considering the projection of the whole coupled system to a single one. More precisely, suppose the coupled system is

$$\begin{cases} \dot{x} = F_1(x) + \epsilon(y - x) \\ \dot{y} = F_2(y) + \epsilon(x - y), \end{cases}$$

where $x, y \in \mathrm{R}^n$ and the system has a periodic solution $(\overline{x}(t), \overline{y}(t))$. We call it a coupled cell system with two cells: x-cell and y-cell. Then the x-cell can be written as a system with periodic external perturbation function $\overline{y}(t)$:

$$\dot{x} = \overline{F}_1(x) + \epsilon\overline{y}(t),$$

for which $\overline{x}(t)$ is a periodic solution. It follows that the possible ratios of frequencies between periodic solutions in the two cells is the same as those between the periodic solution and the perturbation function in x-cell system.

Therefore, we consider

$$\dot{x} = F(x) + \phi(t), \tag{5.1}$$

where $x \in \mathbb{R}^n$, $\phi(t) = (\phi_1(t), ..., \phi_n(t))$ and ϕ_i's are periodic functions of period T_ϕ. Suppose that the action of the cyclic group Z_n on $\mathbb{R}^n$ is generated by

$$\sigma : (x_1, ..., x_n) \to (x_n, x_1, ..., x_{n-1}),$$

and the unperturbed system $\dot{x} = F(x)$ is Z_n-equivariant. In other words, $\sigma F(x) = F(\sigma x)$. In the case when there exists a non-trivial periodic solution $X(t)$ in the system, i.e. the spatial symmetry of $X(t)$ is $K = \{1\}$, we are interested in whether this periodic solution has Z_n-symmetry or not, and the ratio of frequencies between the periodic solution and the perturbation function.

The structure of this chapter is as follows. In section 5.2.1, we give a necessary condition of the perturbation functions for system (5.1) to have a non-trivial periodic solution with Z_n symmetry. The ratio of frequencies between a Z_n-symmetric

periodic solution and the perturbation function will be identified in section 5.2.2. The results obtained in these two sections can be easily extended to a general Z_p-symmetric case where Z_p is a subgroup of Z_n. We show these in section 5.2.3 followed by a discussion of the ratio of frequencies of a non-symmetric periodic solution in section 5.2.4. In section 5.3, we consider the Guckenheimer-Holmes system with periodic perturbations as an example to check the validity of the results. By analysing the Poincaré map of the system, we prove results analogous to those in section 5.2.1 and 5.2.2. As a result, we are able to identify the possible positions of the frequency-locking windows where period-1 periodic solutions with Z_3-symmetry exist. Here, we call a periodic solution a period-1 periodic solution if it intersects any cross section at only one point. We then discuss coupled cell systems in section 5.4 where we prove that periodic orbits have the same cyclic symmetry in each of the two cells and also derive the form of the ratio of frequencies between two symmetric periodic solutions in two cells. Tachikawa's system is studied as an example of our analytic results. We close this chapter with discussion in section 5.5.

The periodic solutions we considered in the following sections will always be non-trivial. Therefore, for simplicity, the term 'non-trivial' will be neglected throughout this chapter without further comment. Also, we will always take suffixes to be modulo n in this chapter.

5.2 Symmetric solutions in systems with periodic perturbations

In this section, we study non-trivial symmetric periodic solutions in the system (5.1).

Suppose $X(t)$ is a periodic solution of period P and let τ_s be a temporal op-

erator which translates time by an amount s, i.e. $\tau_s X(t) = X(t+s)$. We firstly consider the Z_n-symmetric case.

5.2.1 Z_n-symmetric periodic solutions

The periodicity of X means that $\tau_P X(t) = X(t)$ and $\tau_P \dot{X}(t) = \dot{X}(t)$ for all t. This implies $F(X(t+P)) + \phi(t+P) = F(X(t)) + \phi(t)$ for all t. Therefore, $P = kT_\phi$ for some $k \in \mathbb{N}$.

Definition 5.2.1 *Suppose $X(t)$ is a periodic solution of system (5.1). $X(t)$ possesses Z_n-symmetry if $\sigma\{X(t)\} = \{X(t)\}$.*

If $X(t)$ possesses Z_n-symmetry, then by the uniqueness of ODE solutions there exists a θ such that $\sigma \circ \tau_\theta X(t) = X(t)$ for all t. By induction, $X(t) = \sigma^n X(t) = X(t - n\theta)$ for all t. Therefore, $\theta = lP/n$ for some integer l. Conversely, it is trivial that $X(t)$ possesses the Z_n-symmetry if $\sigma \circ \tau_{lP/n} X(t) = X(t)$ for all t for some l. In short, a spatial-symmetric periodic solution also induces temporal-symmetry.

Moreover, $X(t)$ has Z_n-symmetry if and only if

$$\sigma^m \circ \tau_{P/n} X(t) = X(t), \tag{5.2}$$

for all t and some integer m with $(m, n) = 1$, i.e. m and n are coprime. This is because that $\{1, \sigma^m\}$ can generate the whole group Z_n if and only if $(m, n) = 1$. More precisely, (5.2) is valid if and only if

$$\sigma^m X(t) = X(t - P/n).$$

Since there exists an integer l such that $\sigma^{lm} = \sigma$, the last equation is equivalent to

$$\sigma X(t) = X(t - lP/n).$$

By the last paragraph, this is equivalent to that $X(t)$ has the Z_n-symmetry. In other words, $X(t)$ has Z_n-symmetry if and only if there exists an integer m with $(m, n) = 1$ such that $\sigma^m X$ is doing at $t = 0$ what X did at a time P/n ago.

For example, in $\mathbb{R}^4$ as depicted in Figure 5.1, a point x_E on a Z_4-symmetric periodic trajectory could arrive at the point σx_E (the case $m = 1$) or $\sigma^3 x_E$ (the case $m = 3$) after a period of time $P/4$. Note that the solution could possess only Z_2-symmetry instead of Z_4 if it takes a quarter of the period P from x_E to $\sigma^2 x_E$ (the case $m = 2$).

Remark 5.2.1 *In the case $X(t)$ is trivial, (5.2) is not a necessary condition for Z_n-symmetry. For example, consider*

$$\dot{x}_i = \gamma \cos t, \ \textit{for } i = 1, ..., 4.$$

Then $X(t) = (\gamma \sin t, \gamma \sin t, \gamma \sin t, \gamma \sin t)$ is a periodic solution with Z_4-symmetry. However,

$$\sigma \circ \tau_{2\pi/4} X(t) = X(t + \pi/2) \neq X(t).$$

Condition (5.2) can be achieved by the following two conditions:

$$\sigma^m \circ \tau_{P/n} X(t_0) = X(t_0), \ \text{for some } t_0, \tag{5.3}$$

and

$$\sigma^m \circ \tau_{P/n} \dot{X}(t) = \dot{X}(t), \ \text{for all } t. \tag{5.4}$$

The first condition states that there exists an initial point where (5.2) is true, whilst the second one ensures that the tangent vectors at each point on $X(t)$ also satisfy this spatio-temporal condition. Hence, by integration along $X(t)$, these two conditions are equivalent to (5.2).

Condition (5.4) is equivalent to $\sigma^m F(\tau_{P/n} X) + \sigma^m \phi(t + P/n) = F(X) + \phi(t)$. Therefore, if $X(t)$ is Z_n-symmetric, then $\sigma^m F(\tau_{P/n} X) = F(X)$ and hence we have the following proposition since $P = kT_\phi$:

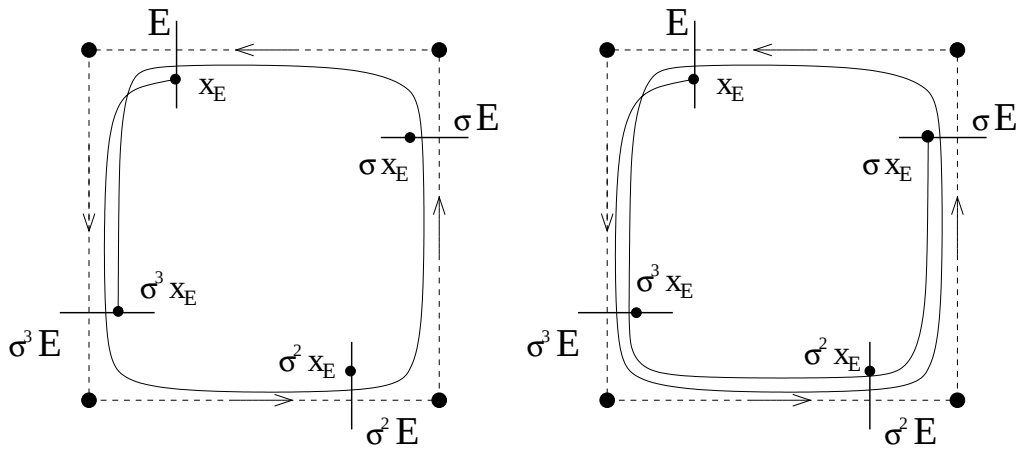

Figure 5.1: Schematic diagrams depicting the two cases of a Z_4-symmetric periodic solution in $\mathbb{R}^4$: (a) $m = 3$ and $j = 2$, (b) $m = 1$ and $j = 2$. Here, m is taken to be the integer such that $\sigma^m x_E$ is the next symmetric copy of x_E along the periodic trajectory $X(t)$, and $j - 1$ is the number of loops that $X(t)$ passes through E. We only show the part of the trajectory between x_E and its next symmetric copy $\sigma^m x_E$ along $X(t)$.

Proposition 5.2.1 *Suppose system (5.1) has a non-trivial periodic solution $X(t)$ with period $P = kT_\phi$. If $X(t)$ has Z_n-symmetry and satisfies (5.2), then*

$$\phi_{i+m}(t + \frac{k}{n}T_\phi) = \phi_i(t), \tag{5.5}$$

for all $t \in \mathrm{R}$, $i = 1, 2, ..., n$.

Proposition 5.2.1 implies that in order to have a Z_n-symmetric periodic solution, the perturbation functions must differ only by a phase shift. By periodicity of ϕ, we can note that both $P = kT_\phi$ and $P = (ln + k)T_\phi$ for some integer l give the same necessary condition (5.5). Conversely, if (5.5) is satisfied and $P = (ln+k')T_\phi$ where $k' \not\equiv k \pmod n$, then the periodic solution is not Z_n-symmetric for otherwise we will end up with a different necessary condition. Therefore, for a fixed m and

k in (5.5), the period of a Z_n-symmetric periodic solution satisfying (5.2) is of the form $(ln + k)T_\phi$ for some non-negative integer l.

In practice, ϕ is fixed at the beginning of the study of a specific collection of ODEs, say $\phi_{i+1}(t + \frac{k}{n}T_\phi) = \phi_i(t)$ for a fixed k. This implies $\phi_{i+m}(t + \frac{mk}{n}T_\phi) = \phi_i(t)$. Therefore, the period of a Z_n-symmetric periodic solution $X(t)$ which satisfies (5.2) is of the form

$$P = (ln + mk)T_\phi,$$

if $\phi_{i+1}(t + \frac{k}{n}T_\phi) = \phi_i(t)$.

Corollary 5.2.1 *Suppose system (5.1) has a non-trivial Z_n-symmetric periodic solution $X(t)$ satisfying (5.2) and $\phi_{i+1}(t + \frac{k}{n}T_\phi) = \phi_i(t)$. Then the period of $X(t)$ is of the form $P = (ln + mk)T_\phi$ for some integer l.*

For example, in $\mathbb{R}^4$, suppose we take $(\phi_1, \phi_2, \phi_3, \phi_4) = (f(t), f(t + T/4), f(t + T/2), f(t + 3T/4))$ where T is the period of f. In this case, $\phi_{i+1}(t + 3T/4) = \phi_i(t)$, i.e. $k = 3$. By the results of the last paragraph, the period of a Z_4-symmetric periodic solution could be $(4l + 3)T$ when $m = 1$ or $(4l + 1)T$ when $m = 3$.

5.2.2 The ratio of frequencies

We now consider the ratio of the frequencies between the periodic forcing functions and the Z_n-symmetric periodic solution $X(t)$. Suppose $X(t)$ satisfies (5.2). By Proposition 5.2.1 and Corollary 5.2.1, to ensure the possibility of the existence of a periodic solution with Z_n-symmetry, we assume the period of $X(t)$ is $(ln + mk)T_\phi$ and $\phi_{i+1}(t + \frac{k}{n}T_\phi) = \phi_i$ for all i.

Let E be any cross section of $X(t)$. Then $\sigma^i E$, $i = 0, 1, 2, ..., n - 1$, are the Z_n-corresponding cross sections of $X(t)$. Denote x_E to be a point of $X(t)$ on E. If $X(t)$ satisfies (5.2), then $\sigma^m x_E$ is the next symmetric copy of x_E along $X(t)$. See figure 5.1. Define the frequency of $X(t)$ to be $2\pi/T$ where T is the average of the first

return time for $X(t)$ corresponding to E. The frequency of the forcing functions is defined as usual by $2\pi/T_\phi$.

It can be easily seen that $X(t)$ intersects all the cross sections $\sigma^i E$, for $i = 0, 1, ..., n-1$, a total of $jn - m$ times between x_E and $\sigma^m x_E$ for some integer j, and n times between x_E and its first return point. Since the time $X(t)$ spends between x_E and $\sigma^m x_E$ is P/n, T is therefore equal to

$$\frac{P}{n} \times \frac{n}{jn - m},$$

which simplifies to

$$\frac{ln + mk}{jn - m} T_\phi.$$

So, we have

Proposition 5.2.2 *Suppose $X(t)$ is a non-trivial periodic solution of system (5.1) satisfying (5.2) and $\phi_{i+1}(t + \frac{k}{n}T_\phi) = \phi_i(t)$ for all i, then the ratio of the frequencies between the periodic forcing function and $X(t)$ is of the form*

$$\frac{ln + mk}{jn - m}, \tag{5.6}$$

where l and j are non-negative integers.

Again, let us consider the same example in $\mathbb{R}^4$ in which we take $(\phi_1, \phi_2, \phi_3, \phi_4) = (f(t), f(t + T/4), f(t + T/2), f(t + 3T/4))$ where T is the period of f. In this case, $\phi_{i+1}(t + 3T/4) = \phi_i(t)$, i.e. $k = 3$. By Proposition 5.2.2, the ratio of the frequencies between ϕ and a Z_4-symmetric periodic solution could be

$$\frac{4l + 3}{4j - 1} \quad \text{for the case} \quad m = 1,$$

or

$$\frac{4l + 1}{4j - 3} \quad \text{for the case} \quad m = 3,$$

for some integers l and j.

Proposition 5.2.2 also implies that a regular pattern exists for the positions where Z_n-symmetric period-1 periodic solutions could occur. Here, a periodic solution is called period-1 if it intersects any transversal cross section at only one point. To have a period-1 periodic solution, m must be $n-1$ and also j must be 1. The following corollary then follows:

Corollary 5.2.2 *Suppose $X(t)$ is a non-trivial period-1 periodic solution of system (5.1) with Z_n-symmetry and $\phi_{i+1}(t+\frac{k}{n}T_\phi) = \phi_i(t)$ for all i, then the ratio of the frequencies between the periodic forcing function and $X(t)$ is of the form $ln-k$, where l is a positive integer.*

We will present an example to demonstrate this result in Section 5.3.

5.2.3 Z_p-symmetric periodic solutions

Suppose Z_p is a subgroup of Z_n, i.e. $n = pq$ for some positive integer q. We can easily derive results analogous to those in sections 5.2.1 and 5.2.2 for Z_p-symmetric solutions. Since $Z_p \cong Z_n/\sim$, where $\sim$ defines an equivalence among the members of Z_n by $\sigma^{m_1} \sim \sigma^{m_2}$ if $m_1 \equiv m_2 \ (mod\ p)$, this suggests that we need to define q of the functions in ϕ to construct a system containing Z_p-symmetric solution in $\mathbb{R}^n$. We will see this in Proposition 5.2.3.

In general, $X(t)$ is a Z_p-symmetric periodic solution if and only if

$$\sigma^{mq} \circ \tau_{P/p}(X(t)) = X(t), \tag{5.7}$$

for all t and for $(m,p)=1$. Since $\sigma^{mq-l} \circ \tau_{P/p}(\sigma^l X(t)) = \sigma^{mq} \circ \tau_{P/p}(X(t)) = X(t)$, for $l = 1,2,...,q$, there are exactly q distinct copies of Z_p-symmetric solutions without Z_{jp}-symmetry for $j = 2,3,...,q$: $\sigma^l\{X(t)\}$, $l = 1,2,...,q$.

By replacing n by p and m by mq in (5.2), the necessary condition for $X(t)$ to be Z_p-symmetric is

$$\phi_{i+mq}(t+\frac{k}{p}T_\phi) = \phi_i(t), \tag{5.8}$$

for all i. In other words, the perturbation functions ϕ_i's can be divided into q groups each of which consists of p functions which differ only by a phase shift $\frac{k}{p}T_\phi$.

Suppose $\phi_{i+q}(t+\frac{k}{p}T_\phi) = \phi_i(t)$ for all i. Again, the period of $X(t)$ is of the form $(lp+mk)T_\phi$ then the averaged return time T is

$$\frac{P}{p} \times \frac{n}{jn-mq},$$

which is equal to

$$\frac{lp+mk}{jp-m}T_\phi,$$

for some positive integers l and j. We summarize this by the following proposition:

Proposition 5.2.3 *Suppose $X(t)$ is a non-trivial periodic solution of system (5.1) satisfying (5.7) and $\phi_{i+q}(t+\frac{k}{p}T_\phi) = \phi_i(t)$ for all i, then the ratio of the frequencies between the periodic forcing function and $X(t)$ is of the form*

$$\frac{lp+mk}{jp-m}, \tag{5.9}$$

where l and j are nonegative integers.

It is clear that condition (5.5) implies condition (5.8). In a system satisfying condition (5.5), a Z_n-symmetric periodic solution is automatically Z_p-symmetric, which is reflected by the fact that (5.6) is also of the form as (5.9).

For example, in $\mathbb{R}^4$, consider Z_2-symmetric solutions. Suppose we take

$$(\phi_1,\phi_2,\phi_3,\phi_4) = (f(t), f(t+T/4), f(t+T/2), f(t+3T/4)),$$

where T is the period of f. In this case, $\phi_{i+2}(t+T/2) = \phi_i(t)$, $m=1$ and $k=1$. So the period of a Z_2-symmetric periodic solution is $(2l+1)T$ and the ratio of the frequencies is of the form

$$\frac{2l+1}{2j-1},$$

for some integer l and j.

In fact, (5.8) and (5.5) share the same form. Note that m is always taken to satisfy the condition $(m, p) = 1$ in the Z_p case or $(m, n) = 1$ in the Z_n case. As for k, it is determined by the value of the phase-shift between perturbation functions.

In the following, we demonstrate with an example in $\mathbb{R}^6$ how to classify all the possible ratio of frequencies where a periodic solution with cyclic symmetry could exist.

Instead of taking $\phi_i(t) = f(t + (i-1)T/6)$ for some periodic function f with period T, we take $\phi_i(t) = f(t - (i-1)T/6)$ this time. This is equivalent to

$$\phi_{i+1}(t + \frac{1}{6}T) = \phi_i, \tag{5.10}$$

for all i. The ODE system is as usual assumed to be Z_6-symmetric in the absence of the forcing terms. Under this framework, a periodic solution could possess Z_6, Z_3, Z_2 or no symmetry. In each case, (5.10) gives us a fixed k by comparing the condition $\phi_{i+q}(t + \frac{k}{p}T_\phi) = \phi_i(t)$ in Proposition 5.2.3. The number of distinct possible ratios depends on how many values of m, $1 \le m < p$, are relatively prime to p.

- Z_6 **ratio:** $p = 6$, $q = 1$, and (5.10) implies $k = 1$. There are two possible m: $m = 1$ or $m = 5$. Therefore, according to (5.9), the ratio of frequencies can be
$$\frac{6l+1}{6j-1} \quad \text{or} \quad \frac{6l+5}{6j-5}.$$
- Z_3 **ratio:** $p = 3$, $q = 2$, and (5.10) implies $\phi_{i+2}(t + \frac{1}{3}T) = \phi_i$. Hence $k = 1$. There are two possible m: $m = 1$ or $m = 2$. Therefore, according to (5.9), the ratio of frequencies can be
$$\frac{3l+1}{3j-1} \quad \text{or} \quad \frac{3l+2}{3j-2}.$$

Symmetry	Z_6	Z_3	Z_2	None
Ratio	$\frac{6l+1}{6j-1}$, $\frac{6l+5}{6j-5}$	$\frac{3l+1}{3j-1}$, $\frac{3l+2}{3j-2}$	$\frac{2l+1}{2j-1}$	otherwise

Table 5.1: The classification of the ratio of frequencies of a periodic solution with cyclic symmetry. The underlying 6-dimensional system has the Z_6-symmetry in the absence of forcing term ϕ and ϕ is taken to be $\phi_{i+1}(t + \frac{1}{6}T) = \phi_i$.

- Z_2 **ratio:** $p = 2$, $q = 3$, and (5.10) implies $\phi_{i+3}(t + \frac{1}{2}T) = \phi_i$. Hence $k = 1$. There is only one possible m: $m = 1$. Therefore, according to (5.9), the ratio of frequencies must be
$$\frac{2l + 1}{2j - 1}.$$
- **Non-symmetric:** Otherwise.

This classification is summarized in Table 5.1.

5.2.4 Non-symmetric periodic solutions

In this section, we discuss whether a given rational number could be the ratio of frequencies of a symmetric solution. This question arises from the various equivalent forms of a rational number. For example,

$$\frac{8}{7} = \frac{16}{14} = \frac{24}{21} = ...,$$

each of which demonstrates a ratio formed in different ways in terms of Z_5-symmetry:

$$\frac{1 \cdot 5 + 3}{2 \cdot 5 - 3} = \frac{3 \cdot 5 + 1}{3 \cdot 5 - 1} = \frac{5 \cdot 5 - 1}{4 \cdot 5 + 1} = ...$$

Nevertheless, by Proposition 5.2.3, if a rational number α/β cannot be written in the form (5.9), then it cannot be the ratio of frequencies of any Z_p-symmetric periodic solution. Hence, we can identify those periodic solutions without Z_p-symmetry by the ratio.

Firstly, note that the forms in (5.9) for different m with $(m, p) = 1$ are interchangeable. This is because $(m, p) = 1$ implies the existence of integers n_1 and n_2 such that $n_1 p + n_2 m = 1$. So multiplying both the denominator and numerator of (5.9) by n_2 gives

$$\frac{n_2(lp + mk)}{n_2(jp - m)} = \frac{n_2 lp + (1 - n_1 p)k}{n_2 jp + n_1 p - 1} = \frac{l'p + k}{j'p - 1},$$

where $l' = n_2 l - n_1 k$ and $j' = n_2 j + n_1$.

Moreover, $jp + m'$, where $(p, m') \neq 1$, cannot be transformed into the form $j'p + m$, where $(p, m) = 1$. Therefore, for a rational number α/β, if $\beta = jp + m'$ with $(p, m') \neq 1$, then the periodic solution is not Z_p-symmetric. We then have the following proposition:

Proposition 5.2.4 *Suppose $\phi_{i+q}(t + \frac{k}{p}T_\phi) = \phi_i(t)$ for all i in system (5.1) and $\alpha/\beta = (lp + k')/(jp - m')$ is a rational number, where l, j, m' and k' are integers and $(\alpha, \beta) = 1$. If $(p, m') \neq 1$ or $k' \not\equiv m'k \pmod{p}$, then the non-trivial periodic solution with frequency ratio α/β is not Z_p-symmetric.*

We close this section with a brief remark showing that it is possible for non-symmetric periodic solutions to nevertheless have frequency ratios of the form (5.9). This demonstrates that condition (5.9) might be not sufficient to guarantee the existence of a Z_p-symmetric periodic solution.

Consider a four-dimensional case of (5.1) with $\phi_{i+1}(t) = \phi_i(t + T_\phi/4)$. In this case, $k = 3$ and $m = 1$ or $m = 3$. A Z_4-symmetric periodic solution then must have one of the following ratios of frequencies:

$$\frac{4l + 3}{4j - 1} \text{ or } \frac{4l + 1}{4j + 1},$$

for some integers l and j, by Proposition 5.2.3. For example, $7/3$ is in this form. Suppose now that $X(t)$ is a non-symmetric periodic solution with period $P = 7T_\phi$

and it intersects $3 \cdot 4$ times with the cross sections, $E, \sigma E, \sigma^2 E$ and $\sigma^3 E$, which are defined in the same way as we did in the previous sections, through a whole period. Then the averaged return time T is

$$P \times \frac{4}{3 \cdot 4},$$

which is $7T_\phi/3$. In other words, the ratio of frequencies of this non-symmetric solution is $7/3$, a Z_4-symmetric ratio, even though this periodic orbit $X(t)$ has no symmetry.

5.3 The positions of period-1 periodic solutions with symmetry – an example

In this section, we consider a 3-dimensional system:

$$\begin{cases} \dot{x} &= x(1-(x+y+z)-cy+ez)+\gamma\phi_1(2\omega t) \\ \dot{y} &= y(1-(x+y+z)-cz+ex)+\gamma\phi_2(2\omega t) \\ \dot{z} &= z(1-(x+y+z)-cx+ey)+\gamma\phi_3(2\omega t) \end{cases}, \tag{5.11}$$

where ϕ_1, ϕ_2 and ϕ_3 are non-negative periodic functions of period 2π. A similar system was studied in the previous two chapters in which we observed the existence of a sequence of intervals in which frequency-locking occurs. We use this system to check the validity of the results obtained in the previous sections. Specifically, we only focus on the period-1 periodic solutions which produce the frequency-locking windows. Recall that a periodic solution is classified as period-1 if it intersects any cross section at only one point. The positions of the windows where Z_3-symmetric period-1 periodic solutions exist will be identified. Instead of applying the previous results directly, we study the system by analyzing its Poincaré map and then prove results analogue to Proposition 5.2.1 and 5.2.2. The

numerical simulations in section 5.3.3 confirm that the positions of these windows are at exactly the locations predicted by the analytic results.

5.3.1 Poincaré map

By the same method of calculation as presented in Chapter 3, we can easily derive the Poincaré map of (5.11). We will omit the detailed derivation but only demonstrate the map from H_3^{in} to H_1^{in} briefly in the following. The notations we use here will be completely the same as those in Chapter 3.

Near P_3, the system can be approximated up to $O(\gamma)$ by:

$$\begin{cases} \dot{x} &= ex + \gamma\phi_1 \\ \dot{y} &= -cy + \gamma\phi_2 \\ \dot{w} &= -w - (1+c)x + (e-1)y + \gamma\phi_3 \end{cases}, \tag{5.12}$$

where $w = z - 1$. Suppose that the trajectory of (5.12) starting at time $t = s$ from $(x_1, h, z_1) \in H_3^{in}$ intersects H_3^{out} at the point (h, y_2, z_2) at time $t = T_1$. Integrating (5.12) implies

$$\begin{cases} y_2(\gamma) &= h^{1-c/e}x_1^{c/e} + h^{1-c/e}x_1^{c/e}\left[\frac{c}{e}x_1^{-1}\int_s^{T_1(0)} \mathrm{e}^{-e(\tau-s)}\phi_1(2\omega\tau)d\tau \right. \\ & \quad \left. + \frac{1}{h}\int_s^{T_1(0)} \mathrm{e}^{c(\tau-s)}\phi_2(2\omega\tau)d\tau\right]\gamma \\ T_1(\gamma) &= s + \log(\tfrac{h}{x_1})^{1/e} - \left[x_1^{-1}\tfrac{1}{e}\int_s^{T_1(0)} \mathrm{e}^{-e(\tau-s)}\phi_1(2\omega\tau)d\tau\right]\gamma \end{cases}.$$

Since the plane $\{y = 0\}$ supporting the connection between P_3 and P_1 is no longer invariant, the intersections of the unstable manifold of P_3' and the cross sections H_3^{out} and H_1^{in} are relative to the y-coordinate of P_3' and P_1' respectively. Following the same calculation as in Remark 3.2.1, the y-coordinate of P_3' is

$$\left(\frac{1}{\mathrm{e}^{c\pi/\omega} - 1}\int_0^{\pi/\omega} \mathrm{e}^{c\tau}\phi_2(2\omega(t+\tau))d\tau\right)\gamma,$$

and the y-coordinate of P_1' is

$$\left(\frac{1}{\mathrm{e}^{-e\pi/\omega} - 1}\int_0^{\pi/\omega} \mathrm{e}^{-e\tau}\phi_2(2\omega(t+\tau))d\tau\right)\gamma.$$

Therefore, the map between H_3^{in} and H_1^{in} is

$$\Phi_1 : \begin{cases} \bar{x} &= x^{c/e} + \mu_1\gamma \\ &\quad +\mu_2 x^{c/e}\left[\frac{c}{e}x^{-1}\int_t^g \mathrm{e}^{-e(\tau-t)}\phi_1(2\omega\tau)d\tau + \frac{1}{h}\int_t^g \mathrm{e}^{c(\tau-t)}\phi_2(2\omega\tau)d\tau\right]\gamma \\ &\quad +\mu_4\left[\frac{1}{\mathrm{e}^{c\pi/\omega}-1}\int_0^{\pi/\omega}\mathrm{e}^{c\tau}\phi_2(2\omega(t+\tau))d\tau\right]\gamma \\ &\quad +\mu_5\left[\frac{1}{\mathrm{e}^{-e\pi/\omega}-1}\int_0^{\pi/\omega}\mathrm{e}^{-e\tau}\phi_2(2\omega(t+\tau))d\tau\right]\gamma \\ \bar{t} &= t + \mu_3 - \frac{1}{e}\log x - \left[\frac{1}{e}\int_t^g \mathrm{e}^{-e(\tau-t)}\phi_1(2\omega\tau)d\tau\right]x^{-1}\gamma \end{cases},$$

where, as before, $g = t + \mu_3 - \frac{1}{e}\log x$ and μ_i, $i = 1, ..., 5$, are constant. Note that the integrals involving g can be written as

$$\int_0^{g'} \mathrm{e}^{-e\tau}\phi_1(2\omega(\tau+t))d\tau,$$

where $g' = \mu_3 - \frac{1}{e}\log x$ by changing variable $\tau' = \tau - t$. This is useful because g' is independent of t.

Since system (5.11) stays the same by cyclic-permutating its suffixes, the Poincaré map $\Phi : H_3^{in} \to H_3^{in}$ is given by the composition of the three maps Φ_i, $i = 1, 2, 3$:

$$\Phi_i : \begin{cases} \bar{x} &= x^{c/e} + \mu_1\gamma \\ &\quad +\mu_2 x^{c/e}\left[\frac{c}{e}x^{-1}\int_0^{g'} \mathrm{e}^{-e\tau}\phi_i(2\omega(\tau+t))d\tau + \frac{1}{h}\int_0^{g'} \mathrm{e}^{c\tau}\phi_{i+1}(2\omega(\tau+t))d\tau\right]\gamma \\ &\quad +\mu_4\left[\frac{1}{\mathrm{e}^{c\pi/\omega}-1}\int_0^{\pi/\omega}\mathrm{e}^{c\tau}\phi_{i+1}(2\omega(t+\tau))d\tau\right]\gamma \\ &\quad +\mu_5\left[\frac{1}{\mathrm{e}^{-e\pi/\omega}-1}\int_0^{\pi/\omega}\mathrm{e}^{-e\tau}\phi_{i+1}(2\omega(t+\tau))d\tau\right]\gamma \\ \bar{t} &= t + \mu_3 - \frac{1}{e}\log x - \left[\frac{1}{e}\int_0^{g'} \mathrm{e}^{-e\tau}\phi_i(2\omega(\tau+t))d\tau\right]x^{-1}\gamma \end{cases}, \tag{5.13}$$

where $\Phi_2 : H_1^{in} \to H_2^{in}$ and $\Phi_3 : H_2^{in} \to H_3^{in}$. That is, $\Phi = \Phi_3 \circ \Phi_2 \circ \Phi_1 : H_3^{in} \to H_3^{in}$.

5.3.2 Periodic solutions with symmetry

In this section, we give a necessary condition for system (5.11) to have periodic solutions with Z_3-symmetry. We will consider only period-1 solutions in which the period T is equal to $\frac{k\pi}{\omega}$, $k = 1, 2, 3, ...$

Suppose $(x(t), y(t), z(t))$ is a periodic solution of system (5.11) with Z_3-symmetry and $H_3^{in} = \{y = h\}$. Let $(x_0, h, z_0) \in H_3^{in}$ be a point of the periodic solution at time t_0. Then the periodic solution intersects $H_1^{in} = \{z = h\}$ and $H_2^{in} = \{x = h\}$ at (z_0, x_0, h) and (h, z_0, x_0) respectively. By definition, the Poincaré map $\Phi = \Phi_3 \circ \Phi_2 \circ \Phi_1$ for the system (5.11) acts in the way depicted in the following diagram:

$$(x_0, t_0) \overset{\Phi_1}{\to} \left(x_0, t_0 + \frac{k\pi}{3\omega}\right) \overset{\Phi_2}{\to} \left(x_0, t_0 + \frac{2k\pi}{3\omega}\right) \overset{\Phi_3}{\to} \left(x_0, t_0 + \frac{k\pi}{\omega}\right). \tag{5.14}$$

Proposition 5.3.1 *Suppose* $\Phi_1(x_0, t_0) = (x_0, t_0 + \frac{k\pi}{3\omega})$ *for a fixed k. If* $\phi_{i+1}(2\omega t + \frac{2k\pi}{3}) = \phi_i(2\omega t)$ *for all t and i, then* $\Phi_2(x_0, t_0 + \frac{k\pi}{3\omega}) = (x_0, t_0 + \frac{2k\pi}{3\omega})$ *and* $\Phi_3(x_0, t_0 + \frac{2k\pi}{3\omega}) = (x_0, t_0 + \frac{k\pi}{\omega})$

Proof: We only prove the Φ_2 case.

The t-coordinate of $\Phi_2(x_0, t_0 + \frac{k\pi}{3\omega})$ is

$$t_0 + \frac{k\pi}{3\omega} + \mu_3 - \frac{1}{e}\log x_0 - \left[\frac{1}{e}\int_0^{g'} \mathrm{e}^{-e\tau}\phi_2\left(2\omega\left(\tau + t_0 + \frac{k\pi}{3\omega}\right)\right)d\tau\right] x_0^{-1}\gamma,$$

which is equal to

$$t_0 + \frac{k\pi}{3\omega} + \mu_3 - \frac{1}{e}\log x_0 - \left[\frac{1}{e}\int_0^{g'} \mathrm{e}^{-e\tau}\phi_1(2\omega(\tau + t_0))d\tau\right] x_0^{-1}\gamma, \tag{5.15}$$

since $\phi_2(2\omega(\tau + t_0 + \frac{k\pi}{3\omega})) = \phi_1(2\omega(\tau + t_0))$ for all τ. In addition, $\Phi_1(x_0, t_0) = (x_0, t_0 + \frac{k\pi}{3\omega})$ gives

$$t_0 + \frac{k\pi}{3\omega} = t_0 + \mu_3 - \frac{1}{e}\log x_0 - \left[\frac{1}{e}\int_0^{g'} \mathrm{e}^{-e\tau}\phi_1(2\omega(\tau + t_0))d\tau\right] x_0^{-1}\gamma,$$

i.e.

$$\frac{k\pi}{3\omega} = \mu_3 - \frac{1}{e}\log x_0 - \left[\frac{1}{e}\int_0^{g'} \mathrm{e}^{-e\tau}\phi_1(2\omega(\tau + t_0))d\tau\right] x_0^{-1}\gamma.$$

Substituting this into (5.15), it follows that the t-coordinate of $\Phi_2(x_0, t_0 + \frac{k\pi}{3\omega})$ is equal to $t_0 + \frac{2k\pi}{3\omega}$.

Since $\Phi_1(x_0, t_0) = (x_0, t_0 + \frac{k\pi}{3\omega})$ and $\phi_{i+1}(2\omega t + \frac{2k\pi}{3}) = \phi_i(2\omega t)$, we have

$$\begin{aligned}
x_0 &= x_0^{c/e} + \mu_1\gamma \\
&\quad +\mu_2 x_0^{c/e}\left[\tfrac{c}{e}x_0^{-1}\int_0^{g'} \mathrm{e}^{-e\tau}\phi_1(2\omega(\tau+t_0))d\tau + \tfrac{1}{h}\int_0^{g'}\mathrm{e}^{c\tau}\phi_2(2\omega(\tau+t_0))d\tau\right]\gamma \\
&\quad +\mu_4\left[\tfrac{1}{\mathrm{e}^{c\pi/\omega}-1}\int_0^{\pi/\omega}\mathrm{e}^{c\tau}\phi_2(2\omega(t_0+\tau))d\tau\right]\gamma \\
&\quad +\mu_5\left[\tfrac{1}{\mathrm{e}^{-e\pi/\omega}-1}\int_0^{\pi/\omega}\mathrm{e}^{-e\tau}\phi_2(2\omega(t_0+\tau))d\tau\right]\gamma \\
&= x_0^{c/e} + \mu_1\gamma \\
&\quad +\mu_2 x_0^{c/e}\left[\tfrac{c}{e}x_0^{-1}\int_0^{g'} \mathrm{e}^{-e\tau}\phi_2\left(2\omega\left(\tau+t_0+\tfrac{k\pi}{3\omega}\right)\right)d\tau + \tfrac{1}{h}\int_0^{g'}\mathrm{e}^{c\tau}\phi_3\left(2\omega\left(\tau+t_0+\tfrac{k\pi}{3\omega}\right)\right)d\tau\right]\gamma \\
&\quad +\mu_4\left[\tfrac{1}{\mathrm{e}^{c\pi/\omega}-1}\int_0^{\pi/\omega}\mathrm{e}^{c\tau}\phi_3\left(2\omega\left(t_0+\tau+\tfrac{k\pi}{3\omega}\right)\right)d\tau\right]\gamma \\
&\quad +\mu_5\left[\tfrac{1}{\mathrm{e}^{-e\pi/\omega}-1}\int_0^{\pi/\omega}\mathrm{e}^{-e\tau}\phi_3\left(2\omega\left(t_0+\tau+\tfrac{k\pi}{3\omega}\right)\right)d\tau\right]\gamma,
\end{aligned}$$

which is the x-coordinate of $\Phi_2(x_0, t_0 + \frac{k\pi}{3\omega})$. Therefore, $\Phi_2(x_0, t_0 + \frac{k\pi}{3\omega}) = (x_0, t_0 + \frac{2k\pi}{3\omega})$. Obviously, the Φ_3 part is similar to the Φ_2 one. ■

In other words, if the perturbation functions differ by only a phase-shift $\frac{2k\pi}{3}$, then (5.14) is valid if one of the three parts of (5.14) is true. This phase-shift condition constrains the form of perturbation functions and hence seems too strong for (5.14) to be valid at first sight. However, the following proposition shows that generically it is a necessary condition for system (5.11) to possess a periodic solution with Z_3-symmetry.

Proposition 5.3.2 *Generically, the existence of a periodic solution with Z_3-symmetry and period $\frac{k\pi}{\omega}$ in the system (5.11) implies $\phi_{i+1}(2\omega t + \frac{2k\pi}{3}) = \phi_i(2\omega t)$ for all t and i.*

By genericity, we mean that a Z_3-symmetric solution always exists in an open interval of c and e of system (5.11) for a fixed ω.

Before proceeding the proof of proposition 5.3.2, we make some remarks on ϕ_i and t_0. Firstly, if $(x_0, h, z_0) \in H_3^{in}$ is a point of a Z_3-symmetric periodic solution at time t_0, then (z_0, x_0, h) and (h, z_0, x_0) are the intersection points of the periodic solution and the cross sections H_1^{in} and H_2^{in} at time $t = t_0 + \frac{k\pi}{3\omega}$ and $t = t_0 + \frac{2k\pi}{3\omega}$,

respectively. The existence of a Z_3-symmetric solution also implies the tangent vectors of the periodic solution must possess Z_3 symmetry. For a Z_3-symmetric periodic solution, the x direction of the tangent vector of the point (x_0, h, z_0) at time t_0 must agree with the y direction of the tangent vector of the point (z_0, x_0, h) at time $t_0 + k\pi/3\omega$. By considering system (5.11), $\phi_2(2\omega t_0 + \frac{2k\pi}{3}) = \phi_1(2\omega t_0)$. Similarly, $\phi_3(2\omega t_0 + \frac{2k\pi}{3}) = \phi_2(2\omega t_0)$.

Secondly, t_0 is in fact a function of c, e and ω. We will assume that t_0 depends smoothly on c, e and ω, and we denote by t_0' the derivative of t_0 with respect to c in the following proof.

Proof of Proposition 5.3.2:

Suppose that there exists a periodic solution with Z_3-symmetry such that

$$\begin{aligned} \Phi_1(x_0, t_0) &= \left(x_0, t_0 + \tfrac{k\pi}{3\omega}\right) \\ \Phi_2\left(x_0, t_0 + \tfrac{k\pi}{3\omega}\right) &= \left(x_0, t_0 + \tfrac{2k\pi}{3\omega}\right) . \\ \Phi_3\left(x_0, t_0 + \tfrac{2k\pi}{3\omega}\right) &= \left(x_0, t_0 + \tfrac{k\pi}{\omega}\right) \end{aligned}$$

By the definition of the x-coordinates of Φ_1 and Φ_2, we have

$$\begin{aligned} x_0 &= x_0^{c/e} + \mu_1\gamma \\ &\quad +\mu_2 x_0^{c/e}\left[\tfrac{c}{e}x_0^{-1}\int_0^{g'} \mathrm{e}^{-e\tau}\phi_1(2\omega(\tau+t_0))d\tau + \tfrac{1}{h}\int_0^{g'} \mathrm{e}^{c\tau}\phi_2(2\omega(\tau+t_0))d\tau\right]\gamma \\ &\quad +\mu_4\left[\tfrac{1}{\mathrm{e}^{c\pi/\omega}-1}\int_0^{\pi/\omega} \mathrm{e}^{c\tau}\phi_2(2\omega(t_0+\tau))d\tau\right]\gamma \\ &\quad +\mu_5\left[\tfrac{1}{\mathrm{e}^{-e\pi/\omega}-1}\int_0^{\pi/\omega} \mathrm{e}^{-e\tau}\phi_2(2\omega(t_0+\tau))d\tau\right]\gamma \\ &= x_0^{c/e} + \mu_1\gamma \\ &\quad +\mu_2 x_0^{c/e}\left[\tfrac{c}{e}x_0^{-1}\int_0^{g'} \mathrm{e}^{-e\tau}\phi_2\left(2\omega\left(\tau+t_0+\tfrac{k\pi}{3\omega}\right)\right)d\tau + \tfrac{1}{h}\int_0^{g'} \mathrm{e}^{c\tau}\phi_3\left(2\omega\left(\tau+t_0+\tfrac{k\pi}{3\omega}\right)\right)d\tau\right]\gamma \\ &\quad +\mu_4\left[\tfrac{1}{\mathrm{e}^{c\pi/\omega}-1}\int_0^{\pi/\omega} \mathrm{e}^{c\tau}\phi_3\left(2\omega\left(t_0+\tau+\tfrac{k\pi}{3\omega}\right)\right)d\tau\right]\gamma \\ &\quad +\mu_5\left[\tfrac{1}{\mathrm{e}^{-e\pi/\omega}-1}\int_0^{\pi/\omega} \mathrm{e}^{-e\tau}\phi_3\left(2\omega\left(t_0+\tau+\tfrac{k\pi}{3\omega}\right)\right)d\tau\right]\gamma, \end{aligned}$$

which implies

$$\begin{aligned}
&\mu_2 x_0^{c/e}\left[\frac{c}{e}x_0^{-1}\int_0^{g'}\mathrm{e}^{-e\tau}\left(\phi_1(2\omega(\tau+t_0))-\phi_2\left(2\omega\left(\tau+t_0+\tfrac{k\pi}{3\omega}\right)\right)\right)d\tau\right.\\
&\left.+\tfrac{1}{h}\int_0^{g'}\mathrm{e}^{c\tau}\left(\phi_2(2\omega(\tau+t_0))-\phi_3\left(2\omega\left(\tau+t_0+\tfrac{k\pi}{3\omega}\right)\right)\right)d\tau\right]\gamma\\
&+\mu_4\left[\tfrac{1}{\mathrm{e}^{c\pi/\omega}-1}\int_0^{\pi/\omega}\mathrm{e}^{c\tau}\left(\phi_2(2\omega(t_0+\tau))-\phi_3\left(2\omega\left(t_0+\tau+\tfrac{k\pi}{3\omega}\right)\right)\right)d\tau\right]\gamma\\
&+\mu_5\left[\tfrac{1}{\mathrm{e}^{-e\pi/\omega}-1}\int_0^{\pi/\omega}\mathrm{e}^{-e\tau}\left(\phi_2(2\omega(t_0+\tau))-\phi_3\left(2\omega\left(t_0+\tau+\tfrac{k\pi}{3\omega}\right)\right)\right)d\tau\right]\gamma\\
=\;&0.
\end{aligned}$$

In the generic case, this equality holds in an open interval of c and e. Since each collection of terms multiplying one of μ_2, μ_4 and μ_5 has a different functional dependence on c and e, the integrals in each collection can be considered to vanish independently of each other, i.e. the above equality implies conditions:

$$\begin{aligned}
\int_0^{g'}\mathrm{e}^{-e\tau}\left(\phi_1(2\omega(\tau+t_0))-\phi_2\left(2\omega\left(\tau+t_0+\tfrac{k\pi}{3\omega}\right)\right)\right)d\tau &= 0\\
\int_0^{g'}\mathrm{e}^{c\tau}\left(\phi_2(2\omega(\tau+t_0))-\phi_3\left(2\omega\left(\tau+t_0+\tfrac{k\pi}{3\omega}\right)\right)\right)d\tau &= 0\\
\int_0^{\pi/\omega}\mathrm{e}^{c\tau}\left(\phi_2(2\omega(t_0+\tau))-\phi_3\left(2\omega\left(t_0+\tau+\tfrac{k\pi}{3\omega}\right)\right)\right)d\tau &= 0\\
\int_0^{\pi/\omega}\mathrm{e}^{-e\tau}\left(\phi_2(2\omega(t_0+\tau))-\phi_3\left(2\omega\left(t_0+\tau+\tfrac{k\pi}{3\omega}\right)\right)\right)d\tau &= 0
\end{aligned}.$$

The third equality can be written in the form

$$\int_0^{\pi/\omega}\mathrm{e}^{c\tau}\phi_3\left(2\omega(t_0+\tau)+\frac{2k\pi}{3}\right)d\tau=\int_0^{\pi/\omega}\mathrm{e}^{c\tau}\phi_2(2\omega(t_0+\tau))d\tau, \tag{5.16}$$

which is valid in an open interval of c. Differentiating the equation with respect to c, we have, for the left hand side of (5.16)

$$\begin{aligned}
\tfrac{d}{dc}\mathrm{LHS} &= \int_0^{\pi/\omega}\tau\mathrm{e}^{c\tau}\phi_3\left(2\omega(t_0+\tau)+\tfrac{2k\pi}{3}\right)d\tau\\
&\quad+\int_0^{\pi/\omega}\mathrm{e}^{c\tau}\phi_3'\left(2\omega(t_0+\tau)+\tfrac{2k\pi}{3}\right)2\omega t_0' d\tau.
\end{aligned}$$

By integration by parts, the last term is equal to

$$\mathrm{e}^{c\pi/\omega}t_0'\phi_3\left(2\omega t_0+\frac{2k\pi}{3}\right)-t_0'\phi_3\left(2\omega t_0+\frac{2k\pi}{3}\right)-ct_0'\int_0^{\pi/\omega}\mathrm{e}^{c\tau}\phi_3\left(2\omega(t_0+\tau)+\frac{2k\pi}{3}\right)d\tau,$$

which is equal to

$$\mathrm{e}^{c\pi/\omega}t_0'\phi_2(2\omega t_0)-t_0'\phi_2(2\omega t_0)-ct_0'\int_0^{\pi/\omega}\mathrm{e}^{c\tau}\phi_2(2\omega(t_0+\tau))d\tau.$$

In other words,

$$\begin{aligned}\tfrac{d}{dc}\text{LHS} &= \int_0^{\pi/\omega} \tau \mathrm{e}^{c\tau}\phi_3\left(2\omega(t_0+\tau)+\tfrac{2k\pi}{3}\right)d\tau \\ &\quad +\mathrm{e}^{c\pi/\omega}t_0'\phi_2(2\omega t_0) - t_0'\phi_2(2\omega t_0) - ct_0'\int_0^{\pi/\omega}\mathrm{e}^{c\tau}\phi_2(2\omega(t_0+\tau))d\tau.\end{aligned}$$

Equivalently, differentiating the right hand side of (5.16) with respect to c, we obtain

$$\begin{aligned}\tfrac{d}{dc}\text{RHS} &= \int_0^{\pi/\omega} \tau \mathrm{e}^{c\tau}\phi_2(2\omega(t_0+\tau))d\tau + \int_0^{\pi/\omega}\mathrm{e}^{c\tau}\phi_2'(2\omega(t_0+\tau))2\omega t_0'd\tau \\ &= \int_0^{\pi/\omega} \tau \mathrm{e}^{c\tau}\phi_2(2\omega(t_0+\tau))d\tau \\ &\quad +\mathrm{e}^{c\pi/\omega}t_0'\phi_2(2\omega t_0) - t_0'\phi_2(2\omega t_0) - ct_0'\int_0^{\pi/\omega}\mathrm{e}^{c\tau}\phi_2(2\omega(t_0+\tau))d\tau.\end{aligned}$$

Comparing the expressions of $\frac{d}{dc}$LHS and $\frac{d}{dc}$RHS, it is obvious that

$$\int_0^{\pi/\omega} \tau \mathrm{e}^{c\tau}\phi_3\left(2\omega(t_0+\tau)+\frac{2k\pi}{3}\right)d\tau = \int_0^{\pi/\omega} \tau \mathrm{e}^{c\tau}\phi_2(2\omega(t_0+\tau))d\tau,$$

i.e.

$$\int_0^{\pi/\omega} \tau \mathrm{e}^{c\tau}\left(\phi_3\left(2\omega(t_0+\tau)+\frac{2k\pi}{3}\right)-\phi_2(2\omega(t_0+\tau))\right)d\tau = 0.$$

Differentiating the last equation again and then by induction, we have

$$\int_0^{\pi/\omega} \tau^n \mathrm{e}^{c\tau}\left(\phi_3\left(2\omega(t_0+\tau)+\frac{2k\pi}{3}\right)-\phi_2(2\omega(t_0+\tau))\right)d\tau = 0,$$

for all integer $n \geq 0$. This implies

$$\int_0^{\pi/\omega} P(\tau)\mathrm{e}^{c\tau}\left(\phi_3\left(2\omega(t_0+\tau)+\frac{2k\pi}{3}\right)-\phi_2(2\omega(t_0+\tau))\right)d\tau = 0,$$

for all polynomials P. Since the polynomial space in dense in the continuous function space with sup-norm, we have

$$\int_0^{\pi/\omega} \left(\mathrm{e}^{c\tau}\left(\phi_3\left(2\omega(t_0+\tau)+\frac{2k\pi}{3}\right)-\phi_2(2\omega(t_0+\tau))\right)\right)^2 d\tau = 0.$$

Therefore,

$$\phi_3\left(2\omega t+\frac{2k\pi}{3}\right) = \phi_2(2\omega t),$$

for all t. Similarly, $\phi_2(2\omega t+\frac{2k\pi}{3}) = \phi_1(2\omega t)$ can be proved by the same way. Hence, we have done. ■

Combining Proposition 5.3.1 and 5.3.2, we are able to identify the positions where the periodic solutions with Z_3-symmetry exist.

Corollary 5.3.1 *Generically, the Z_3-symmetry solutions, with period $\frac{k\pi}{\omega}$, of system (5.11) can occur only for*

1. $k = 3l$, $l = 1, 2, ...$, *if* $\phi_{i+1} = \phi_i$ *for all i, i.e. when* $T = \frac{3l\pi}{\omega}$.
2. $k = 3l + 1$, $l = 0, 1, 2, ...$, *if* $\phi_{i+1}(t + \frac{2\pi}{3}) = \phi_i(t)$ *for all i, i.e. when* $T = \frac{(3l+1)\pi}{\omega}$.
3. $k = 3l + 2$, $l = 0, 1, 2, ...$, *if* $\phi_{i+1}(t + \frac{4\pi}{3}) = \phi_i(t)$ *for all i, i.e. when* $T = \frac{(3l+2)\pi}{\omega}$.

5.3.3 Numerical results

In this section, we consider an example and display figures which illustrate the three possibilities listed in Corollary 5.3.1.

Let $\phi_1(2\omega t) = \sin^2(\omega t + \theta_1)$, $\phi_2(2\omega t) = \sin^2(\omega t + \theta_2)$ and $\phi_3(2\omega t) = \sin^2(\omega t + \theta_3)$. We are interested in the positions where period-1 periodic solutions with Z_3-symmetry exist. Firstly, by (5.13), the Poincaré map of the corresponding ODE system is the composition $\Phi = \Phi_3 \circ \Phi_2 \circ \Phi_1$ of three maps:

$$\Phi_i : \begin{cases} \bar{x} &= x^{c/e} + \mu_1\gamma \\ &\quad + [\mu_2(-a_1\cos(2\omega g + 2\theta_{i+1}) - b_1\sin(2\omega g + 2\theta_{i+1})) \\ &\quad + \mu_4(a_1\cos(2\omega\bar{t} + 2\theta_{i+1}) + b_1\sin(2\omega\bar{t} + 2\theta_{i+1})) \\ &\quad + \mu_5(a_2\cos(2\omega\bar{t} + 2\theta_{i+1}) + b_2\sin(2\omega\bar{t} + 2\theta_{i+1}))]\,\gamma \\ \bar{t} &= t + \mu_3 - \frac{1}{e}\log x - \frac{1}{2e^2}\left[1 - a_2\cos(2\omega t + 2\theta_i) + b_2\sin(2\omega t + 2\theta_i)\right] x^{-1}\gamma \end{cases}, \tag{5.17}$$

$i = 1, 2, 3$. Figure 5.2 shows that the map agrees very well with the original ODE system for $(\theta_1, \theta_2, \theta_3) = (0, \pi/3, 2\pi/3)$, $c = 0.25$ and $e = 0.2$. Here, we take

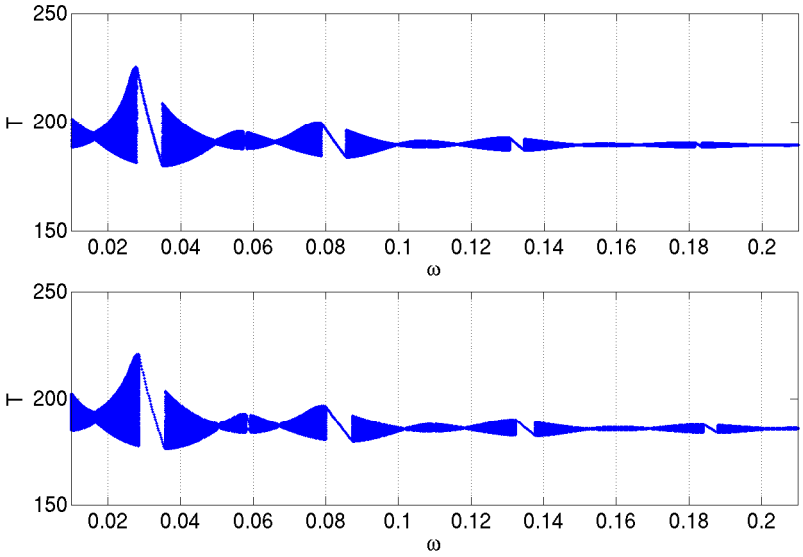

Figure 5.2: The dynamics of the ODEs system (5.11) (upper) and the Poincaré map (5.13) for $c = 0.25, e = 0.2$ and $(\theta_1, \theta_2, \theta_3) = (0, \pi/3, 2\pi/3)$.

parameters $\mu_1 = 9.6$, $\mu_2 = 0.3$, $\mu_3 = 17/3$, $\mu_4 = 26.4$ and $\mu_5 = -35.7$ for the Poincaré map. Note that the parameters $\mu_1, ..., \mu_5$ are the same with the ones in chapter 4 except that the new μ_3 is the original one divided by 3. This reflects the fact that we now divide the whole map into three parts. In the rest of this section, all the figures are plotted for the Poincaré map with this set of parameters.

To detect Z_3-symmetric periodic solutions of the ODE system (5.11), we consider the difference of the y-coordinate and the z-coordinate of points where trajectories intersect H_1^{in} and H_2^{in} respectively. This is equivalent to check if $\Phi_2 \circ \Phi_1(x_0, t_0) - \Phi_1(x_0, t_0) = (0, \frac{k\pi}{3\omega})$ in the Poincaré map. We denote the x-coordinate of this difference by Δx. For each fixed ω, we iterate $1,000$ times for the map, take the last 500 points and then calculate the maximum and minimum of Δx. Periodic solutions with Z_3-symmetry exist generically if and only if $Max(\Delta x) - Min(\Delta x) = 0$ over an open interval in ω.

$(\theta_1, \theta_2, \theta_3)$	$(0, 0, 0)$	$(0, \pi/3, 2\pi/3)$	$(0, 2\pi/3, \pi/3)$
k	3, 6, 9,...	2, 5, 8,...	1, 4, 7,...

Table 5.2: Three possible locations of the k-th frequency-locking windows where Z_3-symmetric solution exists.

Without loss of generality, we may take $\theta_1 = 0$. Figure 5.3, 5.4 and 5.5 show that the periodic solutions with Z_3-symmetry are located at specific frequency-locking windows for the case $(\theta_1, \theta_2, \theta_3) = (0, 0, 0)$, $(0, \pi/3, 2\pi/3)$ and $(0, 2\pi/3, \pi/3)$, respectively. In each upper subplots of these figures, we also plot the hyperbolic curves $k\pi/\omega$, $k = 1, 2, 3, 4, 5, 6$ for reference. It turns out these symmetric solutions occur only at the k-th frequency-locking windows as shown in Table 5.2. This matches the analytic results which we have shown in Corollary 5.3.1.

In addition, we remark that there exist isolated values of ω where $Max(\Delta x) - Min(\Delta x) = 0$ but they are not identified as Z_3-symmetric by Corollary 5.3.1. This happens actually due to a non-generic situation. More precisely, they appear just because we are only comparing the x-coordinates of the points on the cross sections but not looking at the whole trajectories, and as a result, they can be removed by changing c or e slightly. In other words, this is not the case in our disscussion and should be ignored.

5.4 Symmetric solutions in coupled cell systems

In this section, we consider a system formed by coupling two ODE systems:

$$\begin{cases} \dot{x} &= F_1(x) + \gamma(y - x) \\ \dot{y} &= F_2(y) + \gamma(x - y), \end{cases} \tag{5.18}$$

where $x, y \in \mathrm{R}^n$ and both F_1 and F_2 have Z_n-symmetry. We call system (5.18) a coupled cell system with two cells: the x-cell and the y-cell.

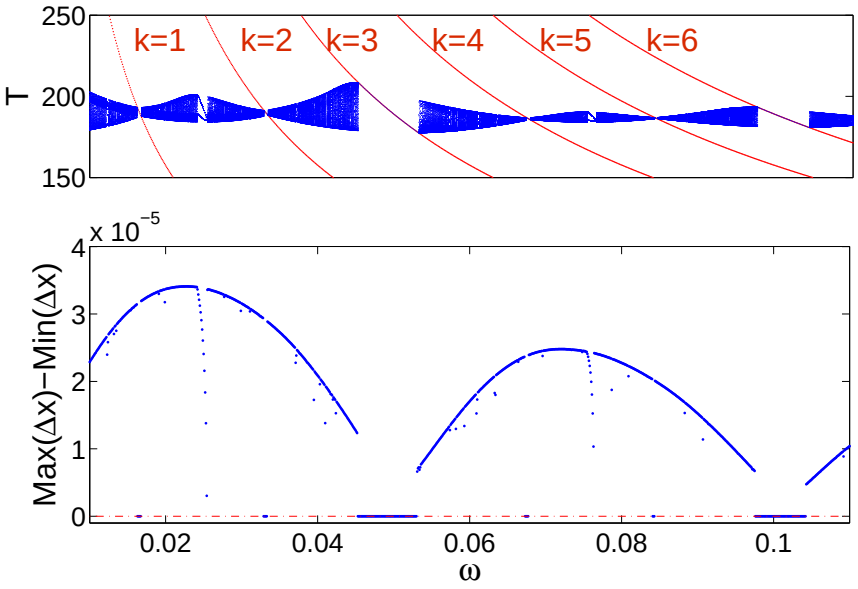

Figure 5.3: The frequency-locking windows where Z_3-symmetric solutions exist for $(\theta_1, \theta_2, \theta_3) = (0, 0, 0)$, $c = 0.25$ and $e = 0.2$. We consider the Poincaré map (5.17) and denote the difference of the x coordinates of $\Phi_1 \circ \Phi^l$ and $\Phi_2 \circ \Phi_1 \circ \Phi^l$ by Δx, where l is an integer. Only the last 500 points of the 1,000 iterations are ploted. If Max(Δx)-Min(Δx)=0 in an open intervals of ω, then the periodic solutions at these ω could be Z_3-symmetric. The red curves on the upper subplot are hyperbolic curves $k\pi/\omega$. The Z_3-symmetric solutions occur only at $k = 3, 6, 9, ...$

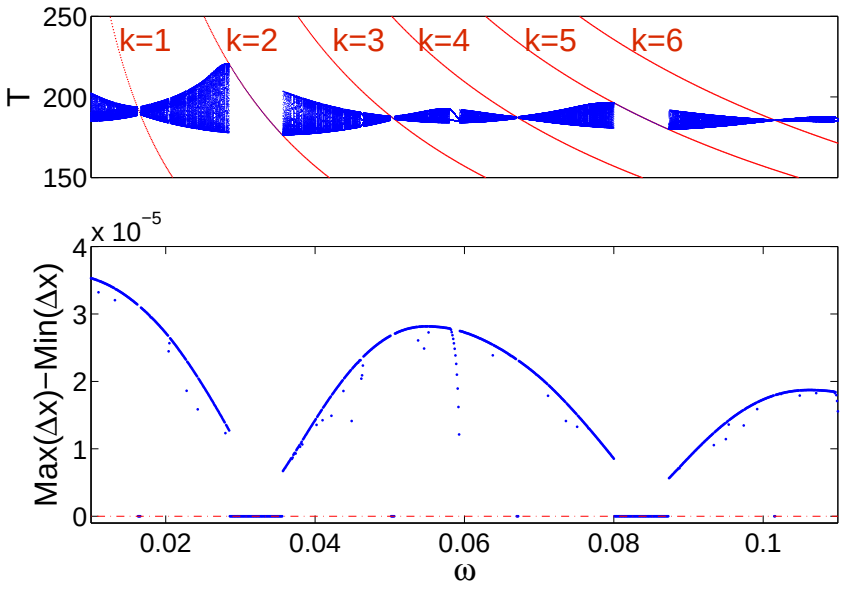

Figure 5.4: The frequency-locking windows where Z_3-symmetric solutions exist for $(\theta_1, \theta_2, \theta_3) = (0, \pi/3, 2\pi/3)$, $c = 0.25$ and $e = 0.2$. We consider the Poincaré map (5.17) and denote the difference of the x coordinates of $\Phi_1 \circ \Phi^l$ and $\Phi_2 \circ \Phi_1 \circ \Phi^l$ by Δx, where l is an integer. Only the last 500 points of the 1,000 iterations are ploted. If Max(Δx)-Min(Δx)=0 in an open intervals of ω, then the periodic solutions at these ω could be Z_3-symmetric. The red curves on the upper subplot are hyperbolic functions $k\pi/\omega$. The Z_3-symmetric solutions occur only at $k = 2, 5, 8, ...$

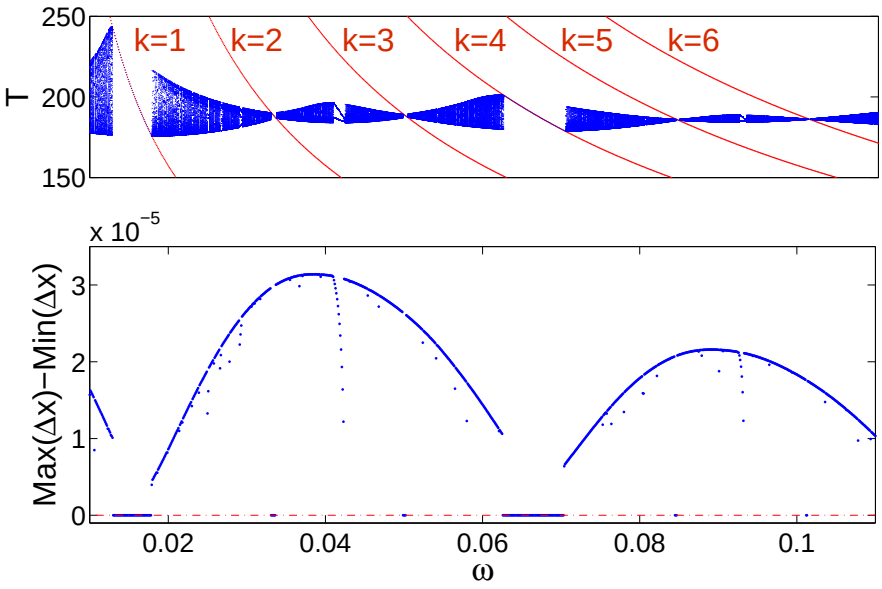

Figure 5.5: The frequency-locking windows where Z_3-symmetric solutions exist for $(\theta_1, \theta_2, \theta_3) = (0, 2\pi/3, \pi/3)$, $c = 0.25$ and $e = 0.2$. We consider the Poincaré map (5.17) and denote the difference of the x coordinates of $\Phi_1 \circ \Phi^l$ and $\Phi_2 \circ \Phi_1 \circ \Phi^l$ by Δx, where l is an integer. Only the last 500 points of the 1,000 iterations are ploted. If Max(Δx)-Min(Δx)=0 in an open intervals of ω, then the periodic solutions at these ω could be Z_3-symmetric. The red curves on the upper subplot are hyperbolic functions $k\pi/\omega$. The Z_3-symmetric solutions occur only at $k = 1, 4, 7, ...$

Suppose there exists a solution $(\bar{x}(t), \bar{y}(t))$ in the system (5.18), for which $\bar{x}(t)$ and $\bar{y}(t)$ are periodic solutions of x-cell and y-cell respectively. We are interested in the ratio of frequencies between $\bar{x}(t)$ and $\bar{y}(t)$, specifically, when they are also Z_n-symmetric.

5.4.1 Synchronisation of periodic solutions

It clearly follows from (5.18) that $\bar{x}(t)$ is a periodic solution of the system:

$$\dot{x} = \bar{F}_1(x) + \gamma\bar{y}(t), \tag{5.19}$$

where $\bar{F}_1(x) = F_1(x) - \gamma x$. Similarly, $\bar{y}(t)$ is a periodic solution of the system:

$$\dot{y} = \bar{F}_2(y) + \gamma\bar{x}(t), \tag{5.20}$$

where $\bar{F}_2(y) = F_2(y) - \gamma y$. Denote by P_x and P_y the period of $\bar{x}$ and $\bar{y}$ respectively. As we have shown at the beginning of section 5.2.1, there exist positive integers k_1 and k_2 such that $P_x = k_1 P_y$ and $P_y = k_2 P_x$. This implies

$$P_x = P_y.$$

We denote this common period P.

Note that both $\bar{F}_1$ and $\bar{F}_2$ are still Z_n-symmetric. The following proposition shows that a kind of synchronisation must occur for $\bar{x}$ and $\bar{y}$ to be Z_n-symmetric.

Proposition 5.4.1 *Suppose system (5.18) has a non-trivial periodic solution* $(\bar{x}(t), \bar{y}(t))$. *Then* $\bar{x}$ *is* Z_n*-symmetric if and only if* $\bar{y}$ *is* Z_n*-symmetric. Moreover,* $\sigma^m \circ \tau_{P/n}\bar{x}(t) = \bar{x}(t)$ *if and only if* $\sigma^m \circ \tau_{P/n}\bar{y}(t) = \bar{y}(t)$, *where* $(m, n) = 1$.

Proof: Since (5.19) is a Z_n-symmetric system with a periodic perturbation, the results obtained in the previous sections can be applied. Suppose $\bar{x}(t)$ is Z_n-symmetric and satisfies $\sigma^m \circ \tau_{P/n}\bar{x}(t) = \bar{x}(t)$, where m is an integer with $(m, n) = 1$.

By Proposition 5.2.1, $\bar{x}(t)$ has Z_n-symmetry only if

$$\bar{y}_{i+m}\left(t+\frac{1}{n}P\right)=\bar{y}_i(t),$$

for all t. This is equivalent to

$$\sigma^m\bar{y}(t)=\bar{y}\left(t-\frac{1}{n}P\right),$$

for all t. In other words,

$$\sigma^m\circ\tau_{P/n}\bar{y}(t)=\bar{y}(t),$$

for all t. Therefore, $\bar{y}(t)$ is also Z_n-symmetric.

Conversely, if $\bar{y}(t)$ is Z_n-symmetric, then by the same argument, we can easily prove that $\bar{x}(t)$ must be also Z_n-symmetric. The proposition then follows. ■

Proposition 5.4.1 is very important as it also shows that the symmetric solutions in both cells are always of the same form. More precisely, if $\sigma^m x_0$ is the next symmetric copy of a point x_0 along $\bar{x}(t)$, then $\sigma^m y_0$ is also the next symmetric copy of a point y_0 along $\bar{y}(t)$. This result further restricts the form of the ratio of frequencies between $\bar{x}$ and $\bar{y}$. We will give an example of this fact in the next section.

The following corollary for the Z_p case is trivial.

Corollary 5.4.1 *Suppose system (5.18) has a non-trivial periodic solution* $(\bar{x}(t),\bar{y}(t))$ *and* Z_p *is a subgroup of* Z_n*. Then* $\bar{x}$ *is* Z_p*-symmetric if and only if* $\bar{y}$ *is* Z_p*-symmetric.*

5.4.2 Ratio of frequencies between two cells

We now turn to study the ratio of frequencies. Again, as we did in section 5.2.2, we define the frequency of $\bar{x}$ to be $f_x = 2\pi/T_x$, where T_x is the average of the first return time corresponding to a cross section. Similarly, the frequency of

$\bar{y}$ is defined by $f_y = 2\pi/T_y$. By Proposition 5.4.1, we suppose both $\bar{x}$ and $\bar{y}$ are Z_n-symmetric satisfying

$$\sigma^m \circ \tau_{P/n}\bar{x}(t) = \bar{x}(t) \tag{5.21}$$

and

$$\sigma^m \circ \tau_{P/n}\bar{y}(t) = \bar{y}(t), \tag{5.22}$$

where $(m, n) = 1$. Then by the same arguments as we had in section 5.2.2, we have

$$T_x = \frac{P}{n} \times \frac{n}{j_1 n - m} = \frac{P}{j_1 n - m}$$

and

$$T_y = \frac{P}{n} \times \frac{n}{j_2 n - m} = \frac{P}{j_2 n - m},$$

for some integers j_1 and j_2. Since

$$\frac{f_y}{f_x} = \frac{T_x}{T_y},$$

we have the following proposition

Proposition 5.4.2 *Suppose $(\bar{x}(t), \bar{y}(t))$ is a non-trivial periodic solution of the coupled cell system (5.18). If both $\bar{x}$ and $\bar{y}$ are Z_n-symmetric satisfying (5.21) and (5.22), then the ratio of frequencies of $\bar{x}$ and $\bar{y}$ is of the form*

$$\frac{f_y}{f_x} = \frac{j_2 n - m}{j_1 n - m}, \tag{5.23}$$

for some integers j_1 and j_2.

Similarly, the following corollary for the Z_p case is a straightforward result. Here, Z_p is a subgroup of Z_n.

Corollary 5.4.2 *Suppose $(\bar{x}(t), \bar{y}(t))$ is a non-trivial periodic solution of the coupled cell system (5.18). If both $\bar{x}$ and $\bar{y}$ are Z_p-symmetric, then the ratio of frequencies of $\bar{x}$ and $\bar{y}$ is of the form*

$$\frac{f_y}{f_x} = \frac{j_2 p - m}{j_1 p - m}, \tag{5.24}$$

for some integers j_1, j_2 *and where* $(m, p) = 1$.

Now, we can identify those rational numbers which are not the ratio of frequencies of any symmetric periodic solutions in two cells.

Corollary 5.4.3 *Suppose* $p = j_1 p + m$ *and* $q = j_2 p + m'$ *are two positive integers such that* $(p, q) = 1$, j_1, j_2, m *and* m' *are integers. If* $(m, p) \neq 1$, $(m', p) \neq 1$ *or* $m \neq m'$, *then* q/p *is not the ratio of frequencies of any non-trivial* Z_p*-symmetric periodic solution in two cells.*

5.4.3 Numerical results- an example

In this section, we use Tachikawa's example to check numerically that the results in the previous sections are valid.

The system consists of two replicator equations coupled diffusively:

$$\begin{cases} \dot{x}_i &= x_i((Ax)_i - x^T Ax) + D(y_i - x_i) \\ \dot{y}_i &= y_i((By)_i - y^T By) + D(x_i - y_i) \end{cases}, \tag{5.25}$$

for $i = 1, 2, 3, 4$. Here, the 4×4 matrices A and B are defined by

$$\begin{aligned} (a_{ii}, a_{i,i+1}, a_{i,i+2}, a_{i,i+3}) &= (0, -2.0, -1.0, 1.0) \\ (b_{ii}, b_{i,i+1}, b_{i,i+2}, b_{i,i+3}) &= (0, -1.0, -0.9, 2.0) \end{aligned},$$

where the suffixes are all taken modulo 4.

Without coupling, i.e. the case $D = 0$, the x-cell has a robust heteroclinic cycle as an attractor. In contrast, an unstable heteroclinic cycle exists in the y-cell and, as a result, the attractor within the y-cell is a periodic orbit. As long as $D > 0$, the attractors in both cells are periodic or quasi-periodic.

Replicator equations describe the dynamics of the frequencies of n-species in an ecological system. More precisely, let x_i denote the frequency of the ith species

and suppose that the rate of increase $\dot{x}_i/x_i$ depends on the difference between the fitness $f_i(\mathbf{x})$ of the ith species and the average fitness $\bar{f}(\mathbf{x}) = \sum x_j f_j(\mathbf{x})$, i.e.

$$\dot{x}_i = x_i(f_i(\mathbf{x}) - \bar{f}(\mathbf{x})), \tag{5.26}$$

$i = 1, ..., n$. Equation (5.26) is called *replicator equation*. Since x_i denotes the frequency of the ith species, the equality

$$\sum_{i=1}^{n} x_i = 1$$

is trivially true. In other words, replicator equations are defined on the n-simplex.

Normally, we take $f_i(\mathbf{x})$ to be a linear functional of $\mathbf{x}$

$$(A\mathbf{x})_i = \sum_{j=1}^{n} a_{ij}x_j,$$

where $A = (a_{ij})$ is a $n \times n$ matrix. In game theory, this matrix A can be considered as the payoff matrix. For example, in the rock-scissors-paper fair game, A can be of the form

$$\begin{pmatrix} a & b & c \\ c & a & b \\ b & c & a \end{pmatrix},$$

where a, b, c denote the payoff obtained by rock against rock, scissors and paper, scissors against scissors, paper and rock, or paper against paper, rock and scissors, respectively. When $f_i(\mathbf{x})$ is linear, which is the case of Tachikawa's paper, the replicator equation (5.26) is in the form

$$\dot{x}_i = x_i((A\mathbf{x})_i - \mathbf{x}^T A\mathbf{x}), \ i = 1, 2, ..., n,$$

$A = (a_{ij})$, which is equivalent to the $(n-1)$-dimensional Lotka-Volterra system [37]

$$\dot{y}_i = y_i\left(r_i + \sum_{j=1}^{n-1} a'_{ij}y_j\right), \ i = 1, ..., n-1,$$

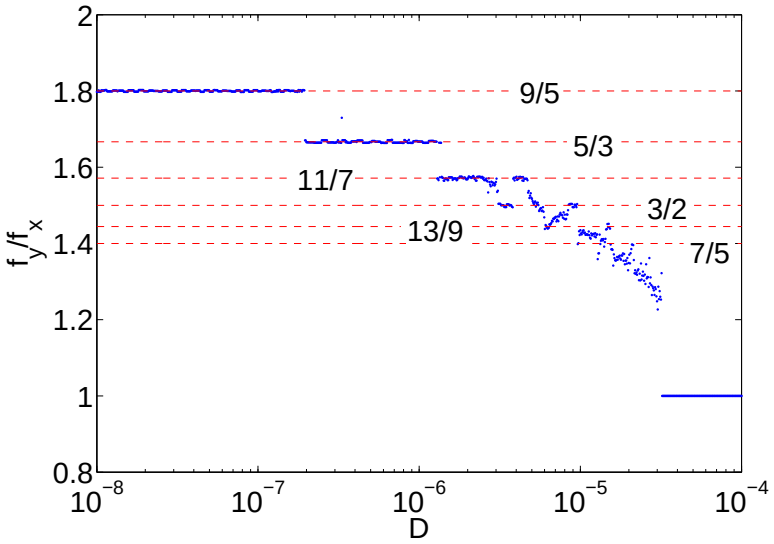

Figure 5.6: The frequency-locking intervals in system (5.25) when varying the coupling strength D. We reproduce this figure from [74].

where $r_i = a_{in} - a_{nn}$ and $a'_{ij} = a_{ij} - a_{nm}$. Specifically, by suitable choice of the payoff matrix A, there exists a stable robust heteroclinic cycle in the replicator system.

Tachikawa compared the frequencies of the attractors in each cells and showed numerically that frequency-locking intervals of D can be observed when varying the forcing strength D. See Figure 5.6. He also explained some of the ratios are due to symmetric periodic solutions in both cells. In the following, we will check that our analytic results are confirmed by numerical investigations for this system. Specifically, we answer the following questions:

- Are the period of periodic solutions in x-cell and y-cell the same?
- Do they both share the same symmetry?
- Does the ratio match the form given in Proposition 5.4.2 or Corollary 5.4.2?

Since both cells have robust heteroclinic cycles connecting the four points $(1,0,0,0), (0,1,0,0), (0,0,1,0)$ and $(0,0,0,1)$, we investigate periodic solutions near the heteroclinic cycles by putting cross sections near these four points. Let $E = \{x_3 = 0.2\}$ be the cross section near $(0,0,0,1)$ in the x-cell, then $\sigma^i E = \{\sigma^i x_3 = 0.2\}$ are the cross sections near $\sigma^i(0,0,0,1)$ for $i = 1,2,3,4$. The cross sections in the y-cell are defined by the same way and denoted by $\sigma^i E'$. See Figures 5.7, 5.8 and 5.9.

Suppose $\overline{x}(t)$ and $\overline{y}(t)$ are periodic solutions in the x-cell and the y-cell, respectively. By Proposition 5.4.2, the ratio of the frequencies of two Z_4-symmetric periodic solutions is of the form $(4j_2 - m)/(4j_1 - m)$, where $m = 1$ or 3. To detect Z_4-symmetric periodic solutions, we record the x_1-coordinate of points in $\overline{x}(t) \cap E$ and the x_4-coordinate of points in $\overline{x}(t) \cap \sigma^3 E$, which are denoted by x_1^E and $x_4^{\sigma^3 E}$ respectively, and then compare the last 50 points to see if there exists the same sequence of points which occurs periodically. If this sequence exists, the periodic solution is a Z_4-symmetric one of $m = 3$ type.

Although the x_2-coordinate of points in $\overline{x}(t) \cap \sigma E$ is not computed, we are still able to identify symmetric periodic solutions of the $m = 1$ type by knowing only x_1^E and $x_4^{\sigma^3 E}$. In fact, the number of loops the periodic solution circle around is different in these two cases. It can be $3, 7, 11, ...$ for $m = 1$, while $1, 5, 9, 13, ...$ for $m = 3$. For example, if both x_1^E and $x_4^{\sigma^3 E}$ are period-7 sequences, we then know the underlying symmetric solution is of $m = 1$ type.

The periodicity and the symmetry of the solutions in the y-cell are studied in the same way and all the cross sections as well as other notations are defined analogously. See Figures 5.7 and 5.8 for schematic diagrams.

In the following, we will consider three values of D for which the system has Z_4, Z_2 and non-symmetric solutions. These values are $D = 10^{-8}$, $D = 2.1 \times 10^{-5}$ and $D = 3.3 \times 10^{-6}$.

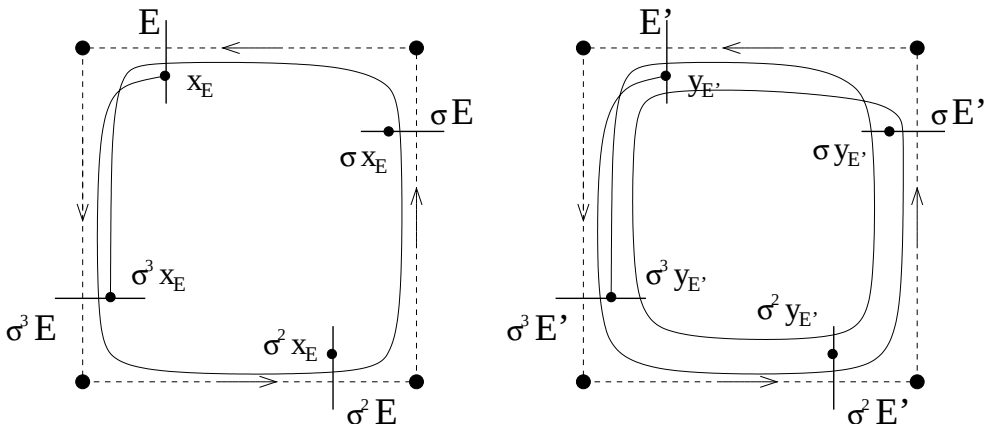

Figure 5.7: Schematic diagram depicting the existence of Z_4-symmetric periodic solutions in the *x*-cell (left) and the *y*-cell (right). In the *x*-cell, $m = 3$ and $j_1 = 2$. In the *y*-cell, $m = 3$ and $j_2 = 3$. The ratio of frequencies $f_y/f_x = 9/5$ in this case.

- Z_4**-symmetry**

  By Proposition 5.4.2, $9/5$ could be the ratio of frequencies of Z_4-symmetric solutions in *x* and *y*-cells of $m = 3$ type. From Figure 5.6, $D = 10^{-8}$ gives this ratio. So we integrate the system with initial point $(10^{-4}, 10^{-4}, 10^{-4}, 1 - 3 \times 10^{-4}, 10^{-4}, 10^{-4}, 10^{-4}, 1 - 3 \times 10^{-4})$ for this value of D to look for a Z_4-symmetric solution. As is shown in Table 5.3, there exists a period-5 periodic solution in the *x*-cell and a period-9 one in the *y*-cell. By comparing the sequences of x_1^E and $x_4^{\sigma^3 E}$, the periodic solution is indeed Z_4-symmetric. This is also the case for the *y*-cell. In addition, we note that the period of $\bar{x}$ and $\bar{y}$, which can be calculated by summing up the return times T_x and T_y, are both equal to 407.04, as we expect.

x_1^E	7.288e-09	4.569e-08	4.459e-08	2.038e-11	2.597e-12	7.288e-09
$x_4^{\sigma^3 E}$	4.569e-08	4.459e-08	2.038e-11	2.597e-12	7.288e-09	4.569e-08
T_x	82.62	84.62	84.63	80.50	74.67	82.62
$y_1^{E'}$	1.484e-08	2.487e-10	6.829e-08	7.097e-10	6.382e-08	1.962e-09
	5.475e-09	6.393e-09	2.057e-10	1.484e-08		
$y_4^{\sigma^3 E'}$	6.829e-08	7.097e-10	6.382e-08	1.962e-09	5.475e-09	6.393e-09
	2.057e-10	1.484e-08	2.487e-10	6.829e-08		
T_y	43.62	45.45	46.48	43.12	48.76	41.34
	49.28	41.42	47.56	43.62		

Table 5.3: The x_1 and x_4-coordinates of the last few points of $\bar{x}(t)$ on the cross sections E and $\sigma^3 E$, and the y_1 and y_4-coordinates of the last few points of $\bar{y}(t)$ on the cross sections E' and $\sigma^3 E'$, respectively. The system (5.25) is integrated for $D = 10^{-8}$ starting from the initial point $(10^{-4}, 10^{-4}, 10^{-4}, 1-3\times10^{-4}, 10^{-4}, 10^{-4}, 10^{-4}, 1-3\times10^{-4})$. The data shows that there exists a period-5 Z_4-periodic solution in the x-cell and a period-9 Z_4-periodic solution in the y-cell. This gives the ratio of frequencies $9/5$. By summing the return times T_x and T_y, we see that the period of both periodic solutions is 407.04.

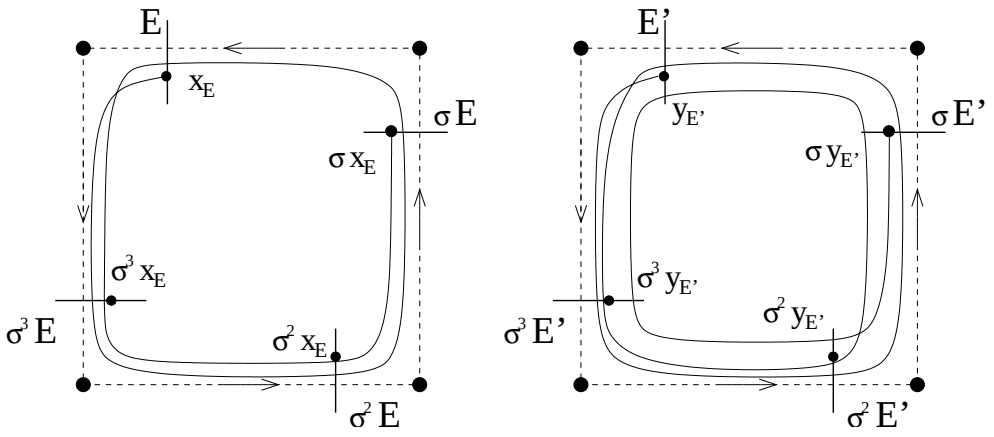

Figure 5.8: Schematic diagram depicting the existence of Z_4-symmetric periodic solutions in the x-cell (left) and the y-cell (right). In the x-cell, $m = 1$ and $j_1 = 2$. In the y-cell, $m = 1$ and $j_2 = 3$. The ratio of frequencies $f_y/f_x = 11/7$ in this case.

- **Z_2-symmetry**

  Here, we consider $7/5 = (2\times4-1)/(2\times4-3)$ as this could be the ratio of a Z_4-symmetric periodic solution of $m = 3$ type in the x-cell and one of $m = 1$ type in the y-cell. See Figure 5.9. By Proposition 5.4.1, this is actually not the case.

  However, by Proposition 5.4.2, $7/5$ could be the ratio of two Z_2-symmetric periodic solutions in the two cells. Figure 5.10 shows how the periodic solutions circle around in two cells to produce this ratio. From Figure 5.6, $D = 2.1\times10^{-5}$ gives this ratio. So we integrate the system with initial point $(10^{-3}, 10^{-3}, 10^{-3}, 1-3\times10^{-3}, 10^{-3}, 10^{-3}, 10^{-3}, 1-3\times10^{-3})$ for this value of D to see if the periodic solutions in both cells are Z_2-symmetric. As is shown in Table 5.4, there exists a period-5 periodic solution in the x-cell and a period-7 one in the y-cell. By comparing the sequences of x_1^E, $x_4^{\sigma^3 E}$ and $x_3^{\sigma^2 E}$, the periodic solution is indeed not Z_4 but Z_2-symmetric. This is also the case for the y-cell. In addition, we notice that the period of $\bar{x}$ and $\bar{y}$

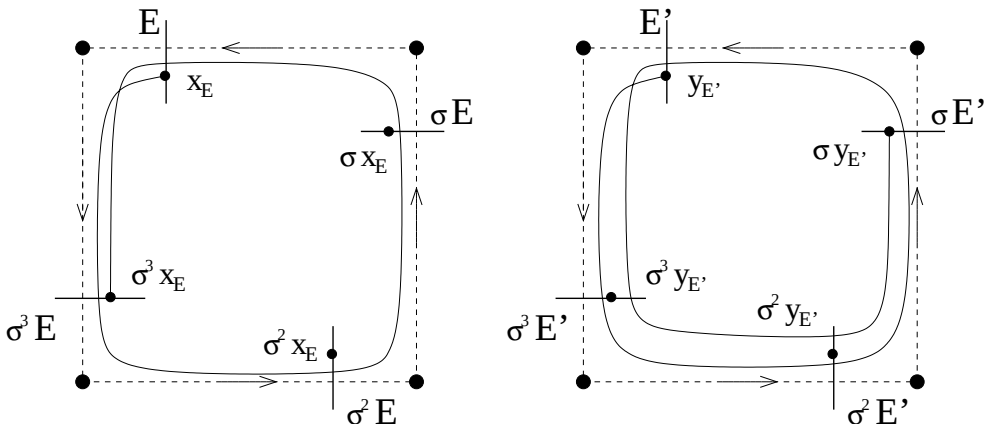

Figure 5.9: Schematic diagram showing a situation which cannot happen in system (5.25). A Z_4-symmetric periodic solution in the x-cell of type $m = 3$ (left) can not accompany a Z_4-symmetric periodic solution in the y-cell of type $m = 1$ (right). In other words, $7/5$ is not a ratio of frequencies of two Z_4-symmetric periodic solutions.

are both equal to 218.64.

x_1^E	4.275e-05	6.907e-05	9.160e-05	2.141e-09	8.130e-05	4.275e-05
$x_4^{\sigma^3 E}$	9.166e-05	5.260e-05	8.693e-05	1.978e-06	7.550e-05	9.165e-05
$x_3^{\sigma^2 E}$	9.160e-05	2.141e-09	8.130e-05	4.275e-05	6.907e-05	9.160e-05
T_x	38.24	51.71	38.50	43.12	47.07	38.24
$y_1^{E'}$	7.272e-06	8.045e-05	3.412e-07	8.702e-07	1.204e-04	4.792e-06
	2.861e-07	7.272e-06				
$y_4^{\sigma^3 E'}$	2.125e-06	1.418e-04	1.138e-06	4.538e-07	3.597e-05	1.447e-05
	2.211e-07	2.125e-06				
$y_3^{\sigma^2 E'}$	1.204e-04	4.793e-06	2.861e-07	7.272e-06	8.045e-05	3.413e-07
	8.702e-07	1.204e-04				
T_y	34.86	26.42	29.68	36.46	31.05	25.59
	34.59	34.86				

Table 5.4: The x_1, x_4 and x_3-coordinates of the last few points of $\overline{x}(t)$ on the cross sections E, $\sigma^3 E$ and $\sigma^2 E$, and the y_1, y_4 and y_3-coordinates of the last few points of $\overline{y}(t)$ on the cross sections E', $\sigma^3 E'$ and $\sigma^2 E'$, respectively. The system (5.25) is integrated for $D = 2.1\times10^{-5}$ starting from the initial point $(10^{-3}, 10^{-3}, 10^{-3}, 1-3\times10^{-3}, 10^{-3}, 10^{-3}, 10^{-3}, 1-3\times10^{-3})$. The data shows that there exists a period-5 Z_2-symmetric periodic solution in the x-cell and a period-7 Z_2-symmetric periodic solution in the y-cell. This gives the ratio of frequencies $7/5$. By summing the return times T_x and T_y, we see that the period of both periodic solutions is 218.64.

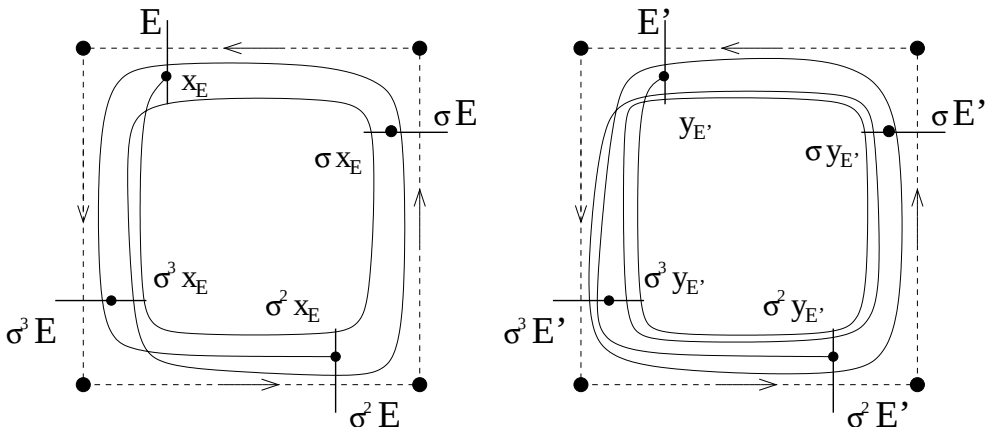

Figure 5.10: Schematic diagram depicting the existence of Z_2-symmetric periodic solutions in the x-cell (left) and the y-cell (right). In the x-cell, $m = 1$ and $j_1 = 2$. In the y-cell, $m = 1$ and $j_2 = 3$. The ratio of frequencies $f_y/f_x = 7/5$ in this case.

- **Non-symmetry**

  Apparently, $3/2$ is the ratio of the frequencies of neither Z_4 nor Z_2-symmetric solutions by Corollary 5.4.3. From Figure 5.6, $D = 3.3 \times 10^{-6}$ gives this ratio. So we integrate the system with initial point $(10^{-3}, 10^{-3}, 10^{-3}, 1 - 3 \times 10^{-3}, 10^{-3}, 10^{-3}, 10^{-3}, 1 - 3 \times 10^{-3})$ for this value of D to see if the periodic solutions in both cells have any symmetry. As is shown in Table 5.5, there exists a period-2 periodic solution in the x-cell and a period-3 one in the y-cell. By comparing the sequences of x_1^E and $x_3^{\sigma^2 E}$, the periodic solution is indeed not Z_2-symmetric. As a result, it is not Z_4-symmetric as well. This is also the case for the y-cell. In addition, we see that the period of $\bar{x}$ and $\bar{y}$ are both equal to 104.86.

x_1^E	1.482e-05	1.841e-08	1.482e-05	
$x_3^{\sigma^2 E}$	1.326e-05	1.982e-06	1.327e-05	
T_x	49.32	55.54	49.32	
$y_1^{E'}$	5.248e-08	2.146e-05	3.409e-07	5.248e-08
$y_3^{\sigma^2 E'}$	1.024e-06	3.594e-06	3.131e-08	1.024e-06
T_y	39.38	35.36	30.11	39.38

Table 5.5: The x_1 and x_3-coordinates of the last few points of $\overline{x}(t)$ on the cross sections E and $\sigma^2 E$, and the y_1 and y_3-coordinates of the last few points of $\overline{y}(t)$ on the cross sections E' and $\sigma^2 E'$, respectively. The system (5.25) is integrated for $D = 3.3 \times 10^{-6}$ starting from the initial point $(10^{-3}, 10^{-3}, 10^{-3}, 1 - 3 \times 10^{-3}, 10^{-3}, 10^{-3}, 10^{-3}, 1 - 3 \times 10^{-3})$. The data shows that there exists a period-2 non-symmetric periodic solution in the x-cell and a period-3 non-symmetric periodic solution in the y-cell. This gives the ratio of frequencies $3/2$. By summing the return times T_x and T_y, we see that the period of both periodic solutions is 104.86.

5.5 Discussion

In this chapter, we have demonstrated a systematic approach to the analysis of coupled cell systems consisting of two cells which are coupled diffusively. We concentrated our investigation on the existence of non-trivial periodic solutions of systems with cyclic symmetry. Such a coupled cell system can be decomposed into two systems with periodic perturbations when periodic solutions occur in both cells. Consequently, we first studied Z_n-symmetric ODE systems perturbed by periodic functions.

For this kind of system, we have shown that to have a non-trivial, cyclically symmetric, periodic solution, the perturbation functions must differ by only a phase-shift. Once we fix a set of perturbation functions satisfying this necessary condition, the ratio of the frequencies between a cyclically symmetric periodic solution and the perturbation functions can be identified.

A Guckenheimer-Holmes system perturbed by periodic functions is then studied as an example to check the validity of results obtained in section 5.2.1 and 5.2.2. Instead of applying these results directly, we calculated the Poincaré map of the system and then give analogous results by studying the map analytically. Our result shows that a regular pattern for the frequency-locking windows where Z_3-symmetric period-1 periodic solution exists can be observed generically.

By applying the results for the system with periodic perturbations, we are able to extend our study to symmetric periodic solutions in coupled cell systems. Our results show that the symmetry is always 'synchronized' between two cells and again the ratio of the frequencies of the non-trivial symmetric periodic solutions in two cells can be identified. Moreover, the symmetric periodic solutions in each of the two cells must be of the same type. These observation help to explain the numerical results given by Tachikawa.

There are still many questions unsolved in the coupled cell systems with cyclic

symmetry. For example, sufficient conditions for the system to have a cyclically symmetric solution are unclear. So far, we only understand that for some ratio of frequencies the periodic solutions could be symmetric. However, knowing the ratio of frequencies is not sufficient to identify what symmetry a periodic solution possesses. An example can be found in Tachikawa's system for $D = 5.5 \times 10^{-7}$ where the periodic solutions in both cells are not Z_2-symmetric even though the ratio of frequencies, $5/3$, is of the Z_2-symmetric form.

Chapter 6

Conclusion and Future Work

Chapters 3, 4 and 5 contain the central results of this thesis, divided into these three parts: the construction of Poincaré maps, the analysis of one specific example, and the investigation of symmetric periodic orbits arising in coupled cell systems. In this chapter, we give concluding remarks on each of these topics in turn and describe directions for future research on each.

6.1 Constructing Poincaré maps for time-periodically forced heteroclinic systems

In Chapter 3, we have presented a systematic method to derive the Poincaré map of the time-periodic forced Lotka-Volterra system in $\mathbb{R}^3$. The derivation involves careful calculation of (i) the local maps by integrating the linearized system near each equilibrium point, and (ii) the global maps by estimating the unstable manifold of each periodic orbit bifurcating from the original equilibrium points due to the perturbation. Unlike the method by Afraimovich et al. [3], we keep the time-dependent terms in each step of the derivation. This complicates the calculations but enables us to obtain a more general and, indeed, correct result. Our result

should be able to be extended to higher dimensional asymptotically stable simple heteroclinic cycles, which by definition are heteroclinic cycles with connections lying in two-dimensional planes.

Essentially, the Poincaré map can be divided into two parts. The time-independent terms reflect a constant forcing term corresponding to the mean of the perturbation function. On the other hand, the oscillating component of the perturbation function contributes to the time-dependent terms by affecting the form of the linearized systems and the unstable manifold of each periodic orbit bifurcating from the original equilibrium points. From this point of view, it is not too hard to write out the form of the Poincaré map.

Finding the parameters in the Poincaré map (3.25) is not straightforward. All we know is that they are functions of c, e and depend on the form of the perturbation function. This results in two difficulties: (i) it is very hard to find a suitable set of parameters for simulating an ODE system (it involves plenty of trial and error), and (ii) it is very hard to analyze the changes of the dynamics of the ODE system when varying c and e because the dependence of the parameters on c and e is not known.

6.2 Analysis for time-periodic forced heteroclinic systems

Based on the Poincaré map we derived, we are able to carry out a thorough mathematical analysis of the dynamics of the systems.

In Chapter 4, we first discuss the asymptotic order of the x-coordinate. The results show that an analytic study of the Poincaré map derived by Afraimovich et al. [3] can not explain the dynamics of the original ODE system. Moreover, the results also predict two different scenarios: the cases 'ϵ near 0' and 'ϵ large',

occur. (Recall that we define $\epsilon = (c/e)^3 - 1$.)

In summary, we are interested in the dynamics of the ODE system when varying the frequency ω of the perturbation function and the main results are:

- If ϵ is near 0, the system is equivalent to a damped pendulum with torque. In this case, bistability arises in some intervals of ω.
- If ϵ is large, the system is equivalent to a circle map. Depending on the frequency of the forcing function, it can be non-invertible, where chaotic dynamics can be observed, or invertible, where only regular (periodic or quasiperiodic) dynamics can exist.

Although we have attempted to understand the dynamics of the system for all ω and c/e, the case ϵ large and ω of medium size remains analytically intractable. So far, we explain the dynamics of the system by consider the case for ω of medium size as some kind of transition state when ω moves from small to near infinity. However, we are not completely sure, in this case (although it seems reasonable), whether the Poincaré map is still equivalent to a circle map and how many bifurcations may take place as the system switches between being equivalent to an invertible and a noninvertible circle map. The difficulty of this case is due to the complicated form of the Poincaré map.

6.3 Symmetric periodic solutions in coupled cell systems

In Chapter 5, we consider coupled cell systems in which two ODE systems with cyclic symmetry Z_n are coupled diffusively. We are interested in the interactions between non-trivial periodic solutions with cyclic symmetry in the two cells.

Specifically, the ratios of the frequencies of periodic solutions in the two cells for which the periodic solutions are symmetric are identified.

To study a coupled cell system when periodic solutions exist, we reduce the coupled system to a single system subjected to a periodic perturbation. Our results prove that to have a non-trivial symmetric periodic solution, the perturbation functions must differ only by a phase-shift. The ratios of frequencies between the non-trivial symmetric periodic solutions and the perturbation functions are also identified.

With these results, we are able to analyze systems composed of two coupled cells. The study proves that a 'synchronization' of symmetry always exists between the non-trivial periodic solutions of two cells. More precisely, if there exist non-trivial periodic solutions in the two cells, then the periodic solution in the first cell is Z_p-symmetric if and only if the periodic solution in the other cell is also Z_p-symmetric. Moreover, they share the same kind of symmetry, i.e. they have the same m defined in (5.2). In addition, all the possible ratios of frequencies of symmetric periodic solutions in these two cells can be classified.

The work in Chapter 5 provides necessary conditions of the existence of symmetric periodic solutions in a coupled system with two cells. This only helps to identify systems which do not have any symmetric solution, and systems which could have a symmetric solution. It is then important to find the sufficient conditions for the existence of symmetric periodic solutions.

As was shown in [74], bistability exists over a range of values of the coupling stength D. Moreover, it is possible to have a Z_4-symmetric ratio (11/7) and, at the same time, a non-symmetric ratio (3/2). In other words, the ratio of frequencies obtained depends on the initial condition.

So far, we have studied the coupled systems of two cells. One trivial extension of our results could be the consideration of lattice coupled cell systems. It

has been reported in the literature that coupled cell systems with symmetry produce spatial-temporal patterns [73]. A question arises concerning the existence of 'synchronization' of symmetry between the periodic solutions of these cells for a coupled system with n cells. A similar question has been studied by M. Golubitsky et al. in [27]. In the following, we briefly review their results and then describe how they may be related.

Golubitsky et al. [27] considered networks of coupled phase oscillators:

$$\dot{\theta} = F(\theta), \tag{6.1}$$

where $\theta = (\theta_1, ..., \theta_N) \in \mathbf{S}^N$, $F = (f_1, ..., f_N) \in \mathbb{R}^N$. Here, $\mathbf{S} = \mathbb{R}/\mathbb{Z} = [0, 1)$.

Firstly, they defined the terms *winding number*, *average frequency* and *coevolve*.

Definition 6.3.1 *([27]) Let $\theta(t)$ be a solution of (6.1) on an interval $\tau = [t_1, t_2]$ and $\theta^L(t)$ be the lift of $\theta(t)$. The winding number of $\theta_j(t)$ on the interval τ is given by*

$$\rho_j^\tau = \theta_j^L(t_2) - \theta_j^L(t_1).$$

If $\theta(t)$ is a T-periodic solution of (6.1), then the lift satisfies

$$\theta^L(t + T) = \theta^L(t) + \rho,$$

where $\rho = (\rho_1, ..., \rho_N) \in \mathbb{Z}^N$ is a vector of integers. The winding number of θ_j in a periodic orbit is defined by

$$\rho_j^{[0,T]} = \rho_j,$$

where T is the minimal period for the solution as a whole.

Definition 6.3.2 *([27]) The average frequency ν_j^τ of $\theta_j(t)$ over τ is defined by*

$$\nu_j^\tau = \frac{\rho_j^\tau}{t_2 - t_1}.$$

If the limit

$$\nu_j = \lim_{|\tau|\to\infty} \nu_j^\tau$$

exists, we say that ν_j is the average frequency of cell j. If $\theta(t)$ is a T-periodic solution of (6.1), then we have

$$\nu_j = \lim_{N\to\infty} \frac{\rho_j^{[0,NT]}}{NT} = \frac{\rho_j}{T}.$$

Definition 6.3.3 *([27]) Two phase oscillators i and j coevolve if the torus $\{\theta \in \mathbf{S}^N : \theta_j = \theta_j\}$ is flow-invariant. They are in the same collection if there exists a chain of distinct oscillators $i = k_0, ..., k_{m+1} = j$ such that all pairs $(k_0, k_1), ..., (k_m, k_{m+1})$ coevolve; m is the length of this chain.*

Then they proved the following results:

Proposition 6.3.1 *([27]) Suppose that oscillators i and j coevolve, then the winding numbers of a periodic solution to a phase oscillator system (6.1) are equal and the winding numbers of any solution to the system (6.1) differ at most by 1. If the average frequency ν_i is defined, then the average frequency ν_j is defined as well and $\nu_i = \nu_j$.*

Proposition 6.3.2 *([27]) The collections of oscillators in a network have the following properties: (a) Winding numbers of a periodic solution are equal for all cells in the same collection. (b) If average frequency is defined for one cell in a collection, then it is defined for all, and this average frequency is the same for all cells in the collection. (c) Let i and j be two cells in the same collection and let m be the length of the shortest chain of oscillators relating them. Then for a general solution, the winding numbers of cells i and j on an interval differ at most by $m + 1$.*

In short, the coevolution of two cells, i and j, states that there exists an invariant torus in the $\theta_i\theta_j$-plane which forces frequency-locking to occur. In their case, the invariant torus is $\{\theta_i = \theta_j\}$ and hence the two cells are $1:1$-locked. However, in the two examples we have considered in Chapter 5, coevolution does not always exist due to that the two oscillators we coupled are not identical. Therefore, we expect the occurence of other locking modes.

Therefore, we might be able to exploit this idea to extend the two-cell systems to N-cell systems. More precisely, if we consider the system:

$$\dot{x}_i = f_i(x_i) + \gamma g(x) \quad i = 1, 2, ..., N, \tag{6.2}$$

where $x_i = (x_{i1}, ...x_{in})$, g is a function depending on how we couple the cells, and f_i's are Z_n-symmetric. We then say that x_i and x_j coevolve if there exists a periodic solution in the x_ix_j-subspace. In this way, we might be able to extract a two-cell system from the n-cell system, and two-cell systems were studied in Chapter 5. A 'collection' of cells can be defined in a similar way. Work on this problem is ongoing.

Bibliography

[1] H.D.I. Abarbanel, R. Brown, J.J. Sidorovich, and L.S. Tsimring. The analysis of observed chaotic data in physical systems. *Rev. Mod. Phys.*, 65:1331–1392, 1993.

[2] V.S. Afraimovich and S-B Hsu. *Lectures on Chaotic Dynamical Systems*. American Mathematical Society and International Press, 2002.

[3] V.S. Afraimovich, S-B Hsu, and H. E. Lin. Chaotic behavior of three competing species of may-leonard model under small periodic perturbations. *Int. J. of Bifur. and Chaos*, 11(2):435–447, 2001.

[4] V.S. Afraimovich, M.I. Rabinovich, and P. Varona. Heteroclinic contours in neural ensembles and the winnerless competition principle. *Inter. J. Biff. Chao.*, 14, 2004.

[5] V.S. Afraimovich, V.P. Zhigulin, and M.I. Rabinovich. On the origin of reproducible sequential activity in neural circuits. *Chaos*, 14(4):1123–1129, 2004.

[6] A.A. Andronov, A.A. Vitt, and S.E. Khaikin. *Theory of Oscillators*. Pergamon, New York, 1996.

[7] F. Antoneli, A.P.S. Dias, M. Golubitsky, and Y. Wang. Patterns of synchrony in lattice dynamical systems. *Nonlinearity*, 18:2193–2209, 2005.

[8] D. Armbruster, J. Guckenheimer, and P. Holmes. Heteroclinic cycles and modulated travelling waves in systems with **O**(2) symmetry. *Physica D*, 29:257–282, 1988.

[9] D.K. Arrowsmith and C.M.Place. *An Introduction to Dynamical Systems*. CUP, 1990.

[10] P. Ashwin, G. Orosz, J. Wordsworth, and S. Townley. Dynamics on networks of cluster states for globally coupled phase oscillators. *SIAM Journal on Applied Dynamical Systems*, 6(4):728–758, 2007.

[11] P.L. Boyland. Bifurcations of circle maps: Arnol'd tongues, bistability and rotation intervals. *Commun. Math. Phys.*, 106:353–381, 1986.

[12] F.H. Busse and K.E. Heikes. Convection in a roating layer: A simple case of turbulence. *Science*, 208:173–175, 1980.

[13] C-W. Chi, S-B Hsu, and L-I Wu. On the asymmetric May-Leonard model of three competing species. *SIAM J. Appl. Math.*, 58(1):211–226, 1998.

[14] R.M. Clever and F.H. Busse. Nonlinear properties of convection rolls in a horizontal layer rotating about a vertical axis. *J. Fluid Mech.*, 94:609–627, 1979.

[15] P. Coullet, J.M. Gilli, N. Monticelli, and N. Vandenberghe. A damped pendulum forced with a constant torque. *American Journal of Physics*, 73:1122–1128, 2005.

[16] J.H.P. Dawes and M.C. Freeland. The '0-1 test for chaos' and strange non-chaotic attractors. *submitted*, 2008.

[17] J.H.P. Dawes, C.M. Postlethwaite, and M.R.E. Proctor. Instabilities induced by a weak breaking of a strong spatial resonance. *Physica D*, 191:1–30, 2004.

[18] J.H.P. Dawes and T.L. Tsai. Frequency locking and complex dynamics near a periodically forced robust heteroclinic cycle. *Phys. Rev. E*, 74(055201(R)), 2006.

[19] M. Dellnitz, M. Field, M. Golubitsky, A. Hohmannan, and J. Ma. Cycling chaos. *Int. J. Bifu. Chao.*, 5:1243–1247, 1995.

[20] R.L. Devaney. *An Introduction to Chaotic Dynamical Systems*. Addison-Wesley Publishing Company, 1989.

[21] A. Epstein, L. Keen, and C. Tresser. The set of map $f_{a,b} : x \mapsto x + a + \frac{b}{2\pi}\sin(2\pi x)$ with any given rotation interval is contractible. *Commun. Math. Phys.*, 173:313–333, 1995.

[22] I. Falconer, G.A. Gottwald, I. Melbourne, and K. Wormnes. Application of the 0-1 test for chaos to experimental data. *SIAM J. Applied Dynamical Systems*, 6(2):395–402, 2007.

[23] M. Field. *Lectures on bifurcations, dynamics and symmetry*, volume 356 of *Pitman Research Notes in Mathematics*. 1996.

[24] M.J. Field and J.W. Swift. Stationary bifurcation to limit cycles and heteroclinic cycles. *Nonlinearity*, 4:1001–1043, 1991.

[25] M. Frean and E.R. Abraham. Rock-scissors-paper and the survival of the weakest. *Proc. R. Soc. Lond. B*, 268:1323–1327, 2001.

[26] J.R. Gog, I. Oprea, M.R.E. Proctor, and A.M. Rucklidge. Destabilization by noise of transverse perturbations to heteroclinic cycles: a simple model and

an example from dynamo theory. *Proc. R. Soc. Lond. A*, 455:4205–4222, 1999.

[27] M. Golubitsky, K. Josic, and E. Shea-Brown. Winding numbers and average frequencies in phase oscillator networks. *J. Nonlinear Sci.*, 16:201–231, 2006.

[28] M. Golubitsky and I. Stewart. *The symmetry perspective: from equilibrium to chaos phase space and physical space*. Birkhäuser, 2002.

[29] G.A. Gottwald and I. Melbourne. A new test for chaos in deterministic systems. *Proc. R. Soc. Lond. A*, 460:603–611, 2004.

[30] G.A. Gottwald and I. Melbourne. Testing for chaos in deterministic systems with noise. *Physica D*, 212:100–110, 2005.

[31] G.A. Gottwald and I. Melbourne. Comment on "reliability of the 0-1 test for chaos". *Phys. Rev. E*, 77(028201), 2008.

[32] G.A. Gottwald and I. Melbourne. On the implementation of the 0-1 test for chaos. *SIAM Journal on Applied Dynamical Systems*, 8:129–145, 2009.

[33] J. Guckenheimer and P. Holmes. Structurally stable heteroclinic cycles. *Math. Proc. Camb. Phil. Soc.*, 103:189–192, 1988.

[34] J. Guckenheimer and P. Holmes. *Nonlinear Oscillations, Dynamical Systems, and Bifurcations of Vector Fields*. Springer, 2002.

[35] J. Hale and H. Koçak. *Dynamics and Bifurcation*. Springer-Verlag, 1991.

[36] J. Hofbauer. Heteroclinic cycles on the simplex. In *Proc. Int. Conf. Nonlinear Oscillations*. Janos Bolyai Math. Soc. Budapest, 1987.

[37] J. Hofbauer and K. Sigmund. *Evolutionary Games and Population Dynamics*. Cambridge University Press, Cambridge, U.K., 1998.

[38] C. Hou and M. Golubitsky. An example of symmetry breaking to heteroclinic cycles. *J. Diff. Eqs.*, 133:30–48, 1997.

[39] J. Hu, W-W Tung, J. Gao, and Y. Cao. Reliability of 0-1 test for chaos. *Phy. Rev. E*, 72:056207, 2005.

[40] R. Ito. Rotation sets are closed. *Math. Proc. Camb. Phil. Soc.*, 89:107, 1981.

[41] V. Kirk and A. M. Rucklidge. The effect of symmetry breaking on the dynamics near a structurally stable heteroclinic cycle between equilibria and a periodic orbit. *Dynamical Systems: An International Journal*, 23(1):43–74, 2008.

[42] M. Krupa. Robust heteroclinic cycles. *J. Nonlinear Sci.*, 7:129–176, 1997.

[43] M. Krupa and I. Melbourne. Asymptotic stability of heteroclinic cycles in systems with symmetry. *Erod. Th. & Dynam. Sys.*, 15:121–147, 1997.

[44] M. Krupa and I. Melbourne. Asymptotic stability of heteroclinic cycles in systems with symmetry, ii. *Proc. Roy. Soc. Edinbrugh*, 134A:1177–1197, 2004.

[45] R. Lauterbach. Forced symmetry breaking from **O**(3). In *Bifurcation and Symmetry*, volume 104, pages 253–262. ISNM, Birkhäuser, Basel, 1992.

[46] R. Lauterbach, S. Maier-Paape, and E. Reissner. A systematic study of heteroclinic cycles in dynamical systems with broken symmetries. *Proc. Roy. Soc. Edinburgh*, 126A:885–909, 1996.

[47] R. Lauterbach and M. Roberts. Heteroclinic cycles in dynamical systems with broken spherical symmetry. *J. Diff. Eqs.*, 100:22–48, 1992.

[48] R.S. Mackay and C. Tresser. Transition to chaos for two-frequency systems. *J. Physique Lett.*, 45:741–746, 1984.

[49] R.S. Mackay and C. Tresser. Transition to topological chaos for circle maps. *Physica 19D*, pages 206–237, 1986.

[50] R.S. Mackay and C. Tresser. Some flesh on the skeleton: the bifurcation structure of bimodal maps. *Physica 27D*, pages 412–422, 1987.

[51] R. Mamon, I.P. Malta, M.J. Pacifico, and F. Takens. Rotation intervals of endomorphisms of the circle. *Ergod. Th. & Dynam. Sys.*, 4:493–498, 1984.

[52] R.M. May and W.J. Leonard. Nonlinear aspects of competition between three species. *SIAM J. App. Math.*, 29(2):243–253, 1975.

[53] I. Melbourne. Intermittency as a codimension-three phenomenon. *Journal of Dynamics and Differential Equations*, 1(4):347–367, 1989.

[54] I. Melbourne. An example of a non-asymptotically stable attractor. *Nonlinearity*, 4:835–844, 1991.

[55] S.E. Newhouse, J. Palis, and F. Takens. Bifurcations and stability of families of diffeomorphisms. *I.H.E.S. Publ. Math.*, 57:5–71, 1983.

[56] M. Nicol, I. Melbourne, and P. Ashwin. Euclidean extensions of dynamical systems. *Nonlinearity*, 14:275–300, 2001.

[57] M.A. Nowak and K. Sigmund. Evolutionary dynamics of biological games. *Science*, 303:793–799, 2004.

[58] M.J. Parker, I.N. Stewart, and M.G.M. Gomes. Partial classification of heteroclinic behaviour associated with the perturbation of hexagonal planforms. *Dynamical Systems: An International Journal*, 23(2):137–162, 2008.

[59] L. Perko. *Differential Equation and Dynamical Systems*. Springer, 3rd edition, 2000.

[60] C.M. Postlethwaite and J.H.P. Dawes. Regular and irregular cycling near a heteroclinic network. *Nonlinearity*, 18:1477–1509, 2005.

[61] C.M. Postlethwaite and J.H.P. Dawes. A codimension-two resonant bifurcation from a heteroclinic cycle with complex eigenvalues. *Dynamical Systems: An International Journal*, 21:313–336, 2006.

[62] M.R.E. Proctor and C.A. Jones. The interaction of two spatially resonant patterns in thermal convection. *J. Fluid Mech.*, 188:301–335, 1988.

[63] M.I. Rabinovich, R. Huerta, and P. Varona. Heteroclinic synchronization: Ultra-subharmonic locking. *Phys. Rev. Lett.*, 96(014101), 2006.

[64] M.I. Rabinovich, R. Huerta, P. Varona, and V.S. Afraimovich. Transient cognitive dynamics, metastability and decision making. *PLoS computational biology*, 4(e1000072), 2008.

[65] M.I. Rabinovich, P.V. Varona, A.I. Selverston, and H.D.I. Abarbanel. Dynamical principles in neuroscience. *Reviews of Modern Physics*, 78:1213–1265, 2006.

[66] M.I. Rabinovich, A. Volkvskii, P. Lecanda, R. Huerta, H.D.I. Abarbanel, and G. Laurent. Dynamical encoding by networks of competing neuron groups: winnerless competition. *Phys. Rev. Lett.*, 87(068102), 2001.

[67] M.T. Rosenstein, J.J. Collins, and C.J. De Luca. A practical method for calculating largest lyapunov exponents from small data sets. *Physica D*, 65:117–134, 1993.

[68] M. Sano and Y. Sawada. Measurement of the lyapunov spectrum from a chaotic time series. *Phys. Rev. Lett.*, 55:1082–1085, 1985.

[69] Y. Sato, E. Akiyama, and J. P. Crutchfield. Stability and diversity in collective adaptation. *Physica D*, 210:21–57, 2005.

[70] K. Sigmund. The population dynamics of conflict and cooperation. *Doc. Math. J. DMV*, Extra Volume ICM I:487–506, 1998.

[71] E. Stone and P. Holmes. Random perturbations of heteroclinic attractors. *SIAM J. Appl. Math.*, 50(3):726–743, 1990.

[72] J.W. Swift. *Bifurcation and Symmetry in Covection*. PhD thesis, Physics, U. C. Berkeley, 1984.

[73] M. Tachikawa. Multiplicity of limit cycle attractors in coupled heteroclinic cycles. *Prog. Theor. Phys.*, 109(1), 2003.

[74] M. Tachikawa. Specific locking in populations dynamics: Symmetry analysis for coupled heteroclinic cycles. *J. Comp. and Appl. Math.*, (201):374–380, 2007.

[75] F. Takens. *Detecting strange attractors in turbulence*, volume 98. Berlin: Springer, 1981.

[76] P. Varona, R. Levi, Y. I. Arshavsky, M. I. Rabinovich, and A.I. Selverston. Competing sensory neurons and motor rhythm coordination. *Neurocomputing*, 58-60:549–554, 2004.

[77] P. Varona, M.I. Rabinovich, A.I. Selverston, and Y.I. Arshavsky. Winnerless competition between sensory neurous generates chaos: A possible mechanism for molluscan hunting behavior. *Chaos*, 12:672–677, 2002.

[78] D. Veitch and P. Glendinning. Explicit renormalisation in piecewise linear bimodal maps. *Physica D*, 44:149–167, 1990.

[79] A. Venaille, P. Varona, and M.I. Rabinovich. Synchronization and coordination of sequences in two neural ensembles. *Phys. Rev. E*, 71(061909), 2005.

[80] Y. Wang and M. Golubitsky. Two-color patterns of synchrony in lattice dynamical systems. *Nonlinearity*, 18:631–657, 2005.

[81] S. Wiggins. *Global bifurcations and chaos*. Springer-Verlag, 1988.